October 2019

SILVER MIRROR SUBSTRATE AND ROLLING METHOD FOR IMPROVED SURFACE-ENHANCED RAMAN SPESCTROSCOPIC ANALYSIS IN FOOD

Yanqi Qu

SILVER MIRROR SUBSTRATE AND ROLLING METHOD FOR IMPROVED SURFACE-ENHANCED RAMAN SPESCTROSCOPIC ANALYSIS IN FOOD

A Dissertation Presented

by

YANQI QU

Submitted to the Graduate School of the
University of Massachusetts Amherst in partial fulfillment
of the requirements for the degree of

DOCTOR OF PHILOSOPHY

September 2019

Department of Food Science

SILVER MIRROR SUBSTRATE AND ROLLING METHOD FOR IMPROVED SURFACE-ENHANCED RAMAN SPESCTROSCOPIC ANALYSIS IN FOOD

A Dissertation Presented

by

YANQI QU

Approved as to style and content by:

_____
Lili He, Chair

_____
Eric A. Decker, Member

_____
Ryan C. Hayward, Member

_____
Eric A. Decker, Department Head
Department of Food Science

DEDICATION

This dissertation is dedicated to my beloved parents Jun and Hongyan, and wife, Jinning, and the best mentor in the world, Dr. Lili He, whose understanding, support, and encouragement inspired me to pursue the competition of this research.

ACKNOWLEDGMENTS

I cannot stop myself to list my Ph.D. advisor, Dr. Lili He, as the first person I want to express my deepest gratitude. I have met many good professors and mentors in my life, but Dr. He is the best one, not one of the best, but the only best. I want to thank her for providing me such a valuable opportunity not only to pursue the doctorate degree but also to bring my wife and I together here in UMASS. I want to thank her for all the right and wise suggestions and guidance which always direct me on the correct path, I would not have done anything in last three years without her support and encouragement. I want to thank her for being such straightforward since the first time I stepped in her office and let me understand what I really want to achieve for my career from the first day of being a doctorate student. I want to thank her for all her trust and understanding to let me handle many important projects, demonstrations, and group events. I truly appreciate her forgiveness for all the mistakes I have made and her kindness, generosity, and patience to make me be a better person. I extremely grateful for all her encouragements and recommendations during my research, job hunting, and any moments I felt perplexed. Dr. He is not only the mentor for my research, but also the mentor for my life. It really is my honor to have her as my advisor for three years and I wish it can be even longer. Again, without her support, I will never be the person I am today!

I also want to express my appreciation to my doctorate committee members, Dr. Eric Decker and Dr. Ryan Hayward. I would love to thank Dr. Decker for all his suggestions for my research, especially in Gas Chromatography. I would love to thank Dr. Hayward for all his advices for my research, especially in statistical analysis. Other than the expertise, I want to thank them for all their valuable comments and even criticisms to my

work and their time and efforts in being a part of my committee, without any one of them, I will never finish this dissertation. I also want to extend my sincere thanks to my great lab mates, Kevin, Alex, Michael, Siyue, Xinyi, Janam, Lourdes, Andy, Tina, Josh, Jason Lin, Jason Yang, and previous lab members, Haoxin, Ana, Dr. Tu, Dr. Zhang, and Dr. Tan, for all their help, supports, and suggestions in my research and life. Thank them all for their trust in me to be the event coordinator and their ever-active participation in all of our lab events.

Additionally, I want to thank Yuheng and Yue from NEC laboratory, Hailing from PepsiCo, and Peter from Diversified laboratory, for their trusts to collaborate us, and for all countless experiences I have gained from these collaborative projects.

Last but not the least, I would love to express my sincerest gratitude to my great family for their countless support and endless love and help. I could not thank my parents more for all the sacrifices they have made and all the most generous love and care they have provided to me since day I was born. I especially want to thank my beloved wife, Jinning, who always provides me the warmest love, the most unforgettable memories, the strongest backup and confidence. I will love, respect and honor every one of them for the rest of my life.

ABSTRACT

SILVER MIRROR SUBSTRATE AND ROLLING METHOD FOR IMPROVED SURFACE-ENHANCED RAMAN SPESCTROSCOPIC ANALYSIS IN FOOD

SEPTEMBER 2019

YANQI QU, B.A., PENNSYLVANIA STATE UNIVERSITY

M.A., PENNSYLVANIA STATE UNIVERSITY

Ph.D., UNIVERSITY OF MASSACHUSETTS AMHERST

Directed by: Professor Lili He

Surface enhanced Raman spectroscopy, short for SERS, is an emerging technology with great potential in food analysis due to rapid detection, high sensitivity, portable instrumentation, and simple sample preparation. However, it is always a bottleneck to obtain reproducible SERS measurements in real analytical cases due to the complicity of food systems and inhomogeneous aggregation of colloidal nanoparticles. To improve its performance for practical applications in food analysis, efforts have been made in improving the reproducibility, enhancing the selectivity and reducing the matrix interference to the analyte. Herein, a self-assembly silver nanoparticles mirror substrate was fabricated to improve the and the quantitative ability and effectiveness of sample preparation for different applications in food analysis, including pesticides detection in beverages, chemical profiling of red wines, and headspace analysis of garlic. The AgNPs mirror was fabricated using the interface between polar and non-polar solvents and showed a uniform arrangement of nanoparticles under the microscope. It demonstrated a great reliability for the detection of a pesticide fonofos in beverages (i.e., apple juice and green tea). AgNPs mirror can also be *in situ* fabricated in red wines to generate a comprehensive spectrum constituted by signals of five wine phytochemicals, which provided a great

potential of SERS in the differentiation, authentication, and quality/safety control of red wines. AgNPs mirror also showed a great potential in the headspace characterization of aromatic compounds from *Allium* species plants. Additionally, a facile rolling method was developed to enrich analyte (i.e., chlordane pesticide) and to amplify its weak SERS activity and a mathematic model was generated and successfully quantified the chlordane in a complicated crude oil sample with a very good recovery. Overall, AgNPs mirror and the rolling method overcame the reproducibility and sensitivity problems for SERS in several challenging food matrices. With these improvements, SERS can be much more reliable for analytical applications and its range of targets can be widely expanded.

TABLE OF CONTENTS

Page

LIST OF TABLES

Table Page

LIST OF FIGURES

Figure Page

CHAPTER

1. INTRODUCTION

Background

In last decades, surface-enhanced Raman spectroscopy (SERS) has been extensively explored and becoming a promising technology to detect various chemical and biological analytes in environmental, agricultural, food, and medical applications[1–7]. SERS combined Raman spectroscopy and nanotechnology. Raman spectroscopy measures the vibration of chemical structure and functional groups and generates a label-free signature fingerprint of the molecule being scattered. Raman scattering is relatively weak, however, after placing the analyte in the close proximity of certain noble metallic nanostructure, the Raman scattering of the analyte can be dramatically enhanced 106 to 108 times. SERS-based methods showed great advantages over the standard methods for food analysis (e.g., UV- vis spectrophotometry, fluorescence, HPLC, GC-MS, etc.)[8]. In terms of simple sample preparation, rapid detection, facile instrumental operation, and cost effective. Furthermore, the commercial availability of handled or portable Raman instrument allows SERS to be an *in situ* analytical solution for the on-site quality and safety analysis during or after the food processing.

The enhancement of Raman scattering is mostly dependent on the SERS substrates. The most traditional SERS active substrates are colloidal nanoparticles, which can be easily fabricated and are already commercially available. It features a very simple sample preparation by mixing the colloidal nanoparticles suspension with analyte in solution. The aggregation of nanoparticles (i.e., coffee ring effect) driven by the surface tension during the mixture evaporation will generate “hot spots” to enhance the signal of target analytes.

However, the aggregation of colloidal nanoparticles during the evaporation cannot be precisely controlled, which could lead to weak reproducibility of the SERS performance[9,10]. The large variation has been considered as the major drawback of the colloidal nanoparticle substrates, along with the lack of quantitative ability due to the same reason. However, the aggregation is sometimes needed to form hotspots and generate Raman intensity enhancement, so it is very critical to control the aggregation of nanoparticles[10,11]. Furthermore, colloidal nanoparticles are lack of selectivity if no surface modification is done and are sensitive to matrix background. Another challenge for real-world application is the lack of sensitivity for certain analytes with a weak Raman-active structure or weak interaction with the SERS substrates. Detection of these analytes in a complex food matrix is extremely difficult.

Therefore, many efforts have been done to improve the reproducibility of SERS, the sensitivity for certain analyte of interest, as well as develop optimum sample preparation to reduce matrix interference. Some examples of reported approaches include self-assembly fabrication, lithography fabrication, microfluidic integration, and functionalization of SERS-active substrates. However, efforts for food application are still not well explored.

Objective

Long term goal of this project is to improve the efficiency of SERS for food analysis. To reach the overall goal, the specific objectives of this project are to fabricate a SERS substrate that can contribute consistent and quantitatively improved results for different targets in varied food systems and to develop a simple sample preparation method to amplify the weak surface enhanced Raman scattering of target analytes.

Objective 1: Development of a facile solvent based method to fabricate AgNPs mirror for improving quantification analysis.

Objective 2: Determination of the reproducibility and quantitative ability of the mirror substrate and its performance in detection of pesticides in water and beverage.

Objective 3: Application of the mirror substrates in red wines profiling.

Objective 4: Application of the mirror substrate in the headspace analysis of food matrices.

Objective 5: Investigation of a facile rolling method to amplify the analyte of weak SERS activity (i.e., chlordane) in food.

The completion of these studies will establish a facile and innovative approach to fabricate a uniform reproducible, and quantitatively improved SERS substrate that can be adapted in detection the trace of contaminants and bioactive compounds in complex food matrices. The development of this substrate can expand the potential applications of SERS for food analysis, including the measurement of targets in complicated aqueous phases and gas phases, the chemical profiling of wine samples and its potential correlation to wine quality. Furthermore, the development of the rolling approach can achieve the intensity amplification of previously reported analytes with weak SERS signals and improve the resolution and the limit of detection of the analyte in food

2. LITERATURE REVIEW

Current methods for food analysis

Food analysis is an important category in analytical chemistry, it can provide chemical information in food matrix including the composition, additives, processing, and contamination, to monitor the overall quality, to ensure the safety characteristics, to implement the law enforcement, to investigate the compliance, to establish standards, and to analyze nutritional value [12]. In terms of the food safety and quality, many foods are threatened with chemical and microbial hazards such as pesticides, food pathogens, antibiotics, banned colorants, and abused preservatives. Therefore, developing accurate analytical methods for monitoring and detecting these targets is in a great need [13]. Currently, standard methods such as chromatographic techniques, UV-visible and spectroscopy methods, and immunoassays were widely explored and applied in chemical characterization of food matrices.

Chromatographic methods

Modern analytical instrumental techniques (e.g., gas chromatography (GC), high performance liquid chromatography (HPLC), mass spectrometry (MS), and etc.)[14], are the gold standard analytical tools and have been extended to the food analysis. Combined with instrumental analytical techniques (e.g., UV-visible spectrophotometry, nuclear magnetic resonance, or mass spectrometry)[15], they are able to identify specific chemical compounds based on their molecular characters [7] and produce highly sensitive results. GC/HPLC analysis has a relatively low detection of limit and is applicable for most bioactive components. Chromatographic techniques show several advantages compared

to liquid chromatography, including fast detection, wide variety of stationary phases, improved resolution, great sensitivity and easy sample recovery. However, disadvantages such as requirement of professional operation, time consuming, and lack of portability were also pointed [13,16].

UV-visible and fluorescence spectroscopy

Both UV-visible and fluorescence spectroscopies are most common analytical techniques in food qualitative and quantitative analysis. The absorbance spectroscopy quantifies the concentration of analyte in a sample solution based on the amount of absorption in a reference beam passing through the sample solution[17]. UV-visible spectroscopy provides a quick and simple analysis of the target and the Beer's law can be quickly applied for quantitative objectives; however, the accuracy and sensitivity are highly dependent on the transparency of the sample and can be easily affected by the impurities and the contaminants in the sample.

On the other hand, fluorescence spectroscopy is about 10-1000 times more sensitive than the absorption spectroscopy. Initially, the analyte absorbs the radiation from the UV/visible range and is activated to a high energy level. Then, it relaxes and emits the electromagnetic radiation from the excited energy level to a its ground state, where the radiant power is measured as the fluorescence signal. The radiation wavelength for each scenario is specific and dependent on the chemical structure of the analyte, so do the excitation and emission wavelengths. The concentration of the analyte is proportional directly to the fluorescence signal[17]. To be noted, the sensitivity of the fluorescence spectroscopy is highly dependent on the power of the incident beam according to the equation, especially for circumstances of low detecting concentration[17]. Fluorescence

spectroscopy is widely used in the food analysis due to it high sensitivity, specificity, wide concentration range and accurate results, however, not every analyte has a fluorescence and the price of instruments is relatively high. The fluorescence reading can also be interfered by the impurities of the sample, presence of the bubbles, and pH of the analyzing environment.

Immunoassays

The immunoassay is based on the high affinity binding of the antibodies to antigens. The most common immunoassay is called enzyme-linked immunosorbent assay, short for ELISA. It involves the binding of the target (antigens or antibodies) to a platform and the removal of unbound molecules through washing steps. Normally, it combines with the colorimetric assay and uses the measurement of color intensity to determine the concentration of analytes. In food analysis, some targets are small molecules, which cannot trigger the formation of antibodies in animals. To ensure the high affinity and specificity of the immunoassays, those small molecular analytes are absorbed by a larger carrier protein and are detected indirectly through the immune binding[18]. Immunoassays provide sensitive results and rapid detection with relative cheap reagents, inexpensive instruments. However, the measurement of enzyme activity sometimes is more complicated than the targets, it might be affected by the chemistry of detecting environment, such as pH. Additionally, the detection of small molecules is still not sensitive due to the lack of selection of the carrier molecules[19].

Summary

Even though above-mentioned analytical methods were well established and considered as standard techniques for food analysis, they were time consuming,

laborious, highly dependent on trained personnel, lack of sustainability for large-scale sample screening, and suffered from interreference from impurity, and complicated sample preparation[7,13]. Therefore, it is crucially for analytical chemists and food scientists to pursue inexpensive, portable, rapid, and reliable techniques with high sensitivity, facile analysis, and high throughput using small volume of samples to trace concerns in food commodities and to satisfy the demand of modern food industry[9,13].

Raman spectroscopy and Surface Enhanced Raman spectroscopy

Raman spectroscopy

Raman spectroscopy was introduced in early 20th century as one of vibrational spectroscopic techniques[20,21]. Once a visible or near infrared laser beam irradiated a sample, a small part of photons was scattered, meanwhile, an inelastic collision occurred between incident photons and molecules in the irradiated subject. Therefore, the vibrational energy of the molecule was changed as well as the wavelength of the scattered light shifted to a different level from the incident light, and the difference of the frequency (i.e., wavelength) of scattered light and incident light is named as the Raman shift[22,23]. The intensity of Raman scattering at each frequency and the Raman shift constitute the Raman spectra. More importantly, the Raman shifts (i.e., spectra bands) are dependent on the chemical bonds or the functional groups of the molecules involved in the scattering. Therefore, the Raman spectra can provide a fingerprint of a specific substance that can be beneficial for chemical characteristic analysis and qualitative analysis[22].

Raman spectroscopy has been performed in food analysis because Raman intensity was found linearly proportional to the concentration of the analyte[22].

Additionally, Raman spectroscopy has significant advantages including high specificity to molecules, short analyzing time, good compatibility with water-based sample, and no requirement of sample preparation[22,24,25]. However, Raman signals are always relatively low and dependent on the high-quality instrumentation because the scattering only happened to a tiny portion of photons from the incident laser[23].

Surface-enhanced Raman Scattering

To enhance the signal of Raman scattering, as shown in Figure 1, when probed molecules are attached with noble metallic nanostructures (e.g., Au, Ag, Cu, Pt, TiO2 or Pt), the Raman scattering signals are significantly enhanced by millions of times because of either the electromagnetic enhancement or the chemical enhancement[3].

Electromagnetic Enhancement

The electromagnetic enhancement mechanism is because of the electromagnetic fields provided by the localized surface plasmon resonance (LSPR) of noble metallic nanostructures surface[13,26]. The incident light hits the surface and excites the localized surface plasmons, therefore, the field enhancement magnifies the intensity of incident light and increase the signal of Raman scattering. Additionally, the surface further magnifies the Raman intensity, to result in the dramatically enhanced Raman scattering[27].

To be noted, the region owning a cluster of strong field enhancements contributed by the LSPR is named as “hot spot”, where can provide considerable enhancement of the SERS intensity[13,28]. Therefore, analytes located closely to the “hot spots” can obtain much higher signals during the measurement[13]. According to the literature, the electromagnetic field is able to generate up to 10^6 times Raman signal enhancement[29].

Chemical Enhancement

Another mechanism is based on the charge transfer, which is named as chemical enhancement. Once the analyte chemically binds to the surface, a resonant charge transfer occurs between molecules strongly absorbed to the surface and the metals, resulting in an increase of the Raman signal[30]. According to the literature, the charge transfer mechanism can only enhance the signal about 100 times[29].

Influent factors for Surface-enhanced Raman scattering

According to several literatures, factors can affect the enhancement of Raman scattering are showed below:

Size and shape: Nanoparticles can provide good enhancement of the of the Raman signal however, the frequency and magnitude of maximum field enhancement are highly dependent on the kind, size, and shape of metallic nanoparticles, such as fractal clusters could provide stronger enhancements[8,10,31].

Surface: Roughness or the arrangement of nanoparticles on the surface generated varied degrees of the enhancement. Larger enhancements can be observed at regions having high field gradients (e.g., two interacted nanoparticles, aggregated nanoparticles) and orienting the spacing between particles can optimize the enhancement factors[31]. As a result, even though the average degree of enhancement for SERS is around 10^6, extremely high levels of enhancement (i.e., 10^{10}) can be achieved at highly efficient sub-wavelength regions at the surface[10].

Absorption of analytes: According to the “hot spot” explanation, the strong absorption of target analytes to the metallic nanostructured surface, even the “hot spot” area can also ensure the sufficient enhancement of the Raman scattering[23,31].

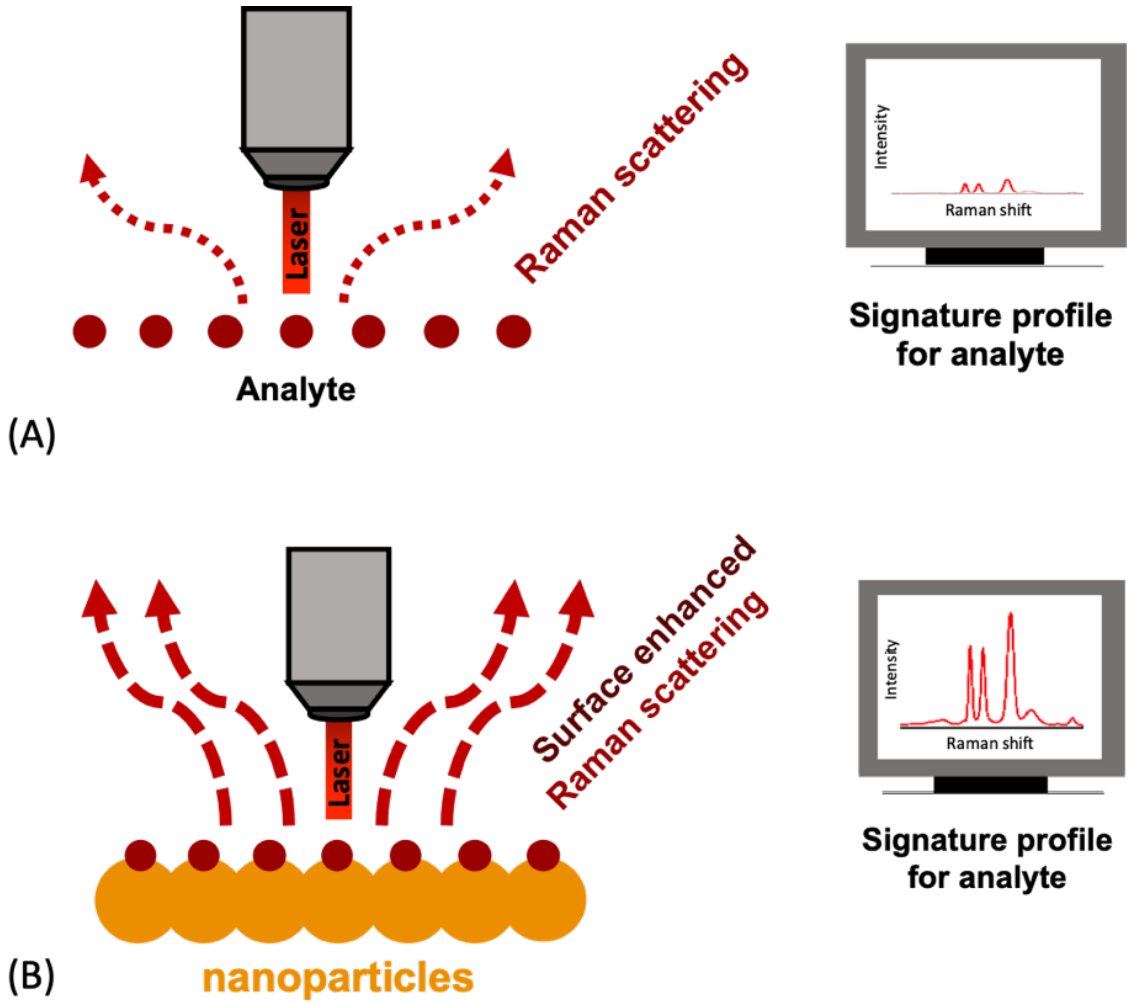

Figure 1 Illustration of surface-enhanced Raman scattering mechanism, (A) Raman scattering, (B) SERS.

Advantages and drawbacks of SERS

In recent 10 years, surface enhanced Raman spectroscopy (SERS) technology emerged into many applications in food analysis. In this section, advantages of SERS as a new analytical technique and challenges that preventing SERS to be further applicable will be thoroughly reviewed.

Advantages of SERS

A powerful fingerprinting and selective tool: Raman scattering is resultant from the vibration of chemical bonds or functional groups; thus, it provides specific fingerprint for each molecule that is being analyzed and works as a good labeling technique[7,13,32].

Rapid measurements and simple operations: Raman spectroscopy collect data in a very short a period of time making the SERS to be applicable in real time detection and there is no requirement of professional trained panel to operate the instrument[22].

Direct and non-destructive identification: SERS can directly acquire signals of analyte on a solid food sample or in the aqueous based water system without the need for sample preparation, destruction or tedious extraction steps[23].

Highly sensitive analysis: SERS is known for its function of single molecule detection, and the limit of detection for specific analytes can reach extremely low levels (i.e., ppb or even ppt) that are favored by the industry and below the requirement of standard regulation[33].

Good compatibility with other techniques: SERS as an analytical tool has been shown to be capable of combining with other techniques such as headspace analysis, immunomagnetic separation, solid phase microextraction (SPME), and microfluidic devices, and filtration methods[13,34–37].

Good portability and *in situ* identification: Portable Raman spectroscopy is commercially available and can be use directly with colloidal nanoparticles for field tests.

Challenges for application of SERS in food analysis

SERS cannot isolate target compounds from a complex sample. This is a significant drawback for SERS to be applied in the food analysis. Food normally is a complicated matrix and the targets such as residual pesticides, antibiotics, or other contaminates are present in relatively concentration levels. Even though sometime extremely low limit of detection was achieved in standard solution, in the real food matrices, other components/ingredients could mask the target signal and make it challenging for SERS measurement[8,9,13].

Background interference is a big challenge for analysis of targets by SERS. Polymerized pigments and proteins in food samples can contribute a huge fluorescence to mask the target signals in the Raman spectra[22,38]. Additionally, the environmental chemistry affects the SERS measurement, such as the change of pH can quench the surface charges of nanoparticles to cause the aggregation and the loss of enhancement functionality. Other species in the sample can also affect the interaction between the analyte and the nanostructured surface to result in the change of the orientation of the surface, so do the spetcra[13,31].

The aggregation of nanoparticles makes the reproducibility of SERS measurements very challenging[7,10]. The easiest formation of "hot spot" is dependent on the surface tension driven natural aggregation of colloidal nanoparticles. Moreover, natural aggregations of nanoparticles result in a disparity in size of metal nanoparticles and inhomogeneous arrangement of analytes on the surface, thus, variations of SERS

signals are observed during the measurement[13,39]. More importantly, the inconsistency of the aggregation of nanoparticles cannot be easily controlled according to current research and makes it significantly challenging to obtain reliable and repeatable performance of SERS[10].

SERS is lack of quantitative ability due to the variation caused by the inconsistent aggregation of nanoparticles and the variations in the substrate preparation[31].

SERS measurements normally require the mixing of colloidal nanoparticles with sample analytes in an aqueous system or on a solid surface, the sampling requirement might limit the extensive applications of SERS[10]. Additionally, current SERS analysis mostly focused on the surface analysis, the internal analysis has not been well studied[8].

Limited range of analytes is another concern for SERS. According to the literature, SERS is very sensitive to symmetric-structure molecules or those molecules can strongly bind to nanoparticles such as chemical structures with thiol group[7,32,40]. However, there are still many concerned targets in food research having weak sensitivities with SERS, and few studies have been done to improve the amplification of SERS signals of those molecules.

Conclusion

Due to the fast and ultrasensitive detection, simple protocols, large-scale screening and in situ sample preparation, surface enhanced Raman spectroscopy (SERS) technology emerged into food analysis techniques and started to be applicable in many areas in the recent one decade.

However, major drawbacks such as the high variations (i.e., low uniformity), lack of quantitative ability and the limited range of analyte are significantly preventing the

SERS to be extended to a real-time analytical technique. Therefore, efforts have been made by analytical chemists and food scientists to modify and evolve the SERS to be a more modern and applicable food analytical tool.

SERS substrates

To overcome the drawbacks, one research suggested that avoid directly measurement of the interested target with SERS, therefore, substrates are important. Since the electromagnetic filed enhancement for SERS is provided by the surface, to obtain improved signal, SERS substrates with functionalized characteristics are in a great demand[9,26,27]. the growing research and fabrication of appropriated SERS-active substrates is driving the development of SERS applications[9]. The enhancement of Raman signal in SERS is not only dependent on the interaction between samples and substrates, but also the functionalization of SERS substrate to improve the measurement and performance. To overcome the drawbacks of SERS, substrates are expected to play an important role[9]. Uniform, sensitive, and functional substrates with different shape, composition, and size have been developed to improve the limit of detection, selectivity, and quantitative ability of SERS.

Three key points were proposed by literatures for a successful fabrication of an appropriate SERS-active substrate[8,41,42]:

The choice of SERS-active materials, such as noble metals (e.g., silver and gold) and semiconductors (e.g., titanium dioxide), is very important for fabrication because of their different enhancement ability.

The affinity of analyte to the SERS-active materials: SERS cannot directly isolate the target signal through a complex food system, so the surface selection ability of a

substrate is very critical during the fabrication to ensure the successfully capture or selection of the target analyte, from the current knowledge, interactions between analyte and the substrate include electrostatic, hydrophobic, and covalent binding. Additionally, absorption of the analyte to the "hot spot" area on the substrate is another key for the acquirement of sufficient signal enhancements.

Resonance Raman effect: Once the incident laser frequency is close in energy to an electronic transition of a compounds, the coincidence or the resonance frequency can trigger an even higher intensity enhancement of the Raman scattering.

Rough metal electrodes were used as the first SERS substrates, but the whole electrode process is not controllable, therefore, it is not considered as a suitable substrate for current fundamental and practical analysis[8]. Current SERS active substrates can be divided into two types based on their physical forms, colloidal substrates and solid surface-based substrates. In the solid surface-based substrates, based on the fabrication methods or specific functionalities, the substrates can be either divided into nanoparticles immobilized on solid substrates, nanostructures fabricated directly on solid substrates, substrate fabricated by using nanolithography methods, molecular imprinting and microfluidic devices; or substrates modified with antibodies and aptamers, respectively[7–10,40].

Colloid-based substrates

Colloid-based substrates are the most direct substrate to obtain enhanced Raman signal, mostly in solution-based aqueous system. Silver and gold nanoparticles colloids in diameters ranging from 10 to 200 nm, are considered as the most traditional substrates for

SERS measurement, they are cost-effective, facile to fabricate in a large scale of production and even commercially available[9].

The synthesis of colloidal nanoparticles are proposed by several groups with chemical, physical, and biological methods[43–45]. The physical methods include the spark discharging and pyrolysis, and the biological methods includes synthesizing nanoparticles via bacterial proteins or plant extracts. Synthesis of nanoparticles chemically happens in water or organic solvents, using the metal precursors (e.g., silver nitrite and gold chloride hydrate), reducing agents, and capping/stabilizing agents. The metal precursors are reduced in two steps, the nucleation of nanoparticle seeds, followed with the growth of nanoparticles[44,46].

Mixing colloidal nanoparticles suspension with a certain concentration of analyte in a food sample/extract is considered as the simplest sample preparation to acquire the SERS signal. Generally speaking, the performance of the colloidal metallic nanoparticles in SERS is dependent on the shape, size and composition of nanoparticles, chemical structure of the target analyte, sample preparation, and the monitoring procedures[9].

Colloidal substrates have been used as the standard sample preparation with targets for analysis, due to its ease of operation and good performance of Raman signal enhancement. However, it suffered from several major disadvantages listed below:

Inconsistent SERS performance. Lack of reproducibility is considered as the main drawback of colloidal nanoparticles for SERS analysis due to the lack of uniform and integrated nanostructures during the synthesis and aggregation after sample preparation. Since colloidal substrates are normally mixed with aqueous sample in suspensions, and the mixture is dried on a surface to form a “coffee ring” (as shown in Figure 2) like

structure for SERS measurement. Therefore, surface tension causes over aggregation of nanoparticles during the drying and accumulated nanoparticles introduce huge variations of signals from one spot and another spot during the Raman detection. Due to the same reason, analytes are also inhomogeneous distributed on the surface to cause the signal inconsistency. On the other hand, the aggregation of nanoparticles is somehow also required to generate the hotspot for SERS enhancement[47,48].

Semi-quantitative ability: Because of the inconsistency of the signal from the colloidal substrates, even though the Raman scattering is reported to be proportional to the concentration of the analyte, the coefficient of determination is still not satisfied for the linear regression analysis. As a result, the quantitative ability of colloidal substrates still needs to be improved.

Requirement of the aqueous system for measurement: Nanoparticles suspension must be mixed with the analyte solution for sample preparation and data collection. This dependency of aqueous environment could limit the application of colloidal substrates in headspace or non-SERS active surfaces[10].

Interreference from the background: Colloidal noble nanoparticles are stabilized by the electrostatic repulsion, components other than the analyte in the sample could break the repulsive state and consequence in the over aggregation and loss of SERS function[8]. Additionally, the charges present in the food sample can also interfere the absorption of analytes to the nanoparticle surfaces.

To improve the performance of the colloidal substrates, advanced colloid-based SERS substrates have been developed, such as AgNPs coated poly (styrene-co-acrylic acid) composite nanospheres, Ag-coated AuNPs, AgNPs-decorated Ag/C nanospheres,

Ag-coated (ferriferous oxide-core silicon shell composite microspheres, Au-core silica-shell NPs (Au@SiO_2 NPs), and AgNPs coated amino modified polystyrene microspheres[7,49–52]. Even though the sensitivity of these substrates is reported to be improved, the aggregation of the colloidal nanoparticles is still hard to control, therefore, more uniform, reproducible, and quantitatively improved substrates, are still in a huge demand for practical analytical applications using SERS.

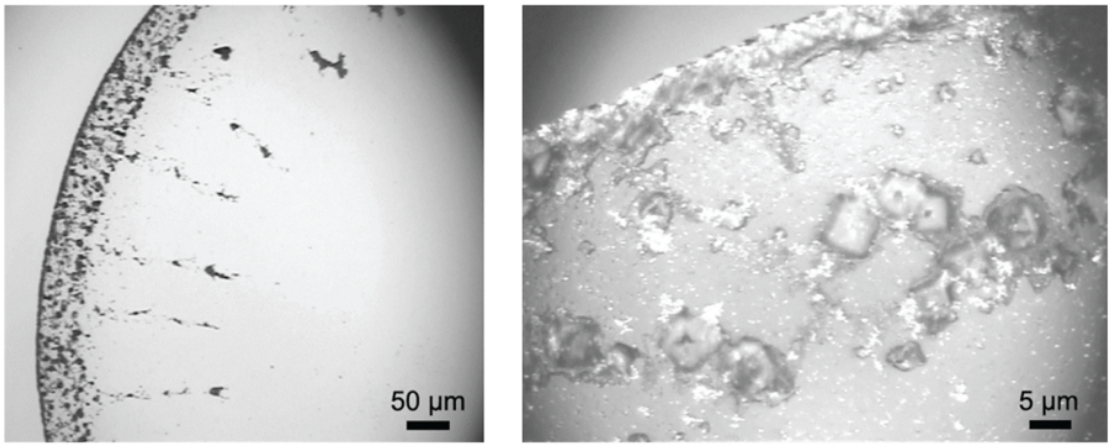

Figure 2 Optical microscope image of a dried Ag colloids: (a) edge part of the drop and (b) detail of the ring[53].

Solid surface-based substrates

Due to the increasing demand for the low level of the limit of detection, SERS applications in food analysis need highly reproducible, sensitive, selective, specific, strongly enhanced, quantitatively improved, and long-term stable SERS substrates to overcome the bottleneck of colloidal nanoparticles. There are already commercial substrates available for simple SERS analysis. However, better performance substrates are normally fabricated by research laboratories. In terms of the solid surface-based substrates, most fabrication protocols focus on the deposition, arrangement, or

modification of nanoparticles to specifically isolate and rapid detect the target on a complex surface. In this section, solid surface-based SERS substrates with different functions, choices of surfaces, and fabrication methods are reviewed.

Commercial SERS substrates

Commercially available substrates such as Klarite™, Ocean Optics SERS substrate, P-SERS, Horiba Scientific SERS substrates, and Q-SERS substrates have been applied in food research to provide consistent measurements with very simple sample preparation (drop analyte suspension to the analyzing area)[7]. It has been reported that commercial SERS substrates have been used in the detection of melamine in standard solution and milk, malachite green in fish fillets, and many pesticides on fruit surfaces. Meanwhile, most commercial SERS substrates are relatively expensive, which prevents their expansion of the universal use in practical cases.

"Hard" and "flexible" SERS substrates

Based on the choice of surface during the fabrication, SERS substrates can be divided into hard and flexible substrates. In the hard substrates, SERS active materials are deposited onto a solid surface such as glass slides and metal films by using self-assembly methods, sputtering methods, layer by layer deposition methods, and Langmuir-Blodgett techniques. In the flexible SERS substrates, SERS active materials are deposited onto surfaces such as tape, filter membrane, paper, and nanofibers, to allow a better application and detection on irregular surfaces[8]. Both hard and flexible SERS substrates include many different fabrication methods and the mechanism and application of them will be detailed elaborated in the later chapters.

Immobilization of nanoparticles on solid surfaces

Immobilization of nanoparticles on a solid support is a way to improve the reproducibility of SERS substrates. These research started from the first report of immobilizing chemically synthesized nanoparticles on an oxide-covered silicon surface[53]. Driven force for the fabrication method of immobilization of nanoparticles on solid surfaces is mostly based on the self-assembly and it can be majorly divided into four detailed fabricating categories: chemical attachment, electrostatic interaction, capillary force, and direct transfer[10].

Chemical attachment of nanoparticles to the surface

This fabrication is based on the decoration of surfaces with bifunctional ligands. One side of the ligand is for fixation to the surface and another side is for absorbing the nanoparticles, as shown in Figure 3. Nathan's group firstly reported the self-assembly fabrication by immersing a thiol or amine modified glass surface into a colloidal nanoparticles suspension for certain periods of time[54]. Four factors have been pointed out despite the choice of glass surface and the nanoparticles, including the concentration of nanoparticles, the choice of functionalized ligand chemicals, the incubation time for fabrication, and the target for analysis. Similar methods were reported such as Au nanoparticles and Au nanorods assembled on quartz slides modified by amine moieties, Ag nanoparticles on silver plate modified by 1, 10-phenanthroline, and immobilization of Ag nanoparticles onto Ag nanowire by using the ligand chemical called 4-aminobenzenthiol[55–58]. Advantages in this fabrication method were suggested to be improved enhance factors, higher reproducibility, and low costs.

Figure 3 Assembly of Au and Ag NPs monolayers. X=CN, NH2, 2-pyridyl, P(C6H5)2, or SH; R=CH3 or CH2CH3, adapted from reference[10].

Based on the similar mechanism, the monolayer structure could be further modified to a multiple-layer-nanoparticles structure by immersing the monolayer substrate (as shown in Figure 3) to a suspension of nanoparticles decorated with bifunctional ligands. According this procedure, layers of nanoparticles can be deposited to the base layer until the optimum performance of SERS is achieved. However, to be noted, the multiple layer deposition may result in the aggregation of nanoparticles and the cluster of nanoparticles can cause the loss of SERS function. This risk pointed out another very important factor in the SERS substrates fabrication, the morphology of the substrate[59,60]. Interestingly, it is also found that the variation is decreasing with the increasing layers of nanoparticle[61].

More complicated fabrication such as immobilizing CATB (i.e., cetyltrimethylammonium bromide) caped nanoparticles to a silicon wafer modified with (3-aminopropyl) trimethoxysilane, 11-mercaptoundecanoic acid (i.e., MUA, a long chain thiol), *N*- hydroxyl succinimide (i.e., NHS), and *N*-(3-dimethylamino- propyl)-*N*''-ethyl carbodiimide hydrochloride (i.e., EDC), can improve the variation to a much lower level as only 5%[62].

Even though such fabrications can achieve superior reproducibility, they are too complex to be apply in food analysis which always require simple procedures.

Electrostatic interaction between nanoparticles and the surface

Some polymers (such as PVP or PDDA) are used as an absorbing agent to self-assembly the nanoparticles onto a metal film surface through the electrostatic interactions. As shown in the Figure 5, poly(vinylpyridine) (i.e., PVP) was firstly used to adhere the silver mirror to a glass slide, to cover it to be a silver film, subsequently was decorated on the surface of the silver mirror to absorb the Ag nanoparticles electrostatically[63].

Nanoparticles on the substrate after fabrication showed a very uniform arrangement. Since the whole procedure of synthesis does not involve the aggregation of nanoparticles (major reason for the variation of SERS), an excellent reproducibility was also reported for the SERS spot-to-spot measurement.

Capillary force as mechanism to form the substrate

Unlike the chemically attachment and electrostatic interaction mechanisms, fabrication of a uniform SERS substrate driven by the capillary force during the evaporation of a nanoparticle droplet is being proposed as another effective method.

According to the literature, an evaporation driven method was proposed by Halas's group. The droplet of gold nanoparticles functionalized with double layer of cetyltrimethyl ammonium bromid (i.e., CATB) was evaporated on a substrate to form a hexagonally packed nanoshell array, which can generate very consistent SERS signals. The CATB in this research not only works as a spacer for each nanoshell to generate extraordinary electromagnetic filed to enhance the SERS signal, but also works as a repulsive agent to prevent the aggregation of nanoshell during the evaporation[64].

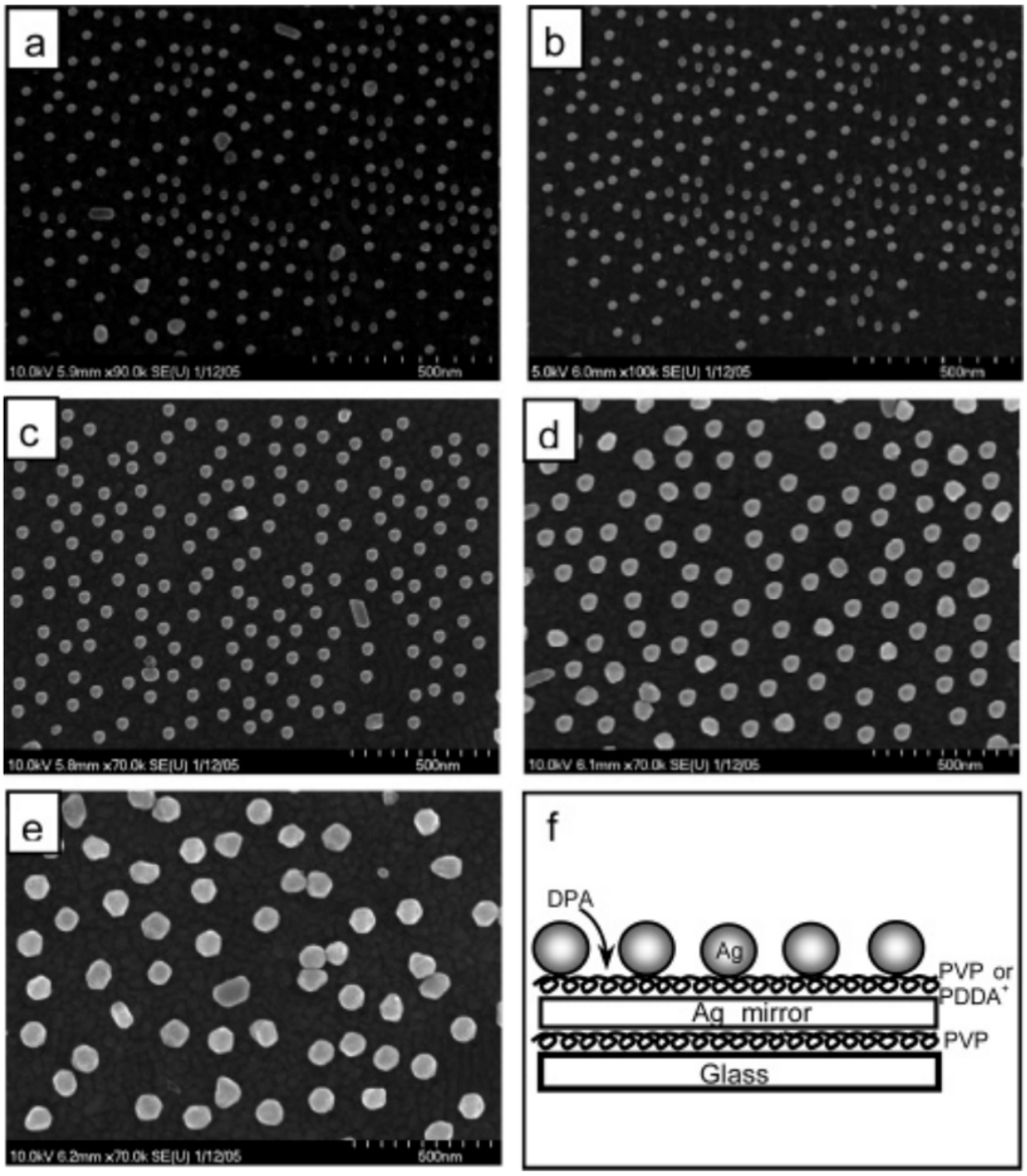

Figure 4 Scanning electronic microscope image of Nanoparticle-Mirror Sandwich Substrates and its fabrication procedure (adapted from reference)[63].

Direct transfer of nanoparticle film to a solid substrate

Another method to immobilize nanoparticles is to transfer a self-assembly monolayer of nanoparticles to a solid substrate, the mechanism is mostly dependent on the Langmuir-Blodgett technique. Nanoparticles monolayers were synthesized at the

interface between water and organic solvents, then a glass slide or a silicon wafer was placed inside the water/solvent/monolayer mixture and gently pulled out vertically. During the process, the monolayer of nanoparticles will hydrophobically bind to the slide/wafer to form a monolayer substrate [65–67]. At the same manner, a monolayer was assembled by silver nanowires using the Langmuir−Blodgett technique[68]. On the other hand, monolayers of gold nanoparticles with different shapes can be assembled by immobilization of nanoparticles sputtered to a 4-mercaptobenzoic acid covered glass slides[69]

After the fabrication, extraordinary SERS reproducibility (i.e., less than 10% relative standard deviation from spot to spot variation) is achieved from all substrates compared to the 50% standard deviation from the aggregated colloidal nanoparticles.

Photosynthesis of nanoparticles on a solid substrate

Nanoparticles can also be grown on a solid surface such as a filter paper or polymer film[42,70]. The photosynthesis can reduce the Ag/Au ions to nanoparticles at certain amount of reacting time and render nanoparticles to grow on a polymer film/wafer. The platform is covered by polymers such as PVP or the semiconductor such as titanium dioxide with nanoparticle seeds to allow a uniform growth of nanoparticles. Additionally, good enhancement factors and reproducibility are reported for both substrates.

Metallic nanostructures fabricated using nanolithography methods

Despite of self-assembly “bottom up” methods, top down methods such as fabricating nanostructures of a solid support are considered as another way to fabricate uniform SERS substrates. The most commonly used method is using the electronic beam

lithography (EBL). As shown in Figure 6, initially, a silicon wafer is etched by EBL in certain depth, then two deposition of the nanoparticles are reported. As the first method, after the removal of resistant area, the nanoparticles are coated onto the etched area through the vapor deposition to form a continuous film substrate; as the second method, the nanoparticles are deposited subsequent with a removal of the resistant to results in a discrete arrangement of nanoparticles on the substrate[71].

Both methods showed good SERS performance such as reproducibility and signal enhancement, and the most important advantage of this method is its capability of accurate controlling of the geometric parameters of the nanostructure which can result in the high uniformity.

Even though above-mentioned methods can fabricate reproducible substrates, the SERS performance has not been challenged with the practical concerns in food samples.

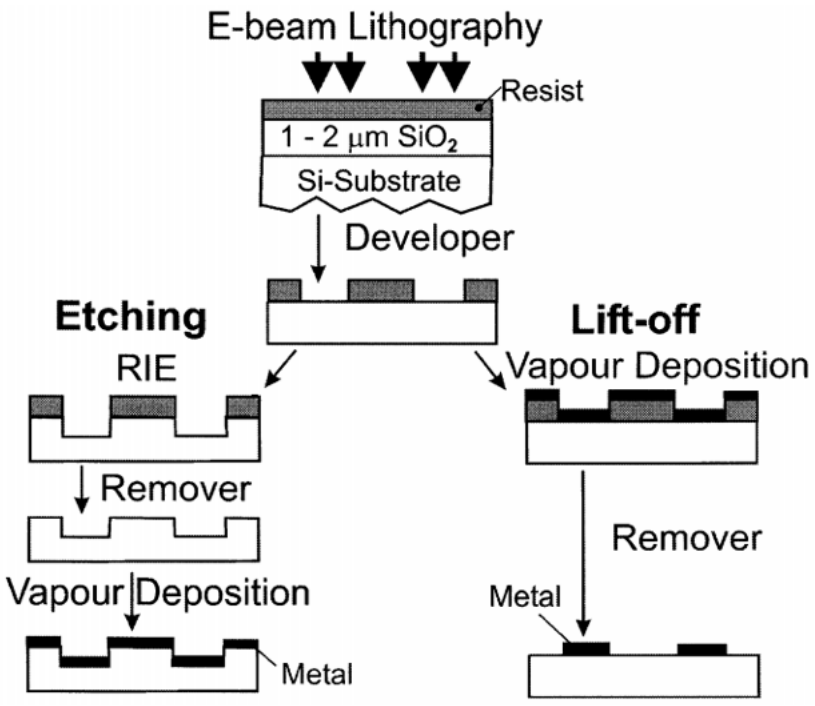

Figure 5 Two methods of substrate fabrication using the electronic beam lithography (adapted from reference)[71].

SERS substrates with microfluidic system

Over the past decade, SERS has been integrated with microfluidic devices to improve the reproducibility of SERS measurement, to provide a platform for more controllable nanostructure substrate fabrication, and to accomplish a real-time and on-site detection of analytes in aqueous food samples[13].

There are two types of microfluidic devices being compatible with SERS detection, the continuous flow platforms and the droplet-based platforms. The integration of SERS substrates with the microfluidic platforms can be divided into three ways, “external injection”, injection of colloidal nanoparticles to microfluidic channels, “ built in”, building solid nanostructures in the microfluidic channels, and “in site fabrication”, in site fabrication of nanostructured substrates in the microfluidic channels[13].

The “external injection” method includes the injecting and mixing colloidal nanoparticles suspension and sample solution in the microfluidic channel and obtaining the SERS signals. Since the colloidal nanoparticles and the sample solution are injected respectively, the degree of mixing could affect the final SERS measurement. However, even though the “external injection” method is very promising for SERS, due to the nature of colloidal nanoparticles, the random aggregation of nanoparticles is still a huge drawback[72]. The external method has been applied in the detection of antibiotics in urine.

To improve the reproducibility, the “built in” method is developed by injecting the sample solution to the microfluidic channel with built in solid nanostructure substrates. Due to more uniform, denser arrangement of nanostructured hotspots, the SERS performance is greatly enhanced. The “built in” method has been applied in the detection of ochratoxin A, melamine in milk, and the dopamine in urine[73,74].

Recently, in site microfluidic fabrication method is becoming much more popular to integrate with SERS due to its better control and more flexibility of precise liquid handling. The mechanism of in situ fabrication of nanostructure substrates is mostly dependent on the galvanic replacement reaction and the reduction of noble metal ions.

For the galvanic replacement reaction, one study deposited Cu-core/C-sheath nanowalls in the microfluidic channel with a subsequent Ag nanoparticle galvanic replacement to in situ form the Ag nanoparticles nanowalls. Due to the dense distribution of Ag nanoparticles, SERS performance was much improved[75]. Another fabrication is based on using silver nitrate to galvanically replace the pre-formed copper block to Ag nanoparticles. The copper blocks are patterned by using lithography, which can precisely

control the size and shape of replaced Ag nanoparticles and provide much more stable SERS performance[76].

For the reduction fabrication, silver nitrate solution was injected to the microfluidic chamber and the femtosecond laser pulse was applied to reduce silver ions to silver nanoparticles. With this method, the size and shape of nanoparticles can be very well controlled, and the deposition of nanoparticles can be flexibly controlled at any locations in the microfluidic channels[77].

Microfluidic methods combined with SERS provided accurately controlled sample preparation including the mixing, concentrating, and trapping, to generate a reproducibly, rapid, label-free, and efficient identification of targets in food matrices[13].

Other silver nanoparticle substrates to improve SERS reproducibility

Other than above-mentioned substrates, other efforts have been done to improve the SERS reproducibility and performance, including sputtering AgNPs to polystyrene spherical beads[78], planting AgNPs on polydopamine pillars[79], arraying silver nanorod on silver film[80], using Ag to shell core Au nanoparticles to provide reliable quantitative abilities in SERS[81] or using Pt, SiO2, Si and Al2O3 to coat core Au nanoparticles to enhance Raman signals[82]. Furthermore, several works suggested that the solvent can also mediate the formation of monolayer of nanoparticles. Previous works found that using an amphiphilic thiol linkage could assemble monolayers of gold nanoparticles at the interface between hexane and water due to the difference of polarity[83], and AuNPs capped with 2,2'-dithiobis[1-(2-bromo-2-methyl-propionyloxy)ethane] (DTBE) formed a monolayer at the interface between water and oil[84]. Moreover, several researches also noticed a monolayer of AuNPs could be spontaneously assembled without any linkages at

the interface between two immiscible solvents, such as water/oil interface[85], or toluene/water interface[86] due to the adsorption of surface charges on AuNPs or the change of contact angle between interface and AuNPs. These works provided a potential of facile fabricated monolayers of nanoparticles, however, only limited choices of organic solvents were demonstrated, and since the mirror was fabricated at the solvents interface, the AuNPs monolayer was hard to collect and transfer. Additionally, the practical applications of these nanoparticles monolayers in SERS have not been studied yet.

Good stability was reported for above substrates while they were also suffering from disadvantages such as complicated fabricating procedures, expensive ingredients, difficult operations, and limited practical applications.

Functionalized SERS substrates

According to the previous chapters, food samples are complex, which makes the direct analysis of targets very challenging for both traditional colloidal substrates and sometimes, even the reproducible self-assembly substrates. Therefore, to improve the selectivity of SERS, functionalized SERS substrates showed a huge potential to repel the interference from the background and to enhance the detection sensitivity of the target[9,87].

Substrates with antibodies

Immunoassay reviewed previously was a unique analytical assay to detect targets selectively based on the antibody-antigen interaction. The use of antibody this is technique can specifically isolate the target antigen from the complex components in a food sample and the interaction between antibody and antigen is very strong and selective[88]. Therefore, the combination of immunoassay with SERS is becoming popular

to achieve very sensitive and selective detection, narrow Raman bands, multiplexed analysis, reduction in analyzing time, and improved limit of detection (LOD) nowadays. Furthermore, due to the ability of immunoassay for detecting molecules with larger molecular weight, SERS-immunoassay based substrates can extend their targets to biomolecules like toxins, proteins, peptides. There are three types of capturing agents in SERS-immunoassay are reported, antibodies, antigens, and the tag molecules (antibody modified nanoparticles with a reporter and antibody modified nanoparticles without reporters) to for the sandwich structure[9].

Two methods were reported to use the immunomagnetic separation kit to capture the foreign protein (i.e., ovalbumin) in milk, and the captured antigen protein was eluted to either mix with Ag nanoparticles or to drop on to a uniform substrate (i.e., Ag dendrite) to acquire the SERS measurement. Both methods were able to obtain good LODs as low as 1 μg/ml ovalbumin in milk. On the other hand, the background interference was also observed in the SERS spectra, which could cause the aggregation of nanoparticles and result in the reduction of SERS signals[36]. Therefore, more complicated fabrication was made to achieve more stable and reproducible results with SERS tag molecules.

The SERS tag molecule fabrication are illustrated in Figure 7 and divided into three steps:

Antibodies are deposited on the solid platforms or the magnetic beads to form the capture agents.

The capture agents are added to food samples to selectively interact with the target antigens.

The nanoparticles decorated with tag/reporter molecules are capped to the antigens absorbed on the capture agents to form a sandwich structure for SERS measurements.

The following washing process will remove the non-specific molecules and to result in an accurate detection without any background interferences. The tag molecules are normally generating very strong and distinctive Raman signals and the successful detection of reporter signal will suggest the detection of presence of antigens. With similar assay, trace levels of cholera toxin and staphylococcal enterotoxin B were successfully detected[78,89].

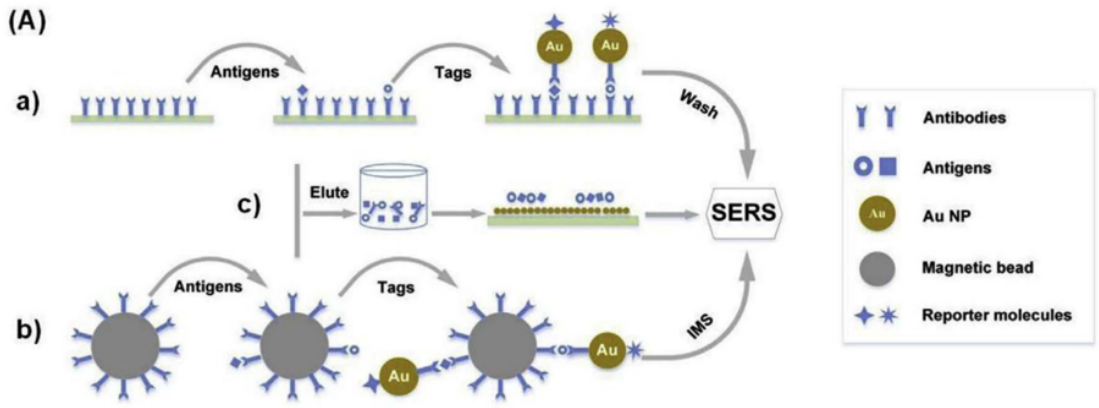

Figure 6 Illustration of three SERS substrates fabricated with tag/reporter molecules (adapted from reference)[9].

Substrates with aptamers

Besides antibodies and antigens, aptamers are recently reported as another capture agent to improve the selectivity of SERS. Aptamers are single-strand nucleic ligands engineered through "systematic evolution of ligands by exponential enrichment" (i.e., SELEX). These aptamers can be bent into a 3D structure to create a specific binding to

the target molecule in complicated food samples to achieve a quick and selective detection of targets.

To make the aptamer SERS sensitive, the aptamer can either be modified with a thiol group to directly bind to the nanoparticles or be labeled with another SERS sensitive group to produce a distinctive signal. SERS-aptamer approach has shown the advantages such as capability of capturing multiple analytes, high level of sensitivities, reliable correlation between Raman intensity with concentrations of targets. The aptamer-SERS approach has been applied in the detection of multiple pesticides in apple juice, toxins in orange juices and milk, pathogens in orange juice, and heavy metals in food samples[90–94].

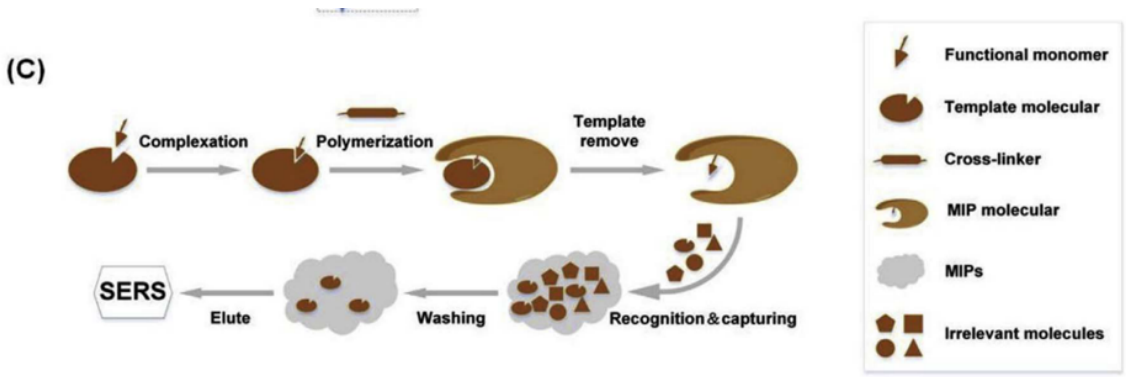

Figure 7 Illustration of SERS substrates with molecular imprinting method (adapted from reference)[9].

One drawback of above-mentioned immunoassay and aptamer methods is reported that the recognition sites of either an antibody or an aptamer, which are both small molecules, are relatively small and may not be sufficient to bind enough target analyte to generate accurate results. Therefore, a molecular imprinting method was proposed to create a specific binding hole in a polymer molecule that can capture sufficient amounts of analytes. As shown in Figure 8, the detection of captured target is following a similar manner to the immunomagnetic separation method, the captured

analytes are eluted from the molecular imprinting polymer and deposited on to a SERS substrate for the analysis.

The molecular imprinting method works as a “lock and key” technique as an artificial antibody can increase the capture efficiency of the target compared to the traditional immunoassay, thus an enhancement of the sensitivity and selectivity for SERS performance[9]. The molecular imprinting method has been applied in the detection of banned artificial colorants in chili powder, histamine in canned tuna, and the assessment of nicotine[95–97].

Application of SERS

Food samples are complex matrices, it is very important to select suitable and functionalized substrates to identify specific targets based on the physical and chemical natures. Additionally, reproducibility, sensitivity, portability, and selectivity are also considered for the practical analysis.

SERS has been proved to be a powerful analytical tool which has broad applications in the assessment of chemical contaminants, pathogenic bacteria, bioactive components, residual pesticides, and banned adulterants. In this section, applications of SERS are detailed reviewed based on the substrates, chemical natures, and the detection limit, according to several published reviews of the SERS and newly reported studies[5,7,100–107,9,10,13,52,78,97–99].

Table 1 shows the current applications of SERS in food analysis, including the analytes, substrates, analytical matrices, and limit of detection. Overall, SERS has been a promising technique for food safety and quality assessment, however, facile fabrication

of substrates, amplification of weak SERS signals, and more practical applications of SERS are still in a huge demand for food industry.

Table 1 Analyte, substrate, limit of detection and food matrices for SERS application in food analysis

Analyte	Substrate	Food matrices	LOD
Food additives			
Benzoic acid	AuNPs colloids	Water solution	-
Phthalic acid	AuNPs colloids	Water solution	-
Sodium benzoate	AgNPs colloids	Water solution	-
Butylated hydroxyanisole	AuNPs colloids	Water solution	10 ppm
Monosodium glutamate	AgNPs colloids	Water solution	10^{-5} M
Iodine	Rh_6G-adsorbed AuNPs colloids	Salt solution	30 ppt
Roxarsone	Silver/Polydimethylsiloxane Nanocomposites	Water solution	-
Acetarsone	Silver/Polydimethylsiloxane Nanocomposites	Water solution	-
4-arsanilic acid	Silver/Polydimethylsiloxane Nanocomposites	Water solution	-
HMB	AgNPs colloids	Potassium chloride solution	-
L-carnitine	AgNPs colloids	Potassium chloride solution	-
Creatine	AgNPs colloids	Potassium chloride solution	-
Vitamin E (α-tocopherol)	Molecular imprinting-SERS	Vegetable oils	-
OVA (egg white protein)	Immunomagnetic separation (IMS) SERS	Milk	1 μg/ml
Melamine	Molecular imprinting SERS	Milk	0.012 mM

Melamine	Aptamer-SERS	Milk	1.0 pg/ml
Melamine	External injection microfluidic AgNPs colloids	-	63 ppb
Melamine	Built in microfluidic AgNPs @ basil-seeds	-	0.68 ppm
Histamine	Molecular imprinting SERS	Canned tuna	3 ppm
Malachite green	External injection microfluidic AgNPs colloid	-	1-2 ppb
	Food colorants		
Sudan-1	AuNPs colloids	Red chili powder	10^{-3}-10^{-4} M
Sudan-1	Molecular imprinting (MIP) thin layer chromatography (TLC) AuNPs colloids	Paprika powder	1 ppm
Azorubine	AuNPs-FON monolayer	Sweet drinks	0.5 ppm
Allura Red AC, Beet Juice Extract, Tartrazine	AuNPs colloids	Water solution	-
Sunset Yellow FCF	AuNPs colloids	Orange Cheddar	-
Brilliant Blue FCF	AuNPs colloids	Candy Cereal	1 ppm
Tartrazine	AgNPs colloids	Water solution	10^{-10} M
Ponceau 4R	AuNPs colloids	Water solution	5 ppm
Sudan II	ZnO/Ag nanoarrays	Ethyl acetate solution	10^{-12} M
Sudan IV	ZnO/Ag nanoarrays	Ethyl acetate solution	10^{-12} M
Methylene blue	SERS activated Ag Electrode	Water solution	-
	Pesticides		
Thiabendazole	Molecular imprinting microextraction SERS	Orange juice	4 ppm
Chlorpyrifos	Molecular imprinting SERS	Apple juice	0.01 ppm
Isocarbophos, Omethoate, Phorate, Profenofos	Aptamer-SERS	Apple juice	1,5,0.1,5 ppm

Thiram, Methyl parathion, Malachite green	AgNPs on the 3D nanotentacle array	Cucumber, Grapes, Apple peels	1.6-10 ng/cm^2
Thiabendazole	Au-glycidyl methacrylate–ethylene dimethacrylate	Apples Potatoes	0.5 mg/kg
Thiabendazole	AuNPs colloids	Spinach leaves	5 ppm
Carnpfuran	In situ fabrication microfluidic AgNPs decorated Cu electrode	-	5 ppb
Malathion	Built-in microfluidic 3D Au nanoarrays	-	1 ppb
Malathion	AgNPs colloids loaded filter membrane	-	62 ppb
Thiram	In situ fabrication microfluidic AgNPs decorated optical fiber tip	-	10^{-8} M
Thiram	Ag coated AuNPs	-	1-7 ng/cm^2
Dimethoate	Metal-doped sol-gel coated capillaries	-	10 ppb
4-Methyl parathion	Metal-doped sol-gel coated capillaries	-	10 ppb
	Toxins		
Ricin B	Aptamer-silver dendrite	Orange juice	50 ppt
Ricin	Aptamer- Silver dendrite	Milk	-
Ochratoxin A	Aptamer-modified Au triangular arrays	-	0.05-4 μM
Mercury (II) ions	External injection microfluidic Aptamer modified Au/Ag core-shell NPs	-	<10 ppm
Mercury (II) ions	External injection microfluidic Rhodamine B modified AuNPs	-	0.1-2 ppb
Aflatoxin B1, Aflatoxin B2, Aflatoxin G1, Aflatoxin G2	Ag nanorod array	-	5×10^{-5} M, 1×10^{-4} M, 5×10^{-6} M, 5×10^{-6} M,
Saxitoxin	AgNPs colloids	-	2×10^{-9} M
	Pathogens		
***Bacillus anthracis* spores**	Aptamer-SERS	Orange juice	10^4 CFU/ml
S. typhimurium	Aptamer-SERS	Pork	4 CFU/ml
E. coli*, *Salmonella*, or *Listeria	AgNPs-Aptamer	Ground beef	10^3 CFU/g

S. aureus*, *E. coli	Polyethylenimine (PEI)-modified AuNPs-coated magnetic substrate	Milk	10^3 CFU/ml
Vibrio parahaemolyticus	Aptamer-SERS	Salmon	14 CFU/ml
8 food-borne pathogens	External injection microfluidic AgNPs colloids	-	-
E. coli	External injection microfluidic AgNPs colloids	-	4.5×10^3 CFU/ml
E. coli	External injection microfluidic AgNPs colloids	-	-
	Antibiotics/Hormones		
Salbutamol	Immunochromatographic test (ICT) SERS	Swine meat	3.0 pg/ml
Brombuterol	Immunochromatographic assay SERS	Swine meat	0.5 pg/ml
Tetracycline	Aptamer SERS	Milk	0.1 ng/ml
Furadantin	AuNPs colloids	-	5 ppm
Enrofloxacin	Klarite™ Au substrate	-	-
Chloramphenicol	Klarite™ Au substrate	-	50 ppb

3. DEVELOPMENT OF A FACILE SOLVENT BASED METHOD TO FABRICATE AGNPS MIRROR FOR IMPROVED SERS QUANTIFICATION

Introduction

Due to its high sensitivity and specificity, surface enhanced Raman scattering (SERS) has been developed and applied as a powerful analytical technique in many areas, such as the detection of food and environmental contaminants, and biological and biomedical sensing.[10,40,108] Colloids-based substrates have been commonly used in SERS because of the ease and low cost of fabrication and application. Nevertheless, low signal reproducibility is often observed from the traditional colloid substrate due to the difficulty in controlling its aggregation process. Many efforts have been made to improve the reproducibility of colloids-based substrates.[45] The shell-isolated approach has successfully improved the signal reproduciblity because the shell can keep the particles from agglomerating.[81,82] Other strategies included assembling NPs into monolayer on a glass slide,[69] assembling hydrophobic thiol capped AgNP or AuNP into monolayer after transferring from water to organic solvents,[83,109] or in the interface of two immiscible solvents with the aid of certain ligand compounds.[68] However, the major disadvantage of these substrates is the involvement of complicated fabrication procedures.

In this work, we demonstrated a facile fabrication of an AgNP mirror substrate, which exhibited high signal reproducibility and sensitivity for SERS applications. The fabrication simply involved commercially available AgNPs and a mediating solvent without the use of any electrical instrument. Different combinations of solvents and

AgNPs were tested for their performance to form the AgNP mirror. The fabricated AgNP mirror was characterized under optical and electron microscopes. Subsequently, a pesticide, fonofos, was tested to determine the limit of detection, quantification capability and signal variation of the mirror substrate as compared to the traditional AgNP aggregates. Finally, the AgNP mirror was applied to quantify trace amount of fonofos in two commercial beverages.

Materials and methods

Chemicals and materials

Silver nanoparticles, 20, 40, 60, 80 nm, 0.02 mg/ml, coated with citrate, PEG, and PVP, were purchased from nanoComposix (San Diego, CA). Fonofos was purchased from Sigma-Aldrich (St. Louis, MO). Hexane, acetonitrile, acetone, ethanol, methanol, dimethyl sulfoxide, cyclohexane, and isooctane were purchased from Fisher Scientific (Fair Lawn, NJ). All chemicals were reagent-grade and used as received. Apple juice and brewed green tea were purchased from grocery stores.

Fabrication of AgNP mirror substrate

A relatively polar (i.e., acetone, acetonitrile, methanol, ethanol, and dimethyl sulfoxide, polarity: 5.1-7.2) organic solvent and a relatively non-polar (i.e., hexane, isooctane, and cyclohexane; polarity: 0.0-0.2) organic solvent were vortexed with a ratio of 1:1. After mixing, non-polar and polar layers were separated (e.g., in hexane and acetonitrile mixture, the volume ratio approximately equals to 43:57). The polar layer was collected and stored as the mediating solvent. Commercial AgNPs were firstly concentrated by centrifugation to 0.2 mg/ml.[111] Then, 50 µl AgNPs was slowly dripping

into 100 µl mediating solvents drop by drop. After about 1 minute, a mirror-like sediment at the bottom was collected then carefully dropped and air dried on a gold coated slide.

Sample preparation for pesticides detection using AgNP mirror substrate and AgNP aggregates

Fonofos of different concentrations (0.01-5 ppm) were prepared in acetonitrile and water mixture (50:50). For mirror substrates, 10 µl of each standard fonofos solution was incubated with 50 µl AgNPs (0.2 mg/ml) for 5 minutes and then gently dripping into 100 µl mediating solvent drop by drop. After incubating for 1 minute, the mirror-like sediment at the bottom was collected then carefully dropped and air dried on a gold coated slide. In addition, fonofos (0.5 ppm) was spiked into commercial apple juice and brewed green tea and detected using the mirror substrates. For detection using AgNP aggregates, 10 µl of each standard fonofos solution was incubated with 50 µl AgNPs (0.2 mg/ml) for 5 minutes. Then 10 µl was dripping on a gold slide and air-dried for Raman measurement.

Instrumentation

The surface morphology of AgNP aggregated substrate and AgNP mirror substrate were characterized by using a FEI Magellan 400 scanning electron microscope (SEM, Hillsboro, OR) with the voltage of 5.0 kV. The SERS measurements were performed using a Thermo Scientific DXR Raman Spectro-microscope with a 780 nm Laser source under the following conditions: 10× objective, 3.1 µm spot diameter, 5 mW laser power, 2s exposure time and 50 µm slit width for fonofos detection. Both AgNP aggregates and AgNP mirror were measured via a selecting mode and a mapping mode.

For the selecting mode, 10-20 spots were randomly selected for each sample on the AgNP aggregates (ring area) and the AgNP mirror substrates, respectively. Under the mapping mode, a 150 μm × 150 μm area containing 81 scanning spots was randomly selected on the AgNP aggregates (ring area) and the AgNP mirror substrate.

Results and discussion

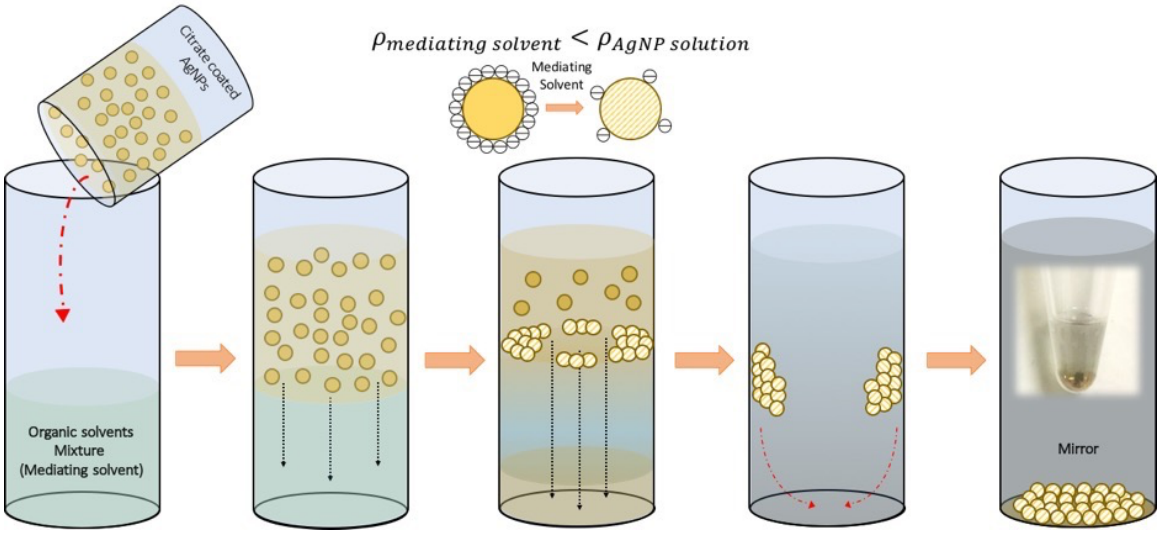

Figure 8 Schematic illustration of steps taken to fabricate the substrates of silver nanoparticles mirror mediated by hexane and acetonitrile mixture.

The fabrication of AgNP mirror substrates is illustrated in Figure 8. The key component in this fabrication is the mediating solvent. The mediating solvent was taken from the polar layer after mixing two immiscible organic solvents. In this polar layer, there were still some parts of non-polar solvents since the immiscible system shares some degree of mutual solubility.[110] We firstly tested the hexane/acetonitrile mediating solvent which contained approximately 7 parts of hexane and 50 parts of acetonitrile. When dropwise adding 0.2 mg/ml citrate coated AgNP solution to the mediating solvent, a blurred interface was observed instantly. At the interface, several small AgNP mirror fractions formed almost immediately. The interface eventually disappeared and AgNP

mirror fractions settled down to the bottom along the wall of the tube, then they were easily taken out by a pipette and deposited on a surface. The whole procedure took approximate 2 min without the use of any electrical instrument.

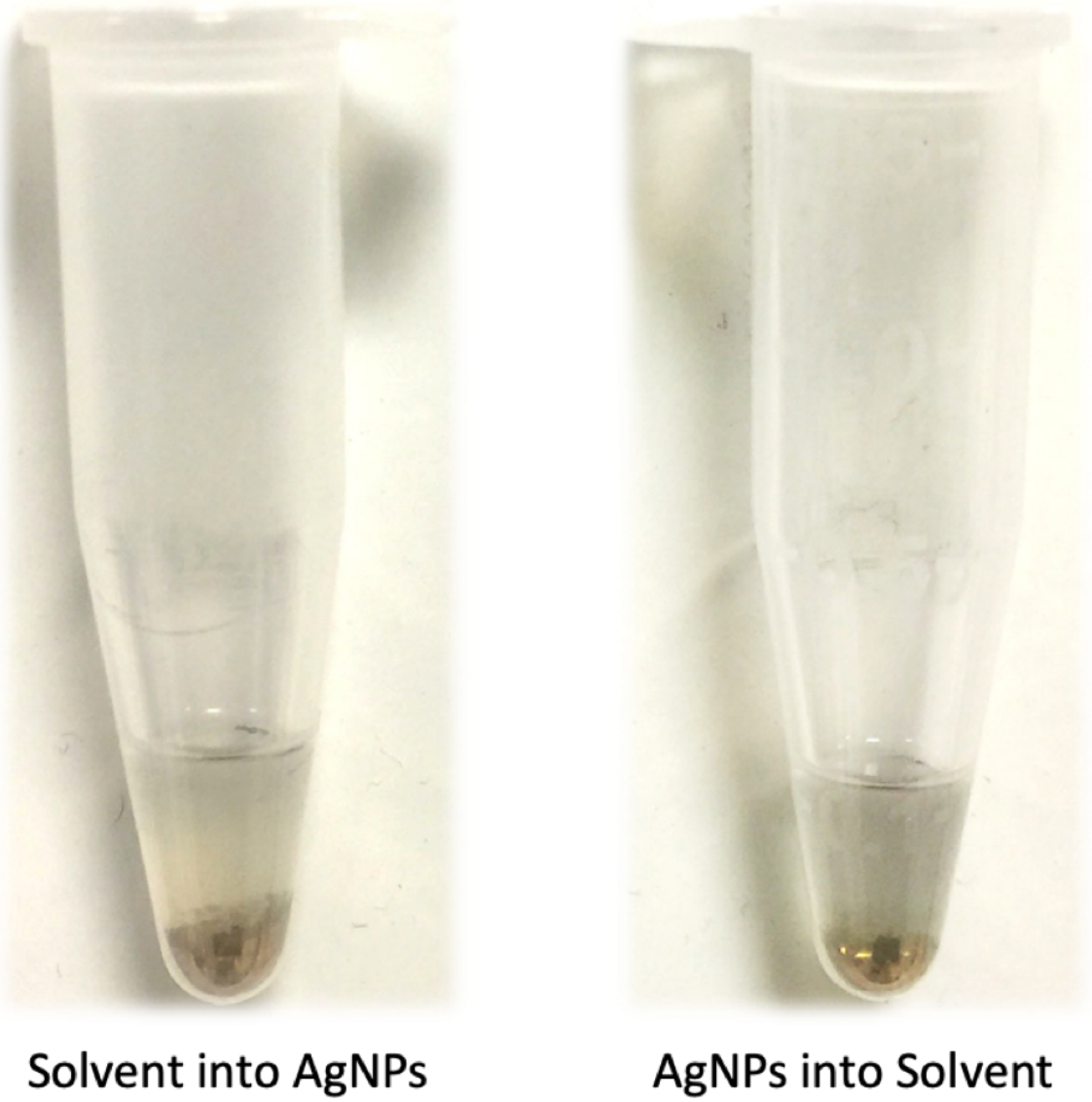

Figure 9 AgNPs mirror formation with different solvent deposition, mediating solvent to AgNPs suspension (on the left) and AgNPs suspension to mediating solvent (on the right).

The reason of forming AgNP mirror can be explained as follows. Due to the higher density than organic solvents, AgNP solution tended to fall through the mediating

solvent phase to the bottom during the addition. Even though the polar fraction of the mediating solvent (i.e. acetonitrile) is miscible with AgNP solution which means they would form a homogenous system quickly, the small fraction of non-polar solvent (i.e., hexane) slightly reduced the environmental polarity of the system and slowed it down from approaching the homogenous equilibrium. Therefore, a blurred and temporary interface was observed when the AgNP layer and the mediating solvent layer encountered. The mediating solvent was continuously upward diffusing to the aqueous phase slowly against the gravity that pulling the AgNP downward. This retained the AgNP and the counteracting forces pressed them into a thin layer at the interface. At the same time, acetonitrile may reduce the surface charges density of citrate coated AgNP and increase their surface tension, which could lead the AgNP form self-assembled monolayer.[85,86] This thin layer looked as a mirror as we can clearly see things reflected from the AgNP layer, that is why we named it AgNP mirror. Duan et al. reported self-assembled AuNP monolayer maintained at the water/toluene interface.[84] However, our system still favored to be homogenous, thus the interface eventually disappeared when polar solvents were completely miscible with water. Subsequently, the AgNP mirror lost the supporting platform and settled to the bottom due to the gravity. The sedimentation step gives more advantages for application, as we can easily take out the AgNP mirror using a pipette and deposited them onto another solid support (e.g. a slide).

Additionally, as shown in Figure 8, two different orders of the solvent deposition were investigated to determine the best AgNPs mirror fabrication protocol. According to the observation, the AgNPs mirror formed by depositing AgNPs to the mediating solvent (on the right) showed much more shinny than the left. This phenomenon was presumably

because of the disparity of the density between mediating solvent (i.e., approximate 0.8 g/ml) and the AgNPs suspension (i.e., approximate 1 g/ml). Due to the higher density, with the help of gravity, AgNPs suspension passed through the mediating solvent, which promoted a better interaction (i.e., surface charge quenching) between solvent and the surface charges on AgNPs and resulted in a better formation of the mirror. However, depositing in a reverse way, the mediating solvent tended to float on the top of the AgNPs suspension, which could cause insufficient surface charge removal in AgNPs and leaded to a bad formation of AgNPs mirror.

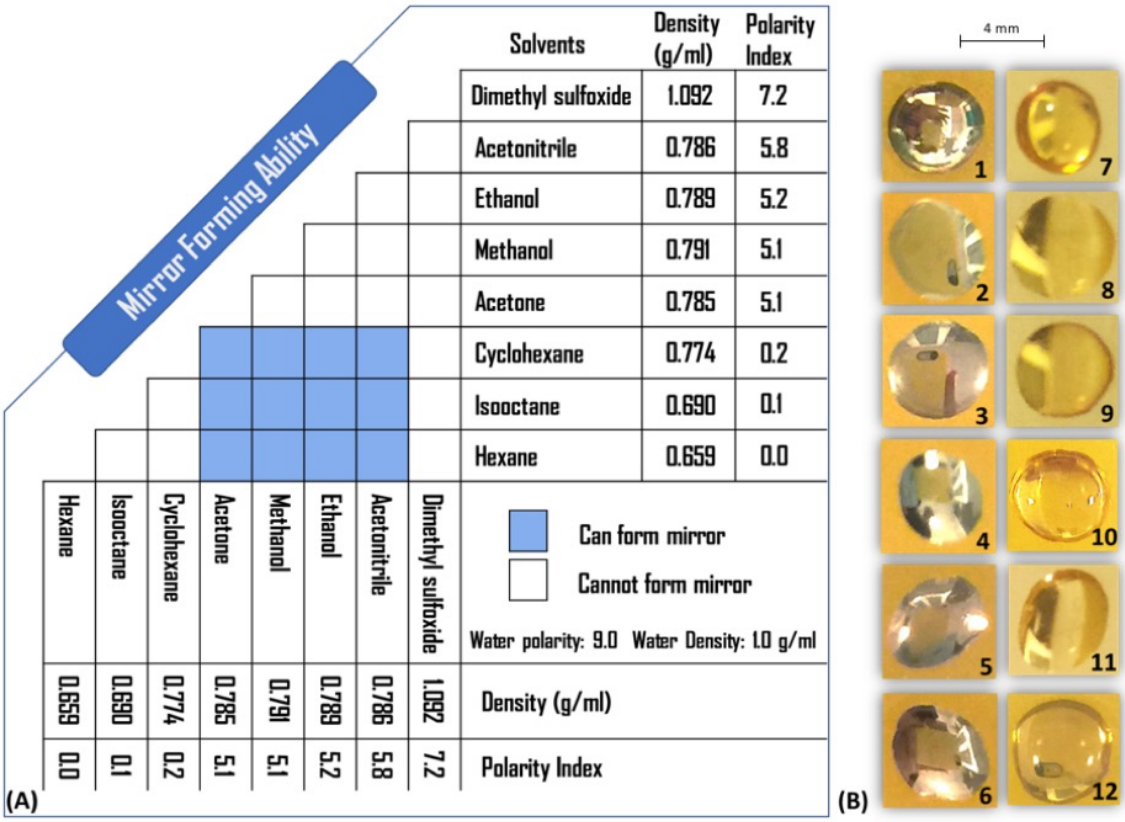

Figure 10 (A) Ability of mirror formation mediated by varied combinations of organic solvents with displayed polarity. (B) Macroscopic images of silver nanoparticles mirror formed by varied combinations of organic solvents: 1. Hexane/acetonitrile, citrate coating 2. Hexane/ethanol, citrate coating 3. Hexane/methanol, citrate coating 4. Hexane/acetonitrile, citrate coating 5. Cyclohexane/acetonitrile, citrate coating 6. Isooctane/acetonitrile, citrate coating 7. Hexane, citrate coating 8. Ethanol, citrate coating 9. Acetonitrile, citrate coating 10.

Hexane/Dimethyl sulfoxide (DMSO), citrate coating 11. Hexane/acetonitrile, PEG coating, 12. Hexane/acetonitrile, PVP coating.

Besides acetonitrile and hexane, other different combinations of polar and non-polar organic solvents and their AgNP mirror forming ability were investigated. Figure 10(A) showed only the mediating solvents constituted by a low polarity (i.e., 0-0.2) and a high polarity (i.e., 5.1-5.8) organic solvent can successfully fabricate AgNP mirror (Figure 10(B) 1-6). However, only hexane, acetonitrile or ethanol was not able to form mirror as shown in Figure 10(B) 7-9. Additionally, Figure 3(B) 10 showed hexane combined with DMSO failed to assemble AgNP into monolayers because the DMSO has a higher density (i.e., 1.092 g/ml) than water, thus could not spontaneously move downward to press the AgNP into a mirror. This phenomenon highlights the importance of density for the mirror formation. In addition, we tested other two commercial AgNP coated with PEG and PVP. They failed for forming AgNP mirror due to the steric repulsion and the low surface tension (Figure 10(B) 11 and 12). Summarizing the above findings, three factors are important to determine the successful fabrication of the AgNP mirror substrate. The first one is the lighter density of the solvents as compared to the water, so that the solvents can move upward into the AgNP solution to create a counteracting force against the gravity for AgNP. The second factor is the different polarity of these two solvents with the large component to be polar and the minor component to be non-polar in the system. The small non-polar component was used for slowing down the mixing equilibrium which produces a temporary interface for retaining AgNP and facilitated the physical pressure. As the polar component was dominant in the system, the equilibrium can be reached eventually, so that the formed monolayer can be settled down in the bottom for the ease of collection. The third factor is the surface

chemistry of AgNP. AgNP stabilized with electric repulsion (e.g., citrate coating) can be reduced easily to increase its surface tension, while AgNP with steric repulsion (e.g., PVP or PEG coating) has no surface charge and low surface tension cannot form a mirror.

In addition, different sizes (20, 40, 60, 80 nm) of citrate coated AgNP were tested and all of them showed the ability of mirror formation (Figure 5). After the comparison, all four AgNPs mirrors with different sizes of nanoparticles showed very good sensitivity, along with very consistent data presentation. In Figure 12 (B), intensity at 1571 cm^{-1} was shown for four AgNPs mirrors. Size of 40 nm and 60 nm AgNPs showed the best SERS performance in terms of the Raman scattering intensity. This finding is following a similar manner to what was reported in the previous work, 40 or 60 nm, citrate coated AgNP showed the best performance in SERS detections.[111] Therefore, citrate coated 40 nm AgNP were used to fabricate the mirror substrates for the subsequent analysis.

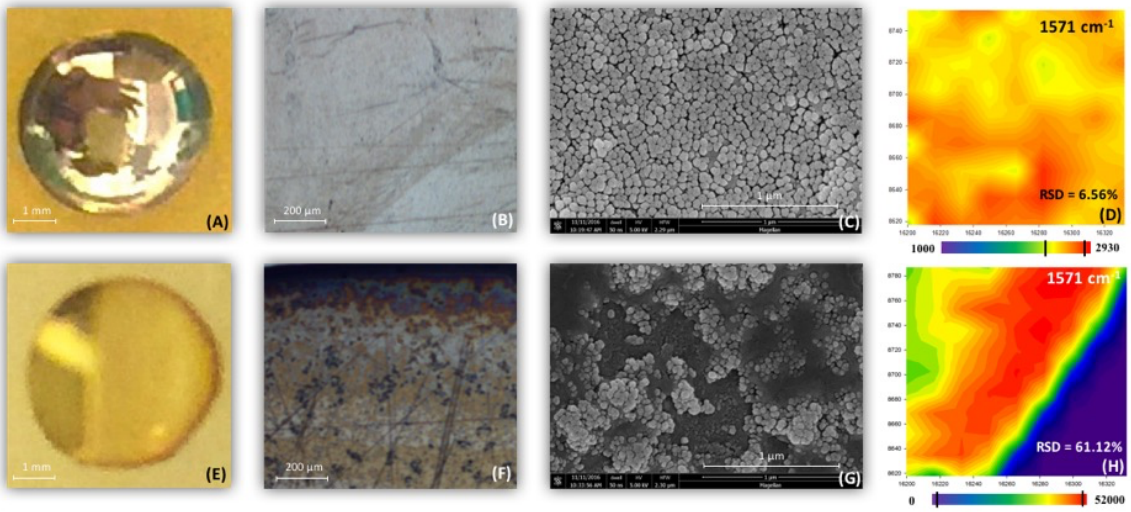

Figure 11 (A) Macroscopic; (B) Optical microscopic; (C) Scanning electron microscopic image; (D) 5 ppm fonofos SERS mapping of AgNP mirror substrates; (E) Macroscopic; (F) Optical microscopic; (G) Scanning electron microscopic; (H) 5

ppm fonofos SERS mapping of A AgNP aggregate substrates (Peak intensity at 1571 cm-1 was selected for mapping measurement and relative standard deviation calculation).

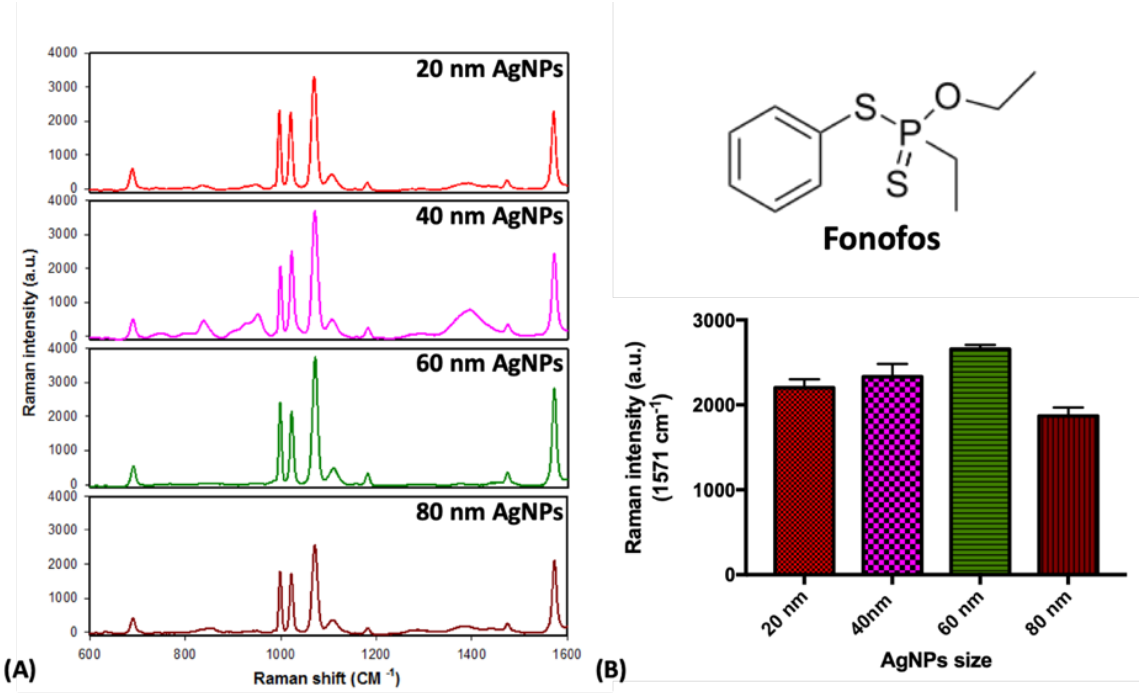

Figure 12 (A) SERS spectra of 5 ppm of fonofos in standard solution obtained with AgNPs mirror formed with different size of nanoparticles (20 nm, 40 nm, 60 nm, and 80 nm). (B) The peak intensity at 1571 cm-1 Raman shift for four sizes of nanoparticles.

The morphologic characterization of the AgNP mirror was showed in Figure 4, the traditional substrate (i.e., AgNP aggregates) was displayed as a comparison. After depositing on the gold slide, the thin monolayer of AgNP was observed as a mirror while the traditional substrate was observed as a drop of clear AgNP solution. After dried, the AgNP mirror and the traditional substrate showed different visual appearances under the optical microscope. Under the optical microscope, the AgNP mirror has no noticeable edge line as compared to the coffee ring formed by the AgNP aggregates. More clear and detailed morphological differences between the AgNP mirror and the traditional substrate were found in the scanning electron microscopic analysis. In Figure 11(C), AgNP

presented the oriented arrangement in a monolayer, however, in Figure 11(G), AgNP aggregated strongly and stacked into multilayers. Additional benefit for the applying the mirror substrates in real analysis is the versatile sample preparation approach, that is, analyte can be directly involved in the solution for the mirror formation or dropped on the air-dried AgNP mirrors. The first approach that involves analyte directly in the mirror formation allows relative more sample volume than the second approach which only puts a few droplets on the dried mirror. In addition, the first approach is most suitable for detecting the target analyte which have strong interaction with the NPs, especially in a mixture. This is because of the dynamic competition between the target analyte with other matrix molecules for the interaction with the NPs during mirror formation. The target analyte with a stronger interaction can be selectively enriched by the mirror. For the second approach, all the molecules are physical put on the mirror surface, therefore, there is no dynamic competition. As a comparison, traditional AgNP colloids are only limited to the solvent interaction method as most of the air-dried colloids were aggregated into the coffee rings.

The morphology of AgNP mirror was further investigated by using the SERS mapping technique. The AgNP mirror and the traditional AgNP substrate were incubated with 5 ppm fonofos and 81 spots were selected for mapping measurements. In Figure 11(D) and Figure 11(H), mapping results of AgNP mirror and AgNP aggregates were showed respectively, and the relative standard deviation (RSD) were calculated to evaluate their uniformity. Low RSD was showed from the mirror substrate (i.e., RSD = 6.27%), because of the uniformity of the AgNP mirror. However, a much higher RSD was observed in the traditional substrate (i.e., RSD = 61.12%). Thus, the results further

suggested that the AgNP mirror substrate can provide much more reliable and reproducible performance in SERS detection than the traditional substrate. To confirm the reproducibility, 25 spectra randomly collected spots on the AgNPs mirror with 5 ppm fonofos were showed in Figure 13 (A). Most spectra presented in a very consistent manner and in Figure 13 (C), another SERS mapping of the intensity at 1024 cm^{-1} Raman shift was conducted to further validate the reproducibility (i.e., low relative standard deviation). In Figure 13 (B), standard deviations for data collected from AgNPs mirror, coffee ring area in the AgNPs aggregate, and the overall area of the AgNPs were presented and it also suggested the AgNPs mirror showed the best consistency.

In addition, as shown in Figure 11(H), strong Raman intensities were only obtained from the coffee ring area, which pointed out another disadvantage of the AgNP aggregates substrate, high dependency on using microscope to choose the spots on a coffee ring. In contrast, high consistency of AgNP mirror make it possible to be used by a portable or handled Raman spectrometers, which usually do not have a microscope to facilitate the measurement on specific locations.

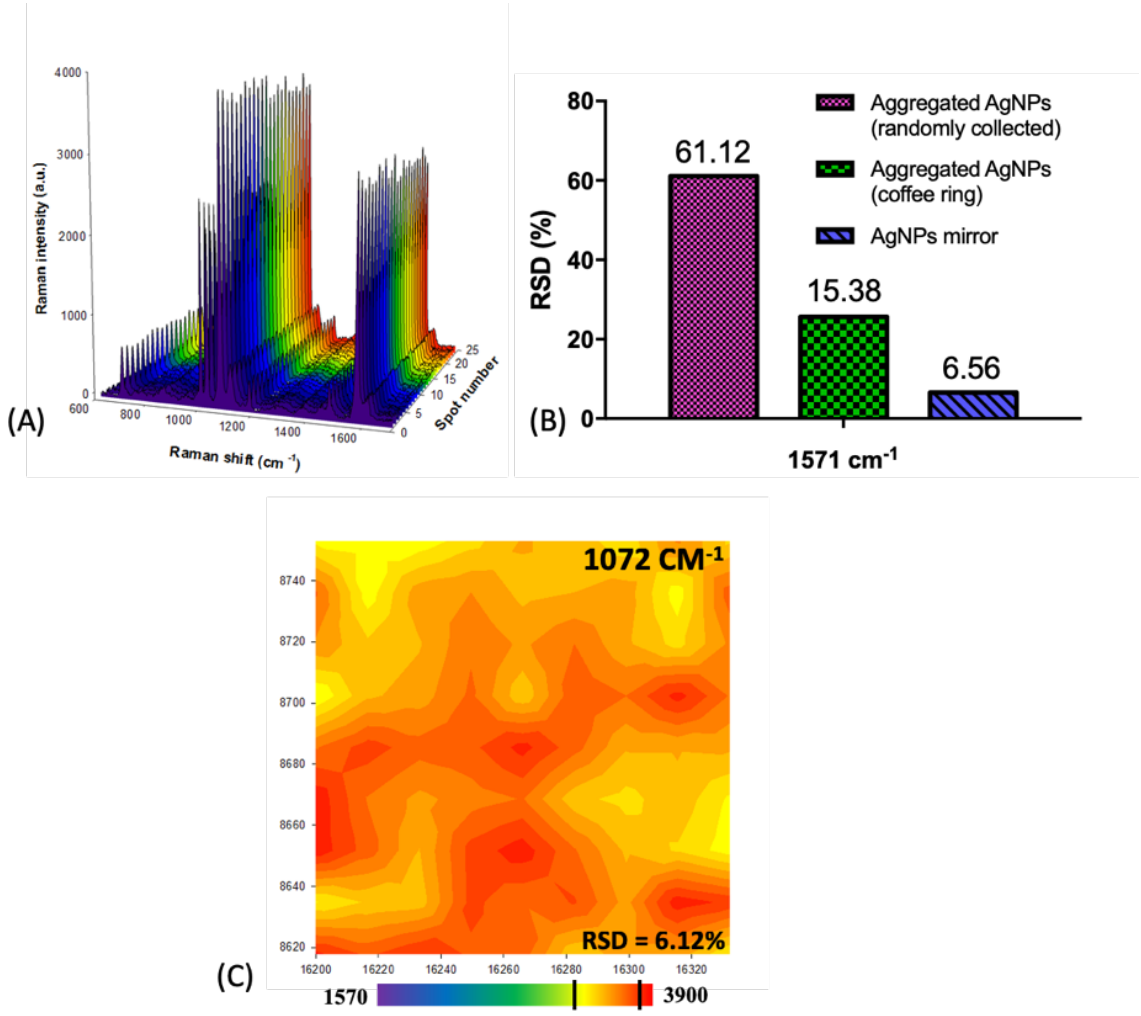

Figure 13 (A) 25 spots randomly collected on AgNPs mirror for Raman intensity of 5 ppm fonofos in standard solution (B) Relative standard deviation for data randomly collected from AgNPs mirror, AgNPs aggregates (on the coffee ring area), and AgNPs aggregates. (C) SERS mapping of 5 ppm fonofos (intensity at Raman peak 1072 cm^{-1}).

Conclusion

In summary, we have successfully fabricated an AgNP mirror sensing substrate using a facile mediation of two organic solvents. The comparison of AgNP mirror to AgNP aggregates was summarized in Table 2. The AgNP mirror substrate provided an improved SERS performance in sensitivity and reproducibility, compared to AgNP aggregates due to the uniformity of the structure.

It offers two breakthroughs for current SERS substrate fabrications,

- Great control of deposition of nanoparticles on the solid platform and reproducible measurements.
- Facile and simple fabrication for self-assembly nanoparticles monolayer substrate.

This nanoscale mirror sensing substrate is also more convenient, versatile and practical to be used under a variety of experimental conditions. Future study will include the quantification evaluation and potential explorations of the application of this substrate for SERS analysis in more real-world samples using a portable or handheld Raman spectrometer.

Table 2 Comparison of AgNP mirror and traditional AgNP aggregates substrate in sensitivity, quantification, variation, ease of performance and versatility.

	AgNP mirror	AgNP aggregates
Variation (average RSD%)	7.30%	33.00%
Ease of performance	1) Form AgNP mirror directly in analyte contained sample or drop analyte on pre-formed AgNP mirror	1) Mix the analyte with AgNP colloids and then deposit on a slide
Versatility	1) No microscope required, potentially compatible with a portable Raman system 2) Portable and facile	1) Highly dependent of microscope for consistency

Acknowledgments

The authors gratefully acknowledge the valuable support from National Institute of Food and Agriculture-USDA and Department of Food Science, University of Massachusetts, Amherst. The research leading to these results are funded by USDA-

NIFA 2015-67021-22993, 2015-67017-23070, 2016-67017-24458, and USDA-NIFA hatch MAS00491.

4. DETERMINATION OF THE REPRODUCIBILITY AND QUANTITATIVE ABILITY OF THE MIRROR SUBSTRATE AND ITS PERFORMANCE IN DETECTION OF PESTICIDES IN WATER AND BEVERAGES

Introduction

Even though SERS has been widely used in food analysis, due to the uncontrollable aggregation of nanoparticles, large variations were preventing the expanding of SERS in more practical applications[9]. Additionally, due to the same reason, SERS cannot be applied as a reliable quantitative tool in food analysis. Therefore, reproducible SERS substrates is in a huge demand by the industry.

Currently, many efforts have been dedicated to developing the uniform substrates by self-assembly the nanoparticles to a monolayer film to contribute very consistent SERS signals. Many uniform SERS substrates have been reviewed in the previous sections, one huge drawback is that most substrates were only tested with SERS sensitive probes in standard solutions, the practical applications of these uniform substrates in complicated food matrices were rarely investigated.

In Chapter 3, a uniform AgNPs mirror substrate was developed with a facile solvent driven fabrication. Results also suggested an extraordinary improvement of the SERS data reproducibility. As hypothesized, a better reproducibility can result in an improved quantitative ability of the substrate, therefore, in this project, the quantitative ability of the AgNPs mirror substrate will be explored. Furthermore, the reliability of AgNPs mirror in pesticides detection in the practical aqueous food samples such as green tea and apple juice will also be investigated. Due to the disparity of the morphology of

AgNPs mirror and colloidal nanoparticles, different sample deposition/sample preparation approaches will also be illustrated.

Material and methods

Materials and chemicals

All materials and chemicals are same as the Chapter 3. Apple juice and green tea are bought from the grocery store.

Sample preparation for pesticides detection in commercial samples using AgNP mirror substrate and AgNP aggregates

For the calibration curve, fonofos of different concentrations (0.01-5 ppm) were prepared in acetonitrile and water mixture (50:50). For mirror substrates, 10 μl of each standard fonofos solution was incubated with 50 μl AgNPs (0.2 mg/ml) for 5 minutes and then gently dripping into 100 μl mediating solvent drop by drop. After incubating for 1 minute, the mirror-like sediment at the bottom was collected then carefully dropped and air dried on a gold coated slide. For the commercial sample testing, 0.5 ppm fonofos was spiked in both commercial apple juice and green tea samples. 10 μl of each spiked apple juice or green tea was incubated with 50 μl AgNPs (0.2 mg/ml) for 5 minutes and then gently dripped into 100 μl mediating solvent drop by drop. After incubating for 1 minute, the mirror-like sediment at the bottom was collected then carefully dropped and air dried on a gold coated slide for SERS measurement. For SERS detection using AgNP aggregates, 10 μl of each standard fonofos solution was incubated with 50 μl AgNPs (0.2 mg/ml) for 5 minutes. Then 10 μl was dripping on a gold slide and air-dried for Raman measurement.

Quantitative and statistical analysis

In this study, all samples were measured within a range of 900-1600 cm^{-1}. The Raman spectra were analyzed using Thermo Scientific TQ Analyst 8.0 software. All Raman intensities were averaged from at least three replicates and standard deviations were recorded. The peak at 1571 cm^{-1} was chosen for further characteristic analysis due to its least interference with the AgNP background. The averaged Raman intensities (i.e., the height of the peak at 1571 cm^{-1}) was plotted as a function of additive fonofos concentrations and then fitted into the linear regression analysis. The coefficient of determination (i.e., R^2) and the trend line equation were analyzed and obtained by Prism 7.0 software. The estimated limit of detection (LOD) was determined based on the following equation,[112]

$$LOD = \frac{3.3 \times \sigma}{b}$$

where σ refers to the standard deviation of blank and b refers to the slope of trend line equations. σ was calculated based on Raman intensity of 10-20 spots randomly collected from AgNP aggregates and AgNP mirror.

The reproducibility of signals from both AgNP aggregates and AgNP mirror substrates were calculated as the relative standard deviation (RSD, i.e., the coefficient of variance).

$$RSD\% = (\frac{sd}{mean}) \times 100$$

where sd and mean refer to the standard deviation and the average of Raman intensity, respectively, obtained from the AgNP mirror and the AgNP aggregates.

The percentage recovery value (RV) was calculated according to the following equation,

$$RV\% = (\frac{[fonofos]_{calculated}}{[fonofos]_{normalized}}) \times 100$$

where $[Fonofos]_{calculated}$ refers to the concentration of fonofos based on the linear regression equation, $[fonofos]_{normalized}$ refers to the actual concentration of used fonofos in sample.

Results and discussion

To investigate the SERS performance on the AgNP mirror as compared to the aggregated AgNP, a pesticide, fonofos was introduced to test the sensitivity and quantitative ability. SERS spectra of fonofos with varied concentrations (0 – 5 ppm) produced from AgNP mirror were shown In Figure 14(A). The intensity of peak at 1571 cm^{-1} was plotted as a function of fonofos concentration for AgNP mirror and AgNP aggregation respectively in Figure 14(B) and 14(C). In terms of peak intensity, the traditional substrate provided a higher Raman intensity than that in the mirror substrate corresponding to the same fonofos concentration. However, due to the large variation for each of the concentration, weak quantitative ability (i.e., R^2=0.9801) was obtained and the calculated LOD was 0.0123 ppm (the standard deviation of blank traditional substrate was 26.63, RSD was 57.41%). On the other hand, the SERS measurements came out very consistently with relatively small error bars. After the linear regression analysis, coefficient of determination (R^2) was indicated as 0.9981, which revealed the much more reliable quantitative ability of AgNP mirror substrate to the traditional substrates. Additionally, according to the linear regression equation, the estimated LOD of AgNP mirror was calculated as low as 0.0081 ppm (the standard deviation of blank mirror substrate was 1.32, RSD was 6.27%), which represents another enhancement of the sensitivity compared to the traditional substrate. Moreover, compared to the previously reported LOD of fonofos (e.g., 0.1 ppm in SERS),[113] our mirror substrate also provided a huge improvement in terms of the detecting sensitivity.

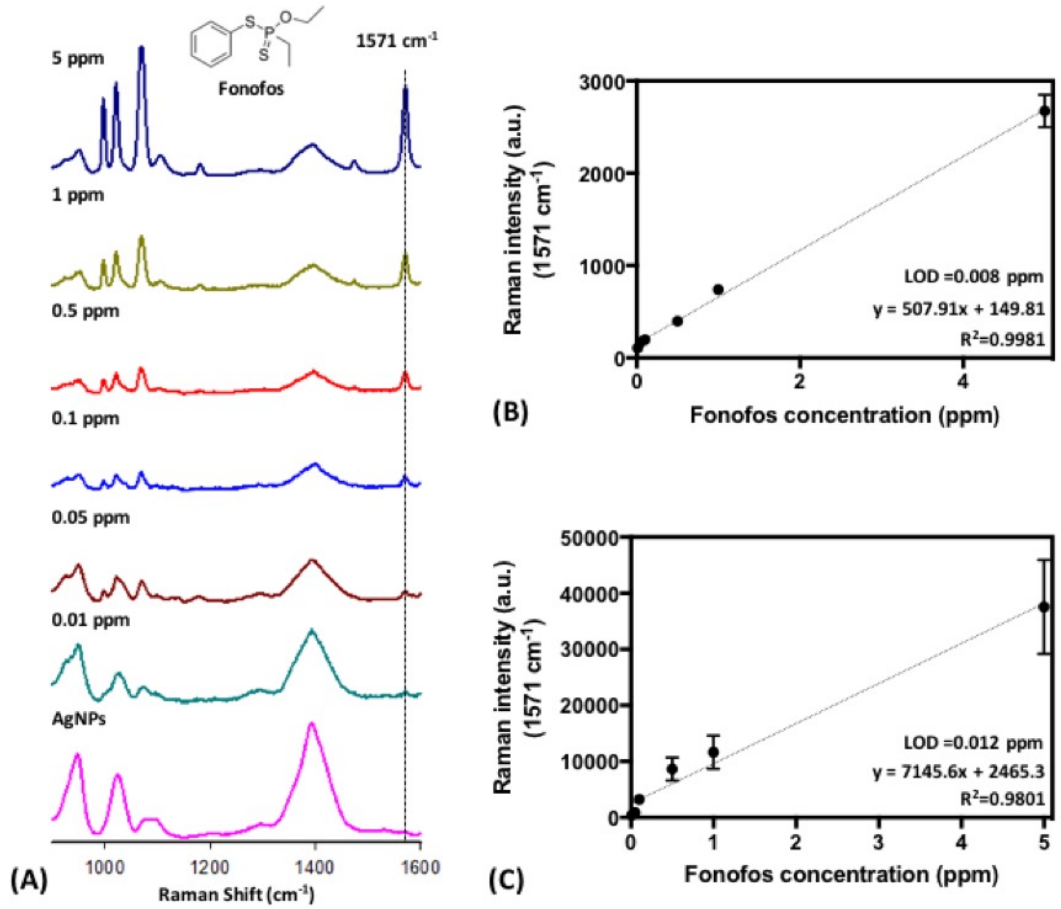

Figure 14 (A) SERS spectra obtained from different concentrations of pure fonofos; Plot of Raman intensity (area under curve) at 1571 cm-1 detected via (B) AgNP mirror substrate and (C) AgNP aggregates as a function of concentration of fonofos. Linear regressions are applied, R-squares and estimated limit of detection are displayed.

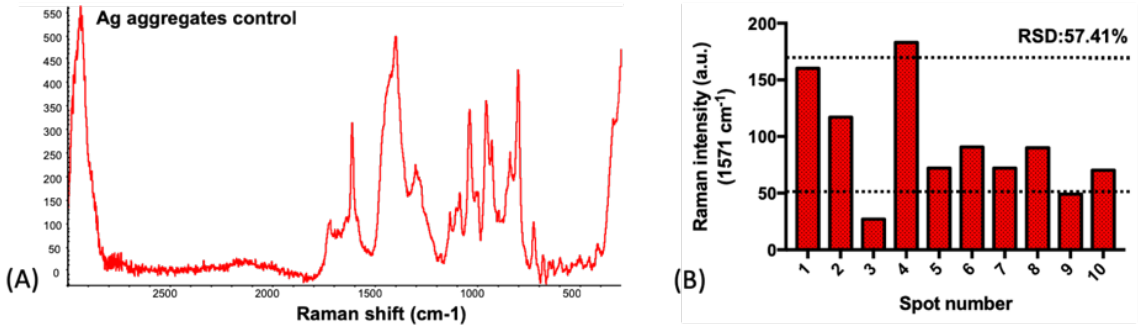

Figure 15 (A) SERS spectra of AgNPs aggregate blank (B) 10 spots randomly collected on the AgNPs aggregate (coffee ring area).

Table 3 Precision of SERS measurements for traditional AgNP aggregates substrate and AgNP mirror substrate (n=20).

Fonofos Concentration *(ppm)*	RSD% （AgNP aggregates）	RSD% （AgNP MIRROR）
5.00	22.35	6.56
1.00	25.63	1.93
0.50	23.98	8.73
0.10	26.20	8.97
0.05	41.06	8.97
0.01	34.38	8.60
0.00	57.41	6.27

Table 3 showed the relative standard deviation (RSD%) of SERS intensity at 1571 cm^{-1} for 0.01-5 ppm fonofos and blanks from AgNP mirror and AgNP aggregates. It is clear that AgNP aggregates showed larger variations even just at the coffee ring area (i.e., RSD ranged from 22.35% to 57.41%). On the other hand, due to the uniform surface, the measurements showed very consistent tendency with low relative standard deviation (i.e., 1.93%-8.97%) which revealed the high reproducibility of AgNP mirror.

According to the literature review, the variation from the AgNPs aggregate is mostly caused by the nature of inconsistent aggregation of colloidal nanoparticles. As shown in Figure 15, 10 spots were randomly collected from the AgNPs aggregates (without any pesticides) on the coffee ring area, and high relative standard deviation also confirmed that large variations from the background.

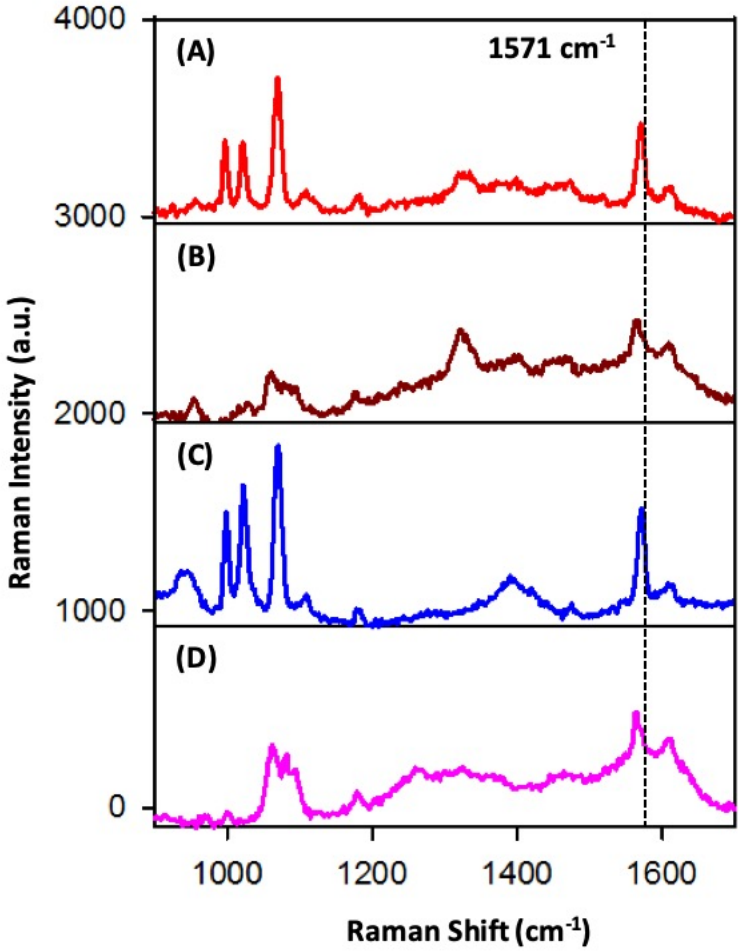

Figure 16 Typical Raman spectra of (A) commercial apple juice and (C) green tea incubated with 0.5 ppm fonofos, Raman spectra of (B) blank apple juice and (D) blank green tea were displayed as control.

After the analytical performance tests of the AgNP mirror, the potential of AgNP mirror for fonofos detection in real food products were investigated. Two commercial food products (apple juice and green tea) were spiked with 0.5 ppm fonofos and then tested with AgNP mirrors. Regardless of the peaks contributed by the background, positive and high-resolution results were found in both products, which suggest the excellent capability of AgNP mirror in real-product pesticides screening (Figure 16). In Table 2, percentage recovery value (RV%) was calculated to be 98.42%-113.63% in

apple juice and 102.18%-107.94% in green tea, demonstrating the high accuracy for the quantification. It suggested the AgNP mirror can be used as a reliable SERS substrate for real applications.

In the literature review section, one drawback of the colloidal AgNPs suspension is that can be only mixed and applied in aqueous sample. Due the disparity of morphology of AgNPs mirrors (solid uniform monolayer film) and colloidal nanoparticles (liquid suspension), the AgNPs mirror shows a much broader application for sample deposition. The AgNPs mirror not only can be *in-situ* fabricated with aqueous samples, but also can be pre-formed and used as a sensing substrate for food samples with different physical forms, such as dipping in aqueous sample, capturing aromatic compounds in the headspace, and holding solid samples for Raman scattering enhancement, as shown in Figure 17.

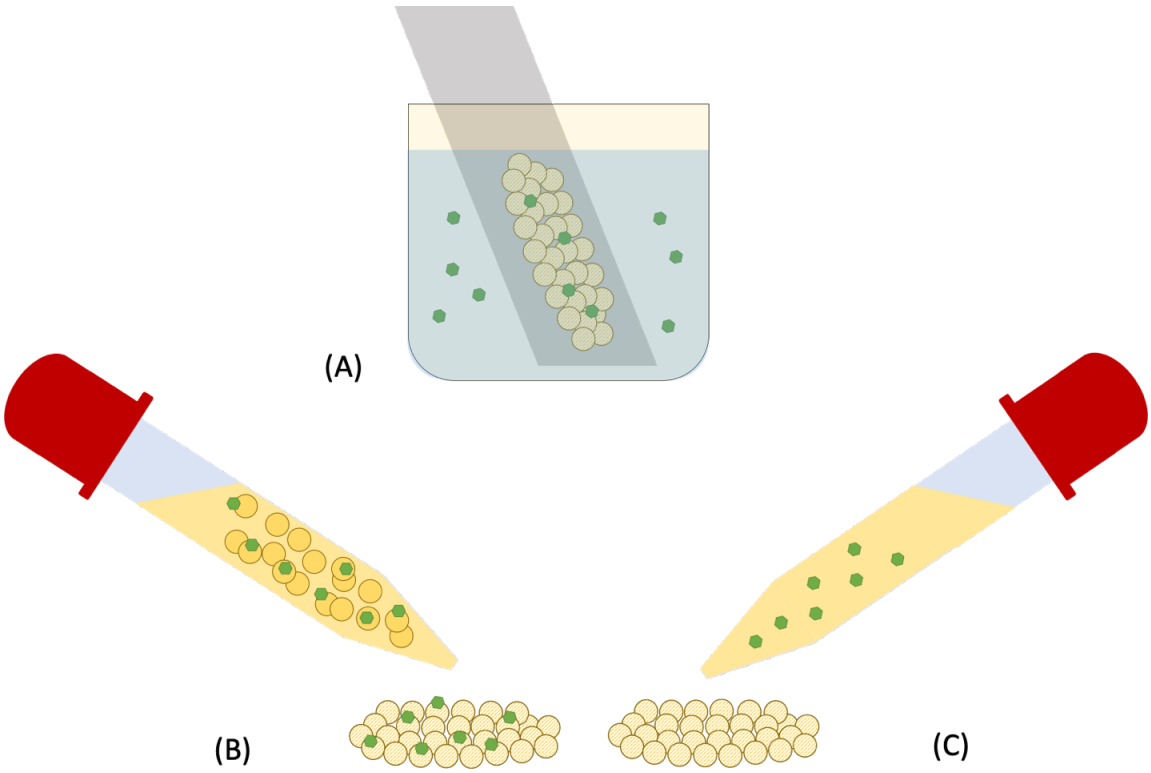

Figure 17 Sample preparations with AgNPs mirror, (A) dipping, (B) in-situ fabrication, (C) deposition on the pre-formed AgNPs mirror.

Table 4 Sensitivity, quantification ability, and sample preparation methods for AgNPs mirror and AgNPs aggregates substrates.

	AgNP mirror	AgNP aggregates
Sensitivity ***(estimated LOD)***	0.0081 ppm	0.0123 ppm
Quantification (R^2)	0.9981	0.9801
Sample Preparation	• Dipping in aqueous sample • Deposition of sample to the pre-formed AgNPs mirror (work for solid, aqueous, and gas samples) • In-situ formation with samples	• Only working in aqueous sample

Conclusion

As shown in Table 4, benefited from the uniform arrangement of nanoparticles, the AgNPs mirror substrate achieved a lower calculated limit of detection for fonofos (i.e., 0.0081 ppm) compared to the AgNPs aggregates. More importantly, a much more improved coefficient of determination was obtained using the AgNPs mirror substrate. Featuring the solid monolayer nature, the AgNPs mirror substrates have broader applications in sample deposition and analysis, compared to the AgNPs aggregates, which can be only used with aqueous samples. Other than the breakthroughs mentioned in Chapter 3, the results of Chapter 4 suggested that the AgNPs mirror can further overcome three drawbacks of current SERS substrates:

- Much more improvement of quantitative reliability
- Expanded applications and sample preparations from only aqueous food to solid and gas food systems.
- *In-situ* fabrication features more

In this project, the AgNPs mirror are proved to be functional in simple aqueous samples, however, its potential in multicomponent food samples have not been fully investigated. In the future chapters, more complicated food samples such as red wines and headspace will be challenged with AgNP mirror substrates.

5. APPLICATION OF THE MIRROR SUBSTRATE IN RED WINES ANALYSIS

Introduction

Chemical profiles are considered as important criteria to evaluate overall quality of red wines, for examples, anthocyanins are responsible for the red color of wines [114], and the perception of astringency in wines is largely credited to the condensed tannins [115]. For the authentication purpose, the characterization of red wine profile is very essential. Standard characterizations and authentications are mostly based on sensory (i.e., tasting), magazine/website rating systems (e.g., Wine Enthusiast, a widely respected website on wines), or chemical analysis such as the infrared spectroscopy, mass spectrometry, the spectrophotometry, and the chromatography [116–120]. However, these standard methods might be expensive, complicated, time-consuming, or not portable to operate. Therefore, a quick but detailed profiling tool is in a great need for authentication, quality control and production monitoring of red wines. In recent studies, Raman scattering showed a potential in wine analysis due to its quick detection and in situ operation. It is reported that Raman spectroscopy, not only can real time monitor sugar, ethanol, and glycerol during the fermentation[121], but also can analyze phenolic acids in white wines or showed some associations of spectra to flavonoids [38,122,123]. However, since red wines are more complex and richer in fluorescent molecules, such as polymerized pigments, Raman spectroscopy or SERS have yet been applied in analysis of red wines to show more detailed chemical profiles[38].

Therefore, in this study, we explored the potential of surface-enhanced Raman spectroscopy (SERS) in red wines chemical profiling with different sample preparations

and compared with Raman spectroscopy result. SERS uses noble metallic nanostructures to enhance the Raman scattering of analytes. Compared to normal Raman, SERS has advantages of higher sensitivity, reduced fluorescence, and enhanced selectivity by combining the Raman techniques with metallic noble nanoparticles. Tradition SERS substrate, i.e., silver nanoparticle aggregates and a highly uniform SERS substrate, AgNPs mirror that we previously developed were used and compared for SERS chemical profiling of red wines[124]. Three approaches of sample preparation for red wine analysis using SERS were developed in this study to characterize the chemical profiles of red wine and to differentiate three red wines, including Chateau de Chantegrive Graves, 2012, Corley Family Cabernet Sauvignon State Lane Yountville, 2011, Gallo Family Vineyards Hearty Burgundy. The first two approaches were based on directly incubating wine samples with AgNPs aggregates and AgNPs mirrors, respectively. The third approach was based on liquid-liquid extraction and in situ forming the mirror substrate in a separated organic phase for SERS analysis. Three sample preparation methods were evaluated, and SERS data was analyzed for its correlation with overall quality of three tested wines.

Materials and Methods

In this work, hydrochloric acid, silver nitrate and sodium citrate were purchased from Thermo Fisher Scientific, Waltham, MA. Adenine, Resveratrol, Malvidin chloride, Catechin, Grape seeds oligomeric proanthocyanidins, and Gallic acid were purchased from Sigma-Aldrich, St. Louis, MO. Two high rating red wines, Chateau de Chantegrive Graves, 2012 (i.e., *WE* rating 93) [125], Corley Family Cabernet Sauvignon State Lane Yountville, 2011 (i.e., *WE* rating 92) [126], and a low rating Gallo Family Vineyards Hearty

Burgundy (i.e., *WE* rating 87) [120], were purchased from *Total Wine and more* store in Manchester, CT. To be noted, the *WE* ratings are given based on the quality, award achievements, affordability, and reviewer recommendations. Additionally, after opening, since wine chemicals could be potentially oxidized to result in a dramatical change of the profile, all red wine samples were analyzed freshly within one hour after opening, to ensure the integrity of their original chemical profiles.

AgNPs synthesis

AgNPs were synthesized according to Gao's protocol [4] 100 ml 1×10^{-3} M silver nitrate solution was heated on the plate under a vigorous stirring at 350°C until boiling. Subsequently, 1 ml 0.1 M sodium citrate solution was added immediately, and the solution was kept boiling for 25 minutes until a greenish brown color was observed to indicate the formation of silver nanoparticles. After cooling down to the room temperature, approximately 70 nm silver nanoparticles were obtained, and nanoparticles were diluted to 100 ml to reach the final concentration of 1×10^{-3} M.

Analysis of red wine samples with Raman spectroscopy

3 ml of red wine sample (i.e., Gallo Hearty Burgundy) was placed at the analyzing chamber directly for Raman measurement.

Directly analysis of red wines with AgNPs aggregate substrates

5 μl 1×10^{-2} M AgNPs solution were mixed with 5 μl of sample red wine (i.e., Gallo Hearty Burgundy) and incubated for 5 minutes, and air dried for Raman measurements.

Directly analysis of red wines with AgNPs mirror substrates

AgNPs mirror substrate was fabricated and deposited on the gold slide. Then, 10 μl of sample red wine (i.e., Gallo Hearty Burgundy) was instilled to the substrate and incubated for 5 minutes for Raman measurements.

Fabrication of AgNPs mirror substrates

According to our previous work [124], mediating solvent (i.e., a mixture of polar and non-polar solvents) is able to assemble AgNPs to a monolayer at the interface between aqueous and solvent phases. 70 μl of the mediating solvent was added to 50 μl 1×10^{-2} M AgNPs solution and pipetted vigorously to enforce the mixing of two immiscible phases. After 20 seconds commingling, an AgNPs mirror-like layer was assembled at the interface once the system reached the stillness. Mediating solvents and extra water were carefully removed and the AgNPs mirror layer was transferred by a pipette to a gold coated glass slides for further analysis.

Wine chemicals extraction and the profiling of red wine samples using AgNPs mirror substrates

In this section, ethyl acetate and hexane were mixed at a ratio of 4:1 to form the mediating solvent to expel water-soluble components. 500 μl of mediating solvent and 500 μl red wine were vortexed vigorously for 30 seconds in a centrifuge vial and incubated on a rotating mixer for 5 minutes. After the system reached equilibrium (i.e., two phases are clearly separated), 70 μl red wine extracts (from the mediating solvent phase, shown in Figure 3 (B)) were added to 50 μl 1×10^{-2} M AgNPs solution and pipetted vigorously for 20 seconds until observing the formation of AgNPs mirror at the interface of two phases. Extra red wine and mediating solvents were carefully removed

and the AgNPs mirror layer was transferred by a pipette to a gold slides for Raman measurement. Additionally, five wine chemicals (i.e., 2000 ppm grape seeds oligomeric proanthocyanidins, 500 ppm catechin, 500 ppm gallic acid, 100 ppm malvidin chloride, and 100 ppm resveratrol) were prepared in 15% ethanolic solutions (i.e., to simulate the practice of red wine environment) as standard stocks. Later, these chemicals went through the same extraction method and SERS spectra were acquired to compare with the wine extract spectra.

Instrumentation

The Surface-enhanced Raman scattering measurement is performed using a ChemLogix EZRaman-I Series High Performance Portable Raman Analyzer with a 785 nm laser source, under following conditions: 170 mW laser power, 5 times integration, and 2 seconds exposure time. Raman intensity was determined based on the height of distinct peaks.

Quantitative and statistical analysis

In this study, all samples were measured within a range of 400-1800 cm^{-1}. Raman spectra were analyzed using Thermo Scientific TQ analyst 8.0 software and the statistical differences of spectra were characterized via principle component analysis. In the principle component analysis, PC scores represent the most distinct regions of the spectra and they are ranked from 1-3 based on the significance of the distinct region in the overall spectrum. PC1, PC2, and PC3 for the PCA of wine spectra were determined and their sum was compared to 80% to suggest a significance of difference among the spectra [127].

Results and discussion

Analysis of red wine with Raman spectroscopy and the AgNPs aggregates

Raman measurement of red wine (i.e., Gallo Hearty Burgundy) and SERS measurements of red wine with AgNPs were shown in **Figure 18** (a) and **Figure 18** (b), respectively. In **Figure 18** (a), one distinct peak at 733 cm^{-1} Raman shift was observed in the spectra, however, the overall resolution of the spectrum is relatively low. According to the literature, this noisiness could be due to the complex constitution of red wine and fluorescent inference given by polymerized pigments [123]. On the other hand, if red wine was mixed with AgNPs and dried for analysis (**Figure 18** (b)), same phenomenon was overserved at the edge area as shown in in **Figure 18** (c). This could be resultant from the aggregation of large wine molecules (i.e., polymerized pigments) at the edge area during the drying process. However, the overall resolution of the spectra was found to be extraordinarily improved if the SERS measurement focused at the middle area as shown in **Figure 18** (d). According to the picture of the dried mixture, most AgNPs were found aggregated at the middle area, which presumably suggested that the exclusion of polymerized pigments (mostly retained at the edge) can reduce the fluorescent interference and hence to improve the overall resolution of the Raman spectra. However, targeting on the distinct peak at 733 cm^{-1}, the variation of Raman intensity was relatively large (i.e., relative standard deviation is 28.9%, as shown in **Figure 18** (e)). Therefore, according to previous study [124], a newly developed uniform SERS substrate, AgNPs mirror was demonstrated to provide more consistent results and more uniform Raman intensities.

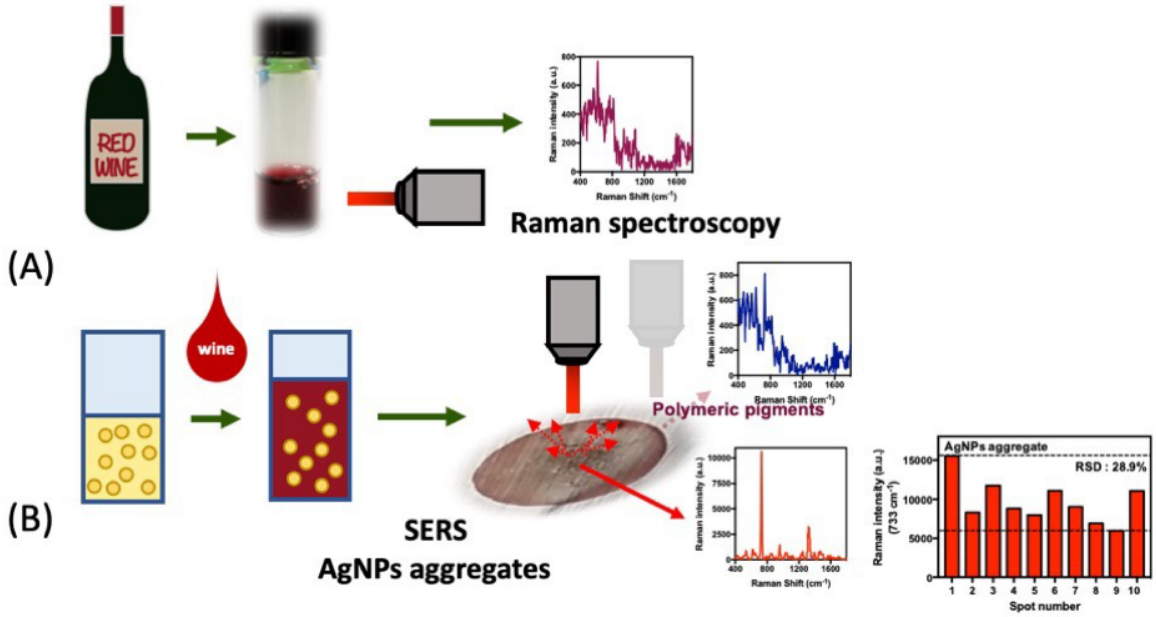

Figure 18 Schematic illustration of (A) direct analysis of red wines with Raman spectroscopy, and (B) direct analysis of red wine with AgNPs aggregates, and SERS intensity distribution for the peak at 733 cm-1 (relative standard deviation is displayed).

Direct wine chemical analyzing method with AgNPs mirror

As shown in **Figure 19** (a) and previous study [124], AgNPs mirror was fabricated with a mediating solvent (i.e., a mixture of acetonitrile and hexane). A drop of model red wine sample (i.e., Gallo Family Vineyards Hearty Burgundy) was carefully dripped on the surface of the premade AgNPs mirror. After the deposition, the AgNPs mirror floated over the wine drop (**Figure 19** (c)) and was able to capture chemicals from the red wine during the incubation. Since the AgNPs mirror is a layer of internally attached nanoparticles, mirror remained intact and stayed at the mid after drying (**Figure 19** (d)). According to **Figure 19**, pigments mostly aggregated at the edge of spots after dried, the phenomenon of mirror staying at mid confirmed that AgNPs mirror can also exclude the pigments and reduce the fluorescence interference as AgNPs aggregates.

Additionally, credit to the uniform arrangement of nanoparticles, data analysis showed that the consistency of Raman intensity at the distinct peak, 733 cm^{-1} (i.e., relative standard deviation was only 8.21%, **Figure 19** (e)), was much improved compared to the AgNPs aggregates and another distinct peak was observed at 1324 cm^{-1} in **Figure 19** (f).

To further investigate the chemical components that are responsible for signature peaks, a dominate and quality-related phytochemical in red wines, condensed tannins (i.e., grape seeds oligomeric proanthocyanidins) were tested via SERS following the same steps of analyzing red wine samples. To mimic the polar environment, condensed tannins were dissolved into 15% ethanolic water solution. SERS spectra of 5000 ppm condensed tannins were shown in **Figure 19** (f) and similar signature peaks were observed as the red wine samples at 733 cm^{-1} and 1324 cm^{-1} Raman shift. However, based on the literature review [128], a DNA fraction molecule, adenine also shared the similar SERS spectra as both red wine and condensed tannins. To confirm the similarity, adenine was analyzed in the ethanolic solution and SERS spectra were acquired following the same steps for condensed tannin and shown in **Figure 19** (f).

After comparison, similar SERS spectra and signature peaks were observed at 1 ppm adenine, 5000 ppm condensed tannins, and sample red wine in **Figure 19** (f). This observation suggested that the distinct peaks observed from red wine and condensed tannins were presumably related to adenines. According to the previous study, DNA fractions in grapes, including seeds, skins, and pulps, were present in the must (i.e., freshly pressed juice containing the skins, seeds, pulps, and stems) and final products [129]. Even though intact DNA could be mostly destroyed during the processing, the residual

fractions, such as adenine, cannot be completely eliminated from red wines. Adenine was known as an extremely sensitive SERS active component [128], according to the our results (shown in supporting information), relatively high signal intensity could be observed at even low concentration at 1 μg/L. This finding suggested that even though the AgNPs mirror can provide consistent results, the dominancy of adenine in the SERS spectra masked other important chemicals such as phenolic acids, anthocyanins, and polyphenols. Thus, a more complex sample preparation method needs to be further developed to comprehensively profile chemicals in red wines. To be noted, since the residual adenine and condensed tannins in wine are mostly released from grapes during winemaking, a potential correlation between adenine and condensed tannins were also found in the study, and the determination of adenine in red wine could be used as an indicator for the concentration of condensed tannins. This prediction of the condensed tannin content in several red wine models was also validated with a standard UV-spectrophotometric condensed tannins determination method, Bate Smith [117]. Validation and modifications are needed in the future for this discovery; therefore, results were shown in supporting information.

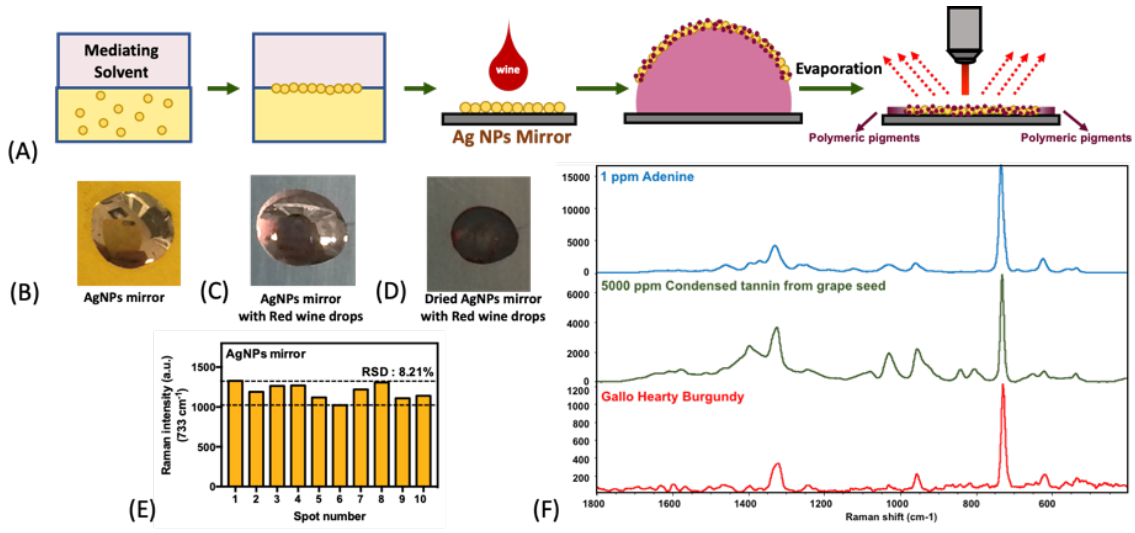

Figure 19 (A) Schematic illustration of the fabrication of AgNPs mirror and the sample preparation for the direct analysis of red wines with AgNPs mirror. Photographs of (B) AgNPs mirror, (C) AgNPs mirror floated on the red wine, and (D) dried AgNPs mirror with red wine. (E) SERS intensity distribution for the peak at 733 cm-1 from the direct analysis of red wine with AgNPs mirror (relative standard deviation is displayed), (F) SERS spectra of adenine (a DNA based molecule), condensed tannin from grape seed extract, and red wine.

Extraction based wine chemical profiling method

As previously mentioned, the mirror was fabricated by a mediating solvent which has different combinations of polar and non-polar organic solvents [124]. These solvents are also effective extracting agents, therefore, we hypothesized that the mediating solvent can also extract the bioactive components from red wines and concentrate them onto the AgNPs mirror substrate for SERS analysis during the fabrication of mirror at interface.

Since adenine is very water soluble [130], the mediating solvent in this study should not only extract sufficient amount of wine chemicals but also suppress adenine in the water phase to eliminate the dominancy of adenine in the wine extract spectra. Therefore, a neutral-polar solvent, ethyl acetate, modified with a minimal amount of hexane was chosen to constitute the mediating solvent.

Sample preparation was illustrated in **Figure 3** (a). The mediating solvents were mixed vigorously with three sample wines and due to the polarity difference, two phases separated once system reached the equilibrium. As shown in **Figure 3** (b), slightly redness in the mediating solvent layer indicated the successful extraction. The mediating solvent with red wine extract was subsequently added to the AgNPs solution and vigorously mixed. The mirror formed at the interface was moved out for measurement. As shown in **Figure 3** (b), compared to a silver color on the mirror blank, a burgundy appearance on the mirror with wine extract indicated that bioactive components were presumably concentrated to the mirror substrate during the fabrication. In **Figure 3** (c), spectra of red wine extracts from three varieties were presented and showed partial similarity to previous reported dry white wine spectra [38]. Furthermore, spectral differences were observed within three tested red wines. After comparing to the spectra obtained by directly dropping red wine to the mirror (**Figure 19** (f)), more peak information, higher resolution, and less intensity of peak at 733 cm^{-1} were acquired in **Figure 3** (c), suggesting that extraction method did provide more chemical details of the red wines other than only adenine from the direct analysis.

Wine chemicals characterization in the wine extract spectra

To confirm the spectral distinctions within three tested red wines, principle component analysis was applied and showed in **Figure 20** (a). Based on the PCA results, PC1 score referred to a 60.23%, PC2 score and PC3 score referred to 20.01% and 9.15%, respectively, in the full spectrum contribution. The sum of three PC scores is larger than 80%, which suggested a presence of significant differences among three red wine spectra [127]. After reviewing of all red wine spectra, dominating peaks were observed at 1603 cm^{-}

^{1}, 1555 cm^{-1}, 1318 cm^{-1}, 1248 cm^{-1}, 950 cm^{-1}, and 650 cm^{-1} in all three red wines, and additional peaks at 1479 cm^{-1}, 1350 cm^{-1} and 1025 cm^{-1} were only found in Chataeu de Chantegrive Graves, as shown in **Figure 20** (b-d). As reported by spectroscopic and theoretical investigation of phenolic acids in white wines [38,131], peaks at 1603 cm^{-1} were presumably contributed by wine polyphenols. Therefore, to potentially identify the assignment of dominating peaks, five representative wine standard chemicals, phenolic compounds (e.g., catechin, oligomeric proanthocyanidins (condensed tannin), gallic acid, resveratrol, and malvidin chloride) were investigated in this study. According to the reported concentrations of standards in red wines (i.e., condensed tannin, 2000-2500 mg/l [132], catechin, 172-637 μM, gallic acid, 130-416 μM, anthocyanins, 101-325 μM, and resveratrol, 2-46 μM [133]), representative chemicals were dissolved in 15% ethanolic solution at according concentrations shown in the method section and were analyzed using the same extracting method as wine samples. SERS spectra of each standard was shown in the supporting information and signature peaks were listed in **Table 5**.

As expected, dominating peaks in **Figure 20** (b-d) were found to share the same Raman bands with five standards, such as peaks at 1555 cm^{-1} and 1248 cm^{-1} were also observed in oligomeric proanthocyanidins (condensed tannins) and malvidin chloride , the peak at 1603 cm^{-1} was observed in gallic acid, resveratrol, and malvidin chloride, the peak at 1318 cm^{-1} was observed in catechin, gallic acid, and malvidin chloride, the peak at 950 cm^{-1} was observed in gallic acid and resveratrol, and the peak at 650 cm^{-1} was observed in oligomeric proanthocyanidins, gallic acid, and catechin. Other than dominating peaks were observed all wine samples, additional peaks at 1350 cm^{-1} and 1025 cm^{-1} in spectra of Chateau were also observed in malvidin chloride and in gallic

acid, respectively, and the peak at 1479 cm^{-1} was observed in oligomeric proanthocyanidins, gallic acid, and catechin. To be noted, other than the five wine chemicals analyzed in this study, many other chemicals that share similar chemical structures or side groups could contribute to the same bands in SERS spectra, such as the peak at 1603 cm^{-1} was reported in other white wine phenolic acids other than the gallic acid [38]. Even though further validation might be needed to study the actual composition, the results suggested that the extraction method combined with SERS showed a huge potential to be a comprehensive screening tool to quickly and simply profile the chemical components of red wines.

In **Figure 20**, differences were observed (e.g., the peak intensity, the appearance of signature peaks, and the pattern of the spectra) within all tested red wines. To further investigate potential differences of three red wines, intensities of peaks at 1603 cm^{-1}, 1555 cm^{-1}, 1479 cm^{-1}, 1350 cm^{-1}, 1318 cm^{-1}, 1248 cm^{-1}, 1025 cm^{-1}, 950 cm^{-1}, 650 cm^{-1}, were compared in Figure 21. At 1603 cm^{-1}, Corley is significantly higher than other two red wines, which could indicate a higher presence of gallic acid, resveratrol, or malvidin chloride. At 1555 cm^{-1}, the highest peak intensity was observed in Chateau, which presumably suggested a higher amount of condensed tannins or malvidin chloride. At 1479 cm^{-1}, a peak was only observed in Chateau, which could illustrate a higher amount of condensed tannin, gallic acid, or catechin. Similar phenomenon was found at 1350 cm^{-1} and 1025 cm^{-1}, only peaks observed in Chateau might suggest a higher concentration of malvidin chloride and gallic acid, respectively. At 1318 cm^{-1}, Corley showed the highest peak intensity which could reveal a higher concentration of catechin, gallic acid, or malvidin chloride. At 1248 cm^{-1}, highest peak intensity occurred with Chateau to

presumably indicate a higher amount of condensed tannins, malvidin chloride. At 950 cm^{-1}, both Corley and Chateau showed significant higher peak intensity than Gallo to suggest potentially higher presences of gallic acid, resveratrol. However, at 650 cm^{-1}, Gallo showed a possibly highest amount of condensed tannin, gallic acid, or catechin. To be noted, since there are no following standard validations due to the lack of instrumentations, detailed differences showed in Figure 21 are mostly speculated and could be also caused by other similar-structure wine chemicals that are not tested. Nevertheless, the noticeable spectral differences reported here suggested a huge potential of SERS in the red wine profiling. According to most results, both Corley and Chateau seem to show relatively more complicated phytochemicals profiles (i.e., higher peak intensity and more peaks) than the Hearty.

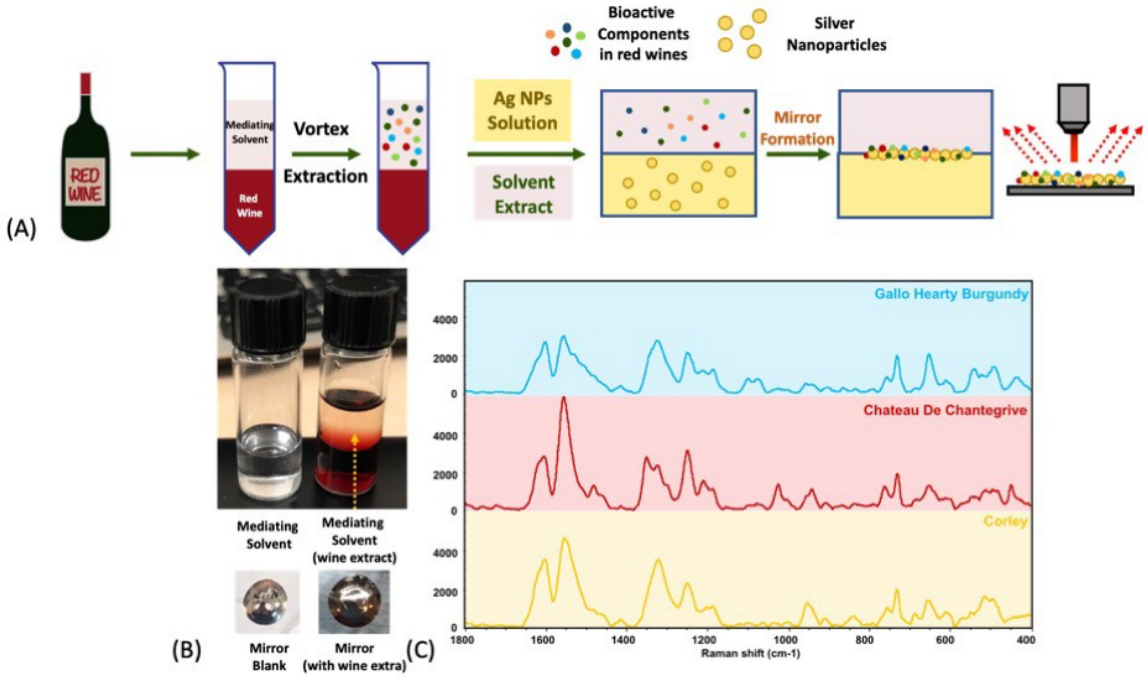

Figure 20 (A) Schematic illustration of the red wine extraction with mediating solvents and the fabrication of the AgNPs mirror with wine extracts. (B) Mediating solvent (top left), mediating solvent layer after red wine extraction (top right), and (bottom left) blank AgNPs mirror substrate after fabrication and (bottom right) AgNPs mirror substrate fabricated with wine extracts. (C) SERS spectra of Gallo

Family Vineyards Hearty Burgundy, Chateau de Chantegrive Graves, 2014, and Corley Family Cabernet Sauvignon State Lane Yountville, 2014.

Table 5 Assignment of signature peaks of standard red wine chemicals.

Raman shift (cm^{-1})	Red Wine Components
1603	Malvidin chloride, Gallic acid, Resveratrol
1555	Condensed tannin, Malvidin chloride
1479	Condensed tannin, Gallic acid, Catechin
1350	Malvidin chloride
1318	Malvidin chloride, Gallic acid, Catechin
1248	Condensed tannin, Malvidin chloride
1025	Gallic acid
950	Gallic acid, Resveratrol
650	Condensed tannin, Gallic acid, Catechin

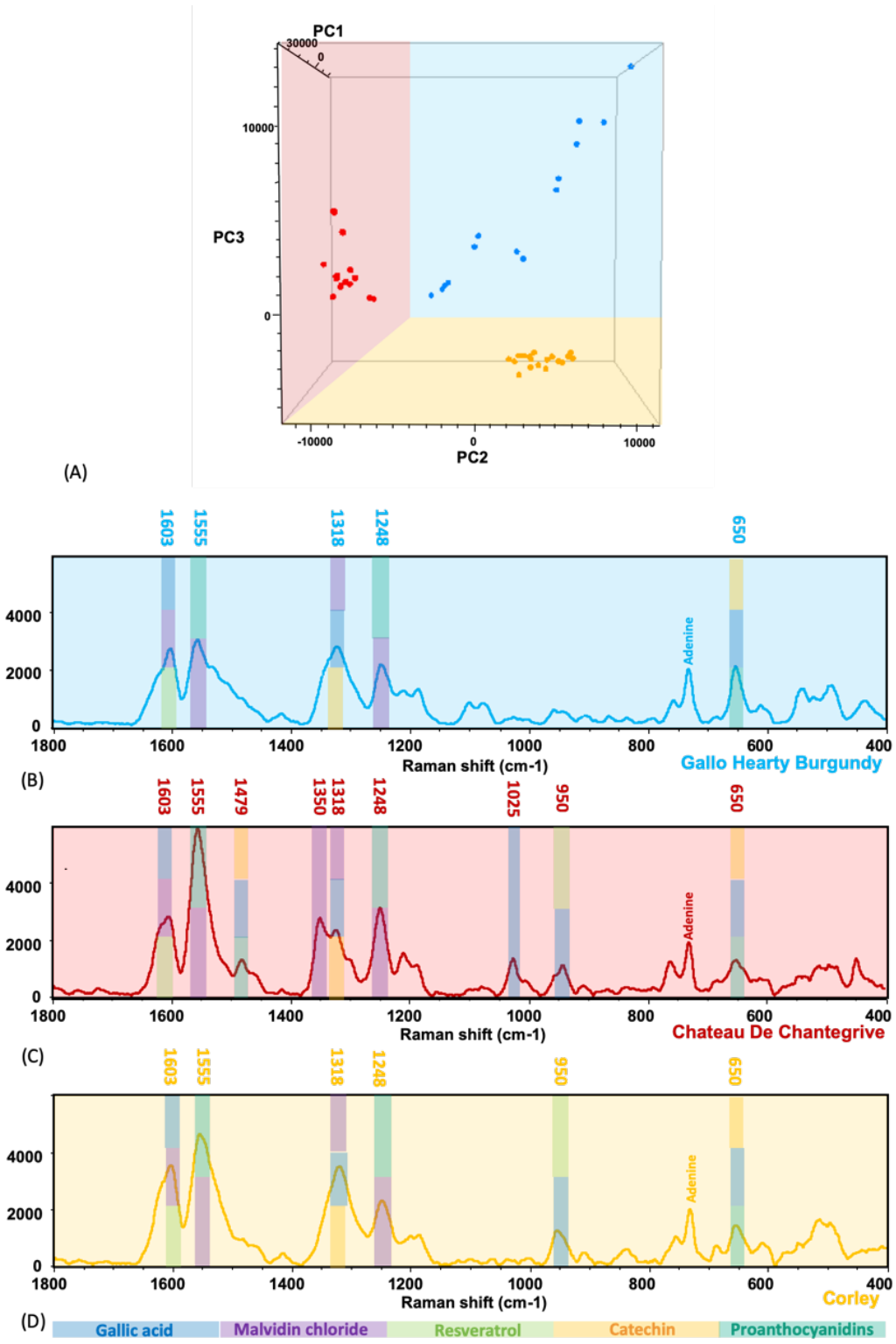

Figure 21 . (a) PCA differentiation of three wine extracts. (b) SERS spectra of Gallo Hearty Burgundy, Chateau de Chantegrive, Corley Family Cabernet Sauvignon State Lane Yountville with peak assignments of tested wine chemicals.

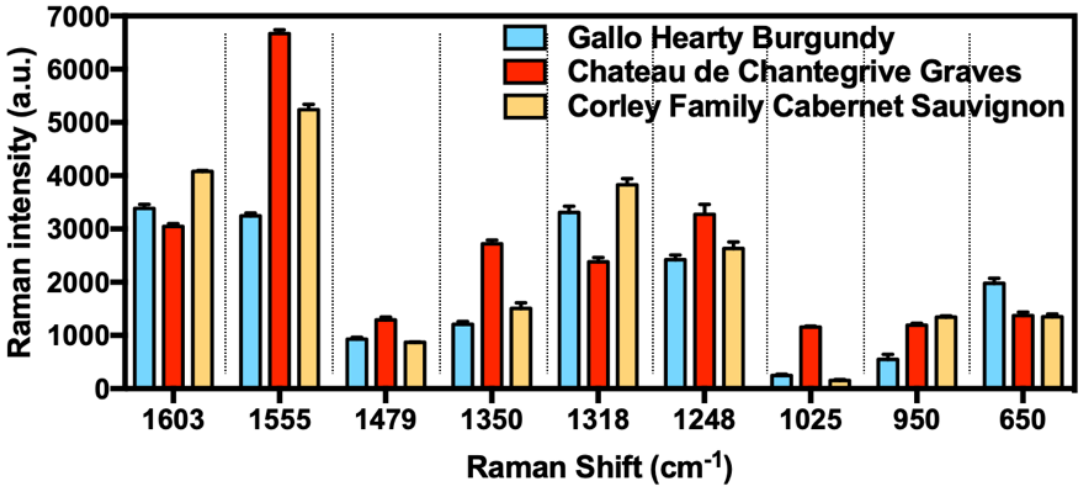

Figure 22 Raman intensities of important peaks in three red wine extract spectra (significant differences within three red wines were observed in each Raman shift).

Additionally, in this case, it is hard to specifically quantify individual chemicals in each red wine sample because many chemicals shared the same peak assignment. For example, oligomeric proanthocyanidins (condensed tannins) always shared same bands with malvidin chloride (anthocyanins) or gallic acid in the spectra and both of them showed potentially higher amount in Chateau.

It was noteworthy that the results from the Bate Smith method in supporting information indicated Gallo Hearty Burgundy also had the lowest content of condensed tannins, which agreed to the findings from the extraction method. Since wine chemicals analyzed in this study are closely related to the overall red wine quality [115], the profiled information can be applied to evaluate the overall quality of red wines. Based on the obtained spectral information in Figure 21 and Figure 22, both Corley Family Cabernet Sauvignon (i.e., *WE* score is 92) and Chateau de Chantegrive Graves (i.e., *WE* score is 93) showed significant higher amount or more information of red wine chemicals which could reveal their higher overall qualities than the Gallo Family Hearty Burgundy (i.e., *WE* score is 87). The results also made an agreement with the *WE* quality scores of three

tested red wines. Since every red wine showed different SERS spectra, all peak assignments can be assembled to a bar code specifically referring to each red wine to illustrate the potential chemical profile of red wines. Overall, the extraction-based method successfully suppressed the interreference of adenine and profiled the wine chemicals in one comprehensive SERS spectra. Additionally, according to the literature, the quality of red wines is closely related to the grape varieties used in the wine making. Some premium-quality red wines are only made from one type of grape to provide a pure taste, such as the Corley is made only from Cabernet Sauvignon. And some red wines, such as Chateau and Gallo Burgundy are blended with a variety of species either to enrich the flavor, or to reduce the cost of ingredients [132]. This might explain why more complexity was observed from the SERS spectra of Corley than Chateau and Gallo Burgundy, since many dominate compounds from Cabernet Sauvignon are presumably diluted during the blending, to result in a disappearance of their signature peaks in the SERS spectra.

However, due to the high cost and the lack of availability of a single wine grape variety, adulteration of foreign species during the winemaking is not a rare case. Since different grape species have distinct chemical profiles, according to the results, SERS showed a great potential to be a fast authentication tool to determine the possible adulteration.

Freshness evaluation using extraction-based profiling method

Other than profiling the important phytochemicals, a freshness study was also demonstrated to compare the SERS spectra of a red wine that is freshly opened and a red wine that is opened for four weeks. Results were shown in Figure 23. In the spectra of

fresh wine, a peak at 500 cm^{-1}-520 cm^{-1} was observed. According to literatures[134,135], this peak was presumably contributed by sulfur dioxide, a preservative that was commonly used in red wine at a relatively high concentration (i.e., 20-200 ppm)[136]. After opening for four weeks, the red wine was considered as spoiled because it produced a strong pungent aroma similar to the nail polish remover (i.e., ethyl acetate, an indicator of the bacterial spoilage of red wine)[137]. In the SERS spectra of spoiled wine, at the similar Raman shift range, an increase of the peak at 500 cm^{-1} was observed. Further principle component analysis also confirmed the difference between two spectra. According to literatures, red wines were oxidized and spoiled quickly after opening, since the contact of oxygen will trigger the growth of acetic acid bacteria and lactic acid bacteria to produce spoilage compounds[138]. In the Raman characteristic group frequencies table[135], the increase of the peak was suspicious to be caused by the production of aromatic disulfides (region from 400 cm^{-1}-540 cm^{-1}) or the polysulfides (region from 450 cm^{-1}-510 cm^{-1}), which were both considered as wine spoilage compounds from the literature.[136] This interesting discovery added an extra potential of the extraction-based method in red wine chemical profiling. However, further analysis still needs to be done to confirm the presence of the sulfur dioxide and the spoilage in red wine after long term storage, such as the increase of volatile acidity a due to the acid production of spoilage bacteria.[137]

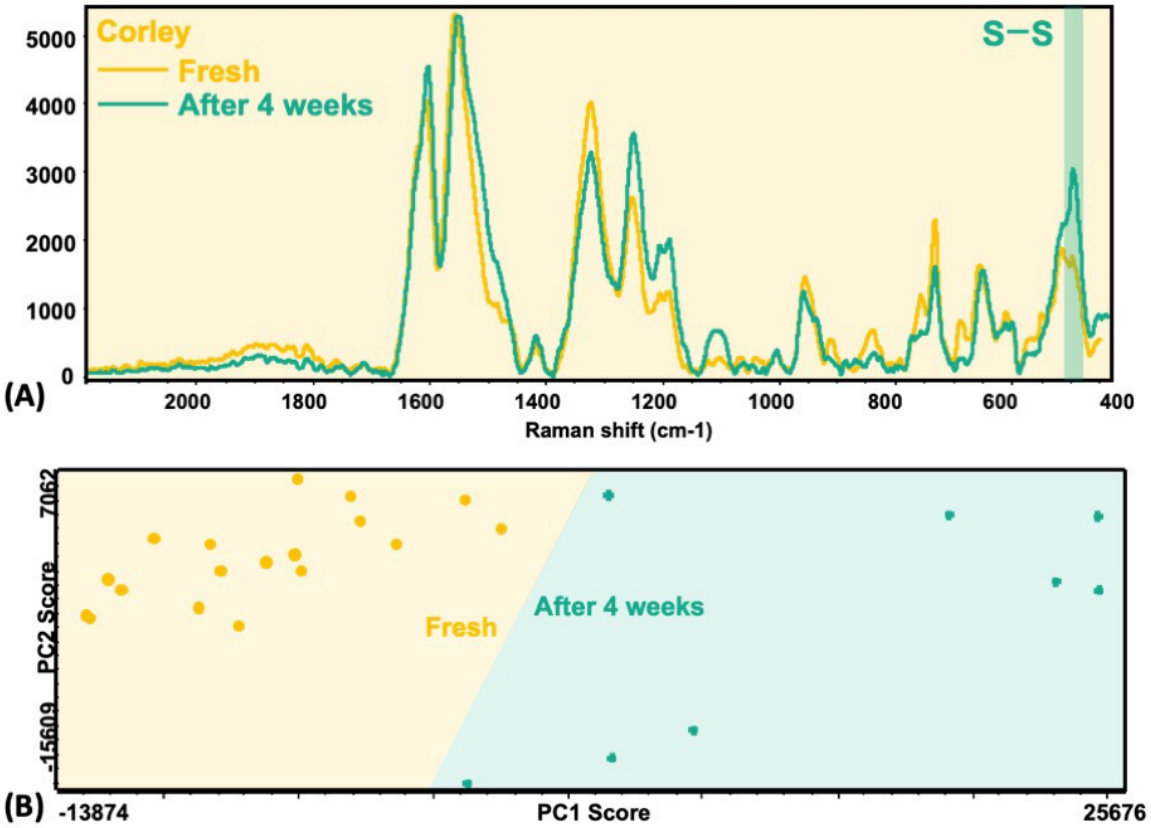

Figure 23 (A) SERS spectra of freshly opened Corley red wine and the red wine after opening for four weeks. (B) PCA differentiation of two SERS spectra.

Conclusion

Herein, several sample preparation methods to profile chemical information of red wines using SERS were demonstrated. Both direct analyses using Raman spectroscopy and using the AgNPs aggregates failed to show clear or consistent spectra due to interference of the pigments and the overgeneration of nanoparticles. The use of AgNPs mirror not only reduced the fluorescent interference but also provided a better data consistency. However, due to the presence of adenine, most chemical information of red wines was masked. Therefore, the extraction-based method was developed to use a specially designed mediating solvent to suppress the dominancy of adenine in the SERS spectra, meanwhile, to extract important phytochemicals in the red wines and to

concentrate to the mirror. Comprehensive chemical profiles were obtained and the spectral differences were clearly observed among three tested red wines. Furthermore, the chemical profiles assembled a bar code that has the potential to for determining the authenticity and monitoring the change of the chemical profiles over time. This study suggests SERS to be a new comprehensive analyzing tool to study the wine components other than UV-spectrophotometry, chromatographic, and sensory methods. Without analyzing each chemical individually, integrating SERS spectra of red wines with data science could be very feasible. In the future study, more wine samples will be tested to establish the data base, and to explore the potential of the data analysis using machine learning algorithms in wine differentiation and quality assessment.

Supporting information

Detection of condensed tannins in red wine samples by the Bate-Smith assay

Grape seeds oligomeric proanthocyanidins (condensed tannins) concentrations in red wine were also determined using the Bate-Smith assay as a validating methodology. Red wine samples were diluted with ultrapure water[117]. Two separate 15 ml test tubes were prepared for every type of red wine, and 4 ml of diluted red wine, 2 ml of ultrapure water, and 6 ml of hydrochloric acid were added in each test tubes. One test tube was water bathed at 100°C for 30 minutes and the other tube (blank) was stored in dark for the same time. After the heating, 1 ml of ethanol was added to each tube and tubes were stored in dark until fully cooling down. The absorbance of each sample was acquired in a spectrophotometer at 550 nm using ultrapure water as the blank. The absorbance difference was then multiplied 19.33 to calculate the final concentration of

proanthocyanidins in red wine samples, and the concentration was expressed in g CE•L-1 (Catechin Equivalence).

Analysis of grape seed oligomeric proanthocyanidins, adenine, and their correlation

Grape seeds oligomeric proanthocyanidins (i.e., condensed tannin) with different concentrations (500-2250 mg/l) and DNA fraction (i.e., Adenine) with different concentrations (2.5-45 μg) were initially dissolved into 15% ethanolic water solution. Then, 10 μl of condensed tannin solution/adenine was instilled onto the surface of AgNPs mirror substrate. After 5-minute incubation, the sample was air-dried for Raman measurements.

All Raman intensities were averaged from at least eight replicates and standard deviation was recorded. For condensed tannin, adenine, the peak at 733 cm^{-1} was chosen and the average Raman intensity was plotted as a function of concentrations of condensed tannin and adenine, respectively. Linear correlations were performed for both condensed tannin and adenine and calibration curves were generated. The correlation was also performed between the concentration of condensed tannin and adenine at the same Raman intensity of 733 cm^{-1} to determine the linear relationship of two wine components. In the direct red wine analysis, the amount of condensed tannins was determined based on the preceding standard curves and the Raman intensity of 733 cm^{-1}. Calculated concentration of condensed tannins was validated with the Bate Smith assay and the recovery value (i.e., RV%) was calculated based on the following equation:

$$\mathrm{RV\%} = \left(\frac{\text{Conc. of condensed tannin}_{\mathrm{SERS}}}{\text{Conc. of condensed tannin}_{\mathrm{Bate-Smith}}}\right) \times 100$$

The concentration of adenine in red wines was hypothesized to indicate the amount of condensed tannins in red wines. To demonstrate the relationship, Raman intensity of adenine and condensed tannins were plotted as a function of their concentrations, respectively (SI 2). After the comparison of two plots, a proportional correlation was observed between adenine and condensed tannins in Figure 2 (C) along with the coefficient of determination (0.9968). Additionally, a mathematic model was presented in Figure 2 (C) to predict the concentration of condensed tannins in red wines based on the concentration of adenine detected using SERS.

Three red wine samples within different quality levels, Corley Family Cabernet Sauvignon State Lane Yountville, 2014 (Corley, high rating), Chateau de Chantegrive Graves, 2014 (Chateau, high rating), and Gallo Family Vineyards Hearty Burgundy (Gallo, acceptable rating) were analyzed using the AgNPs mirror substrate and the spectra were shown in Figure 21 (A). Noticeable differences within three wine samples were observed and further confirmed in the principle components analysis (i.e., PCA) in Figure 21 (B). Distinctions were presumably due to different quality levels and the varied enological nature of three red wines, including origins, viticulture, species, fermentation process, and ages. Nevertheless, even though spectral disparity was observed, signature peaks of adenine still dominated in all red wine spectra. The concentrations of adenine were calculated in each red wine according to the peak intensity at 733 cm^{-1} and the calibration curve (showed in SI). In Figure 21 (C), the concentrations of condensed tannins were estimated via the equation,

$$C_{condensed\ tannin} = C_{adenine} \times 37.2 + 450.53$$

Within three red wines, Corley family Cabernet Sauvignon showed the highest concentration of condensed tannins, followed with the Chateau de Chantegrive and the Gallo Hearty Burgundy. To validate the estimation, a standard UV-spectrophotometer based Bate Smith assay was applied to determine concentrations of condensed tannins in three red wines. After the calculation, a similar tendency of the condensed tannins concentrations in red wines was observed between SERS and Bate Smith Assay in Figure SI2, which indicated that the SERS method is reliable in quantification of condensed tannins.

Therefore, foregoing results suggested that the adenine, a DNA based molecule released along with condensed tannins during the enological process from grapes, can be used as a SERS indicator to estimate the concentration of condensed tannins in red wines. Furthermore, since the amount of condensed tannins is responsible to the reception of astringency [132], which is reported to be positively related to the wine quality, the determination of adenine using SERS can provide a quick predication of the overall quality of red wines.

To be noted, even though Bate Smith method was considered as a validation in this study, the SERS also showed many advantages in the experimental practice such as faster operation (i.e., the whole analysis only took less than 10 minutes including the sample preparation) and simpler preparation, compared to the Bate Smith.

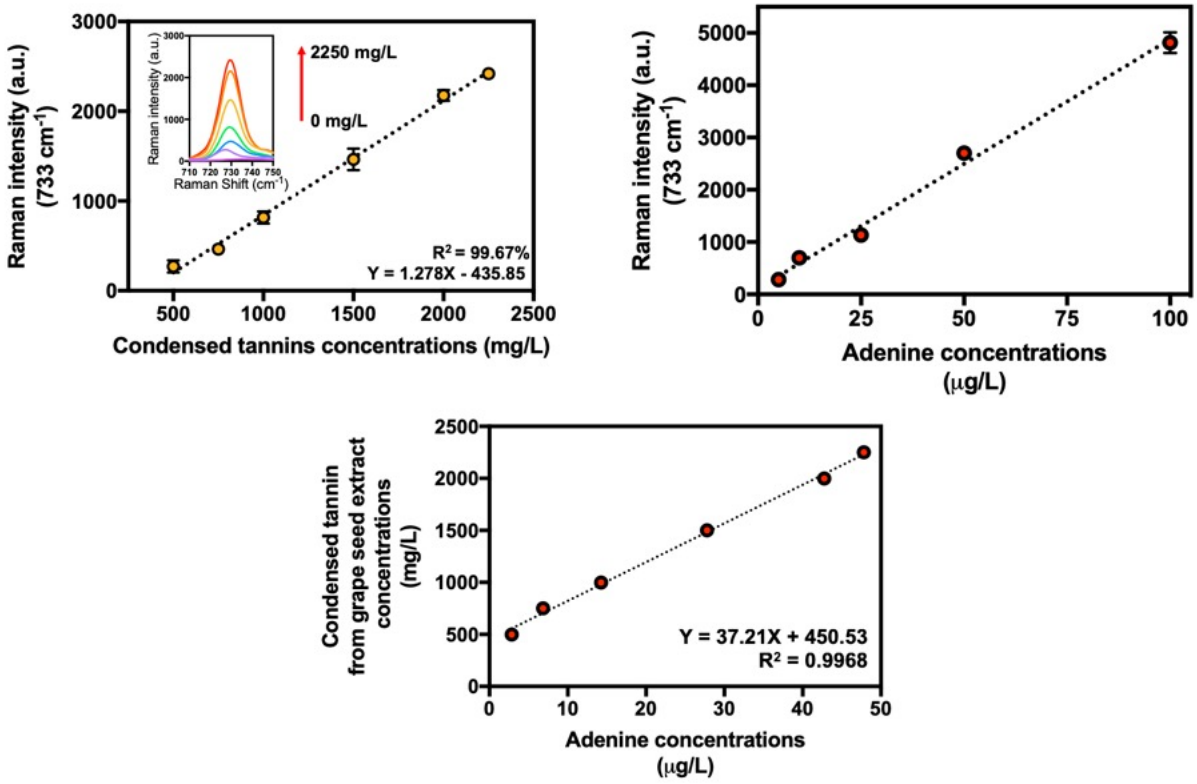

Figure 24 Plots of Raman intensity as a function of concentrations of oligomeric proanthocyanidins and adenine, respectively. Concentration correlations between condensed tannin from grape seed extract and adenine.

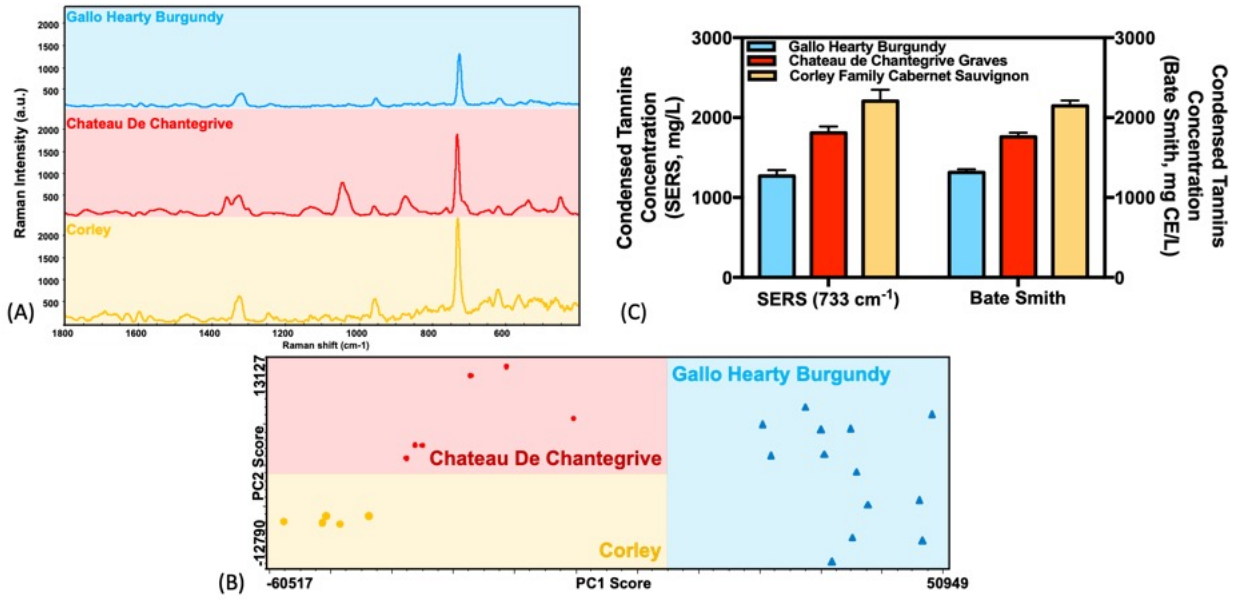

Figure 25 (A) spectra for three wines (B) PCA differentiation of three wines (C) estimation of concentration of condensed tannin in wines and the validation through Bate Smith UV spectroscopic method.

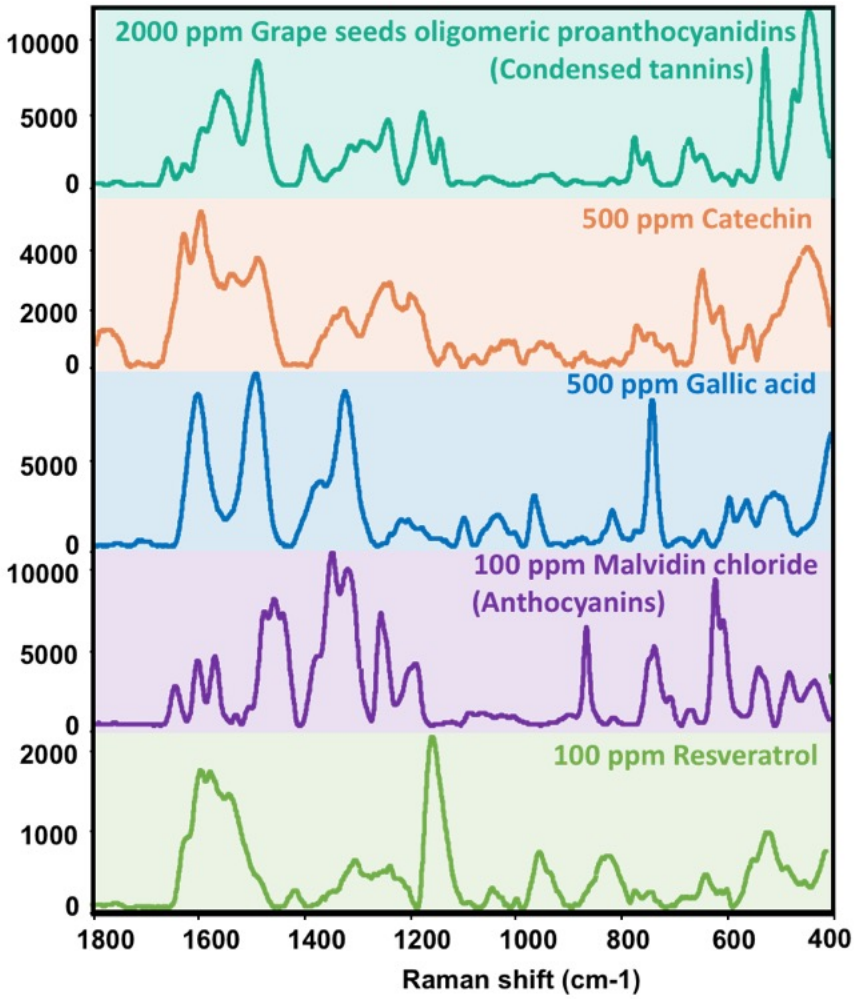

Figure 26 SERS spectra of analyzed wine chemicals.

Acknowledgement

We thank the NEC lab to provide us a valuable internship opportunity to conduct this study, the funding supports in the research on red wines, the UMass summer pre-college program for providing funding supports in lab purchases and the Department of Food Science in UMass, Amherst for providing the analyzing instruments.

6. APPLICATION OF THE MIRROR SUBSTRATE IN THE HEADSPACE ANALYSIS OF FOOD MATRICES

Introduction

Garlic is one of the most representative *Allium* species plants, that is used in food, spices, nutrient supplements, and medicines [139,140]. Garlic yields many heath beneficial compounds, such as an extremely unstable thiosulfinate, allicin, and its decomposed organosulfur compounds, such as diallyl sulfide, diallyl disulfide, and diallyl trisulfide [141]. Due to the reported antimicrobial, anticarcinogenic, and anti-cardiovascular disease properties of these organosulfur garlic derivatives, they have been developed into garlic powders, garlic oils, and other extraction-based dietary supplements [140–145]. Since these organosulfur compounds are not readily stable, characterization of these chemicals in the garlic extract products played a very important role for the quality assurance [139]. The characterization can be conducted through the liquid chromatography (i.e., LC) for products such as garlic oil extract, however, since these organosulfur compounds are mostly aromatic and volatile, characterizing and quantifying them in the headspace of garlic extract using the gas chromatography – mass spectrometry (i.e., GC-MS) is more practical. Chromatographic methods are golden standards and providing accurate analysis, however, it suffers from some drawbacks including complicated instrument operations and/or sample pretreatment, the requirement of trained personnel, and the lack of portability. Therefore, alternative fast, simple, sensitive, and portable techniques are gaining more attentions.

Surface enhanced Raman scattering, short for SERS, combined the nanotechnology and Raman scattering, is an emerging analytical tool for chemical

characterization due to its fast analyzing speed, sensitive detection, simple sample preparation and instrument operation, and great portability. SERS has shown some promising potentials in the detection of volatile compounds. Recently, a gold nanoparticle coated SERS fiber was developed for the solid-phase microextraction and the detection of pesticides in apple juice headspace [35]. Red wine samples were either dropped on a gold nanoparticle coated thin film or filtrated from headspace onto a graphene oxide and gold nanorods hybrid filter paper to analyze the presence of sulfur dioxide, respectively [146,147]. Raman spectroscopy was used to directly measure flavor and aroma from essential oils in quartz cuvettes [148]. Besides the above research, the headspace gas phase of garlic, leeks and Chinese chives, were drawn using a syringe and injected to silver nanoparticle colloids to characterize the volatile compounds using Surface-enhanced Raman spectroscopy [34]. Nevertheless, other than the SERS fiber, few studies analyzed the chemical profiles actually from the headspace, but still by a liquid incubation of sample with SERS substrates. Therefore, the performance of SERS in the actual headspace analysis still need to be further explored.

In this study, the objective is to develop a SERS method coupled with a mirror-in-cap substrate to analyze the the volatile compounds directly in the headspace of garlic extract based on solid phase extraction. Furthermore, the concentration of corresponding compounds in the headspace was determined based on a pre-made calibration curve, and the quantitative performance of this SERS method was compared with the results acquired from an injection GC method.

Material and methods

Materials

Fresh garlic was purchased from the local grocery store. Diallyl sulfide (DAS), diallyl disulfide (DADS), diallyl trisulfide (DATS), 1-propanethiol, 2,5-dimethylthiophene, diallyl sulfide, dimethyl disulfide, dipropyl trisulfide, and s-allyl 2-propene-1-sulfinothioate were purchased from the Sigma Aldrich in St. Louis, MO. Silver nitrate, sodium citrate, and ethanol were purchased from Thermo Fisher Scientific in Waltham, MA.

Synthesis of silver nanoparticles and the fabrication of AgNPs mirror on the cap

AgNPs were synthesized according to Gao's protocol 100 ml 1×10^{-3} M silver nitrate solution was heated on the plate under a vigorous stirring at 350°C until boiling [4]. Subsequently, 1 ml 0.1 M sodium citrate solution was added immediately, and the solution was kept boiling for 25 minutes until a greenish brown color was observed to indicate the formation of silver nanoparticles. After cooling down to the room temperature, approximately 70 nm silver nanoparticles were obtained, and nanoparticles were diluted to 100 ml to reach the final concentration of 1×10^{-3} M.

Acetonitrile and hexane were vortexed with a ratio of 1:1. After mixing, non-polar and polar layers were separated. The polar layer was collected and stored as the mediating solvent. Commercial AgNPs were firstly concentrated by centrifugation to 0.2 mg/ml. Then, 50 μl AgNPs was slowly dripping into 100 μl mediating solvents drop by drop. After about 1 minute, a mirror-like sediment at the bottom was collected then carefully dropped and air dried on an aluminum covered glass slide.

Aluminum film with dried mirrors was cut into proper sizes that can fit in the caps of 2 ml glass vials, and then were attached to the inner side of the cap using double side tapes, to assemble as a mirror in cap SERS active substrate.

Sample preparation of freshly minced garlic, garlic extract, and chemical standards

10 g fresh garlic was minced to store in a 20 ml glass vial and stored in a 20 ml glass vial. For the garlic extract, since the garlic derivatives are unstable, and allicin will quickly decompose to organosulfur compounds after crushing, to prevent a further change of the chemical profile and to achieve a good extraction, 10 g fresh garlic was minced in 10 ml ethanol in a blender, and then the mixture was stored in a 20 ml glass vial. Three organosulfur compounds are analyzed at a pure condition for the best resolution of Raman spectra for peak assignments. To keep the same analytical condition as the garlic extract for the quantitative purpose, diallyl disulfide was prepared in ethanolic solutions with the concentration from 5 to 500 ppm. For all reference standards in the supporting information, all pure standards were mixed with AgNPs at the volume ratio of 1:1, and 10 μl of mixture was dried on a gold covered glass slide to form the "coffee ring" for SERS measurements.

Headspace analysis of garlic headspace using SERS

25 μl of pure organosulfur standards, diallyl sulfide (DAS), diallyl disulfide (DADS), diallyl trisulfide (DATS), and other standard references were transferred to the 2 ml glass vials individually, and the mirror-assembled cap was then placed on the glass vial for a varied of time (under the room temperature) until the distinct SERS spectra was observed. To speed up the release of volatile compounds and to mimic the similar heating

condition of GC, 800 μl diallyl disulfide ethanolic solutions were incubated with the mirror in cap substrate in 2 ml glass vials for 5 minutes (with boiling water bath) for its quantitative analysis.

For freshly minced garlic and garlic extracts, 1 g minced garlic or 1 ml ethanol extract was incubated with the mirror in cap substrate in the glass vial to allow the volatile compounds in the headspace to interact with the substrate for 2 hours (under the room temperature) or for 5 minutes (with boiling water bath), respectively, until the SERS measurement.

The SERS measurements of the captured volatile compounds on mirror in cap substrate were performed using a Thermo Scientific DXR Raman Spectro-microscope with a 780 nm Laser source under the following conditions: 10× objective, 3.1 μm spot diameter, 5 mW laser power, 2s exposure time and 50 μm slit width for headspace analysis.

Headspace analysis of garlic headspace using GC

Headspace analysis of garlic headspace using GC was based on a previous established protocol [149]. The headspace profile was determined by gas chromatography (GC2010, Shimadzu, Columbia, MD) equipped with an auto sampler (AOC-20i, Shimadzu, Columbia, MD). Since the GC is coupled with an injection-based sampler, only ethanolic garlic extract or DADS solutions were analyzed. 1 ml of sample were stored in GC vials and 1 μl of sample solution was injected by an auto sampler and vaporized at 250°C in the injector, and then separated within an SH-Rxi-5 ms capillary column (15m × 0.25mm inner diameter × 0.25 μm). The GC column was programmed with the following settings: temperature starts at 80°C, and then is heated with a rate of

5°C/min to reach 100°C and held for 2 minutes. The overall analyzing time for each sample is 7 minutes. Helium was used as the carrier gas and the flow rate is set at 0.91 ml/min. Headspace profile of garlic was determined based on the matching with retention times of sulfides standards. Concentrations of dominate sulfides were determined based on the peak area and the calibration curve prepared with the sulfide standards.

Statistical analysis

In this study, all samples were measured within a Raman shift range of 400-2000 cm^{-1}. Raman spectra were analyzed using Thermo Scientific TQ analyst 8.0 software and the statistical differences of spectra were characterized via principle component analysis. In the principle component analysis, PC scores represent the most distinct regions and the sample variances of the spectra and they are ranked from 1-3 based on the significance of the variance in the overall spectrum. PC1, PC2, and PC3 for the PCA of spectra of organosulfur compounds and the garlic headspace were determined. Ideally, if the total amount of these variances is greater than 80%, it will suggest a significance of difference among the spectra [127]. The Raman readings at the signature peak 1632 cm^{-1} or the GC peak area of diallyl disulfide at 4.85 min of the headspace of DADS solutions were plotted as a function of DADS concentration, linear regression analysis and the nonlinear fitting analysis were both conducted using the GraphPad Prism to determine the best fitting model for quantification.

Results and discussion

Headspace characterization of minced garlic

The assembly of mirror-in-cap substrate is shown in Figure 27 (A). AgNPs mirror on the aluminum foil was cut into the size fitting in the cap for 2 ml glass vial and fixed

on the cap with a double side tape. The headspace profile characterization of garlic using the mirror-in-cap substrate is illustrated in Figure 27 (B) and the spectra of garlic headspace is shown in Figure 27 (C). High intensity distinct peaks are observed in the Raman shift of 1632, 1400, 1291, 1191, 731, and 577 cm^{-1}. As a representative *Allium* species plant, garlic is rich in organosulfur compounds [150]. Therefore, to determine the corresponding volatile compound in the garlic headspace, a set of organosulfur compounds reported from the *Allium* species plants were tested using the colloidal silver nanoparticles substrate and spectra were shown in the supporting information. After the bands assignment, it was found that diallyl sulfide (i.e., DAS) showed the most similar peak assignments to the distinct bands acquired from the garlic headspace. Even though extra peak and shifted peak were still observed at the Raman shifts of 1606 and 710 cm^{-1} for DAS, this result suggested that the dominate compounds might be corresponding to DAS or other sulfides. To be noted, the headspace SERS spectra showed a much higher resolution than the spectra of chemical standards obtained from coffee rings. This finding agreed with a previous work that headspace showed improved resolution because of the less interreference from the environment [35].

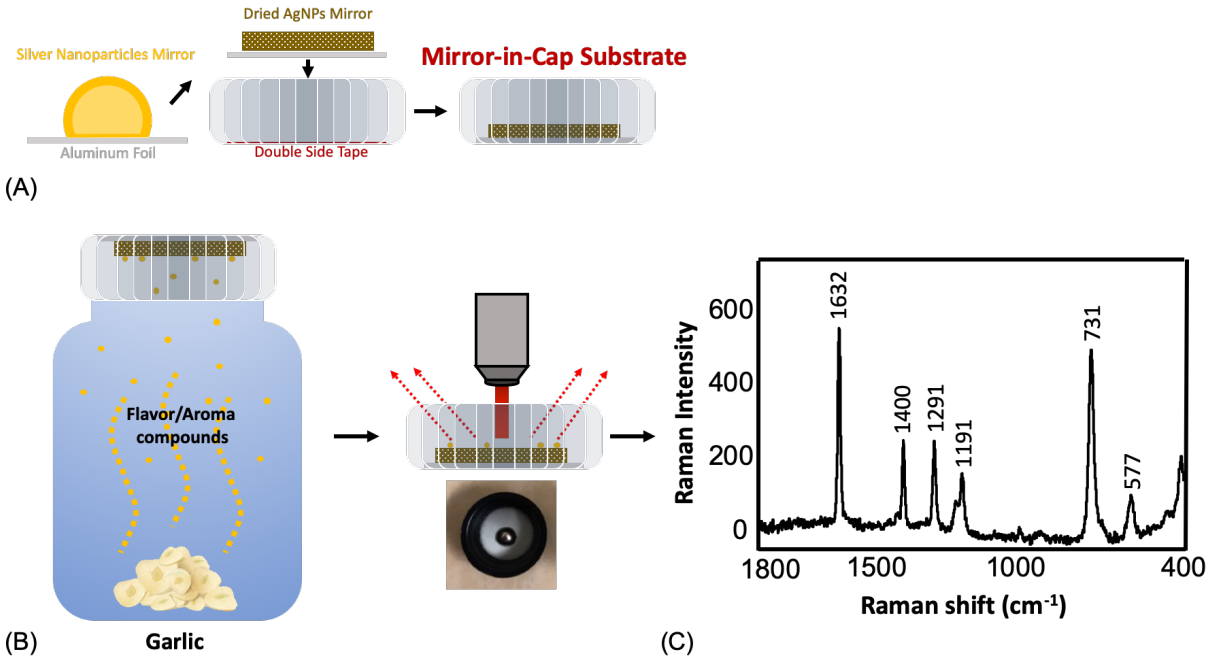

Figure 27 (A) Assembly of the "mirror-in-cap" SERS substrate. (B) Illustration of the headspace analysis of minced garlic. (C) SERS spectra of the headspace of minced garlic.

With more detailed literature reviews, allicin was found to be the dominant flavor compound in the garlic. Due to its unstable chemical structure, allicin can be easily oxidized into a group of organosulfur compounds that are responsible for the garlic flavor and named as the garlic oil. In the garlic oil, the major compounds are diallyl sulfide (DAS), diallyl disulfide (DADS), and diallyl trisulfides (DATS) [150–153].

To further investigate the corresponding organosulfur compound, pure DAS, DADS, and DATS were tested with the mirror-in-cap substrate under room temperature until distinct Raman spectra were obtained. Their SERS spectra and chemical structures are shown in Figure 28 (A). Due to their similar chemical structures, DAS, DADS, and DATS all showed distinct peaks as the garlic headspace spectra at 1632, 1400, 1291, 1191, and 577 cm^{-1}, however, additional peaks were observed from 1606 cm^{-1} for DAS and from 1550 $cm^{-1}$for DATS. Among three compounds, only DADS exact peak

assignments as the garlic headspace spectra. To investigate the matching of spectra, the garlic ethanolic extract was also analyzed under the same condition as standards, and its spectra (in Figure 4 (A)) was compared with spectra of three standards using principle component analysis in Figure 28 (B). According to the PC scores listed in the Figure, the total sample variance is greater than 80%, which suggested the presence of significant differences among spectra. From the cluster analysis, the garlic headspace spectra are completely separated from spectra of DAS and DATS, whereas the DADS spectra are found located at the same cluster. This result demonstrated that the even though the garlic headspace is constituted by many volatile compounds, the diallyl disulfide (DADS) is presumably the dominate and corresponding compound to represent the garlic headspace through the SERS measurement. This speculation actually agreed with a published result and some references also pointed out that the DADS is one of the most abundant compounds in the garlic oil that is occupying 22-40% [34,151]. Interestingly, the pure standard of DATS took significantly longer time (i.e., 2 hours) to appear distinct spectra than other two compounds (less than 1 hour) under room temperature. After the investigation, the delay of appearance of Raman peaks in DATS could be caused by its high boiling point. According to the Food and Agriculture Organization of the United Nations, under 760 mmHg, the boiling point of DAS is 141°C, DADS is 185°C, while DATS is 229°C. Therefore, under the room temperature, both DAS and DADS can be quickly detected by mirror-in-cap substrate under room temperature but DATS cannot.

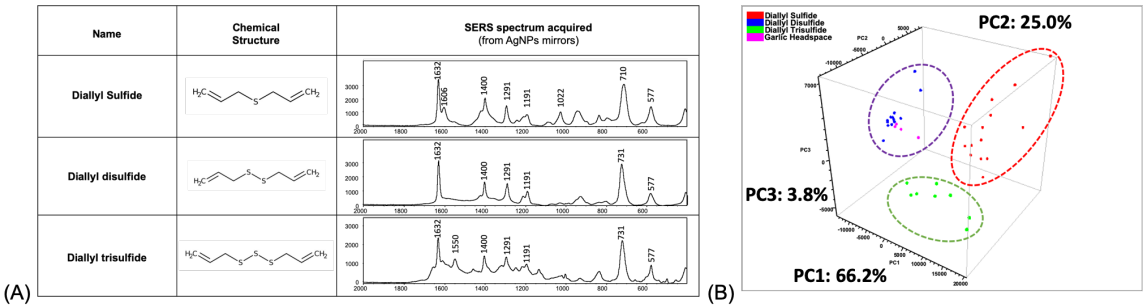

Figure 28 (A) Three major sulfides in garlic oil and their corresponding SERS spectra. (B) Principle component analysis of the SERS spectra of three sulfides and garlic headspace.

Even though distinct SERS spectra can be obtained from DADS and garlic samples, the incubation time is still too long for a fast detection method, especially for lower concentrations. In standard GC method, a heating process is always required for the headspace analysis. Therefore, to mimic the GC analyzing condition and to speed up the release of DADS to the headspace, a boiling water bath incubator was used to provide a temperature-stable heating environment for the DADS samples. 500 ppm DADS in ethanol in the glass vial capped with the mirror was heated in the boiling water bath and its SERS measurement was compared to the DADS sample incubated under the room temperature. As shown in Figure 29 (A), in only 5 minutes, the distinct DADS Raman spectra were observed at a similar intensity level as the sample incubated under the room temperature for 2 hours (Figure 29 (B)). Additionally, as shown in Figure 29 (B), only AgNPs mirror spectra can be observed after 5 minutes incubation under the room temperature. This finding suggested that the heating process is very important to help the release of DADS to headspace and can effectively shorten the sample incubation time.

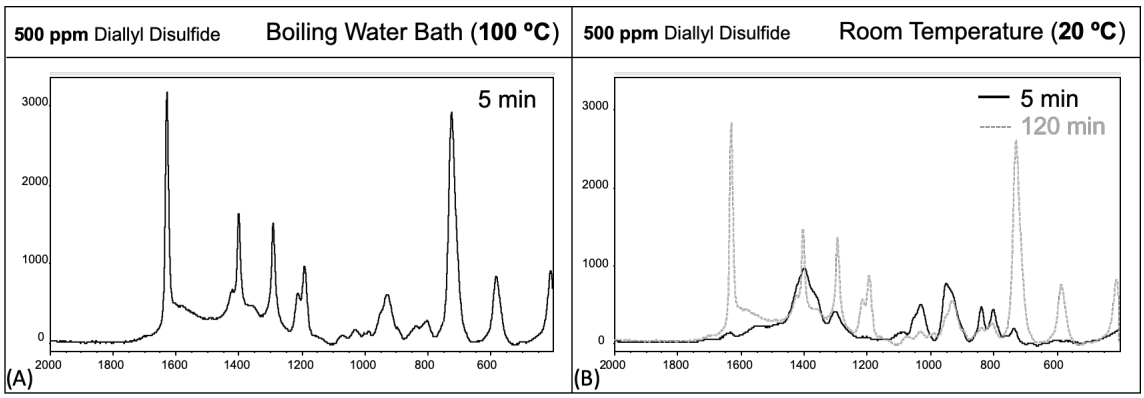

Figure 29 (A) SERS spectra of the headspace of 500 ppm DADS in ethanol incubated with boiling water bath for 5 minutes. (B) SERS spectra of the headspace of 500 pm DADS in ethanol incubated under room temperature for 5 minutes and 2 hours.

Quantification of the concentration of DADS in the headspace of garlic ethanolic extract

After showing SERS's capability in the garlic headspace characterization, the ability of SERS in the quantification of the DADS in the garlic headspace was further investigated. Since it is hard to build the equivalency of the interpretation of concentration between a pile of solid garlic matrix and the DADS in ethanol, and the GC instrument is injection-based, the garlic extract prepared by immersing freshly minced garlic in ethanol (10 g garlic in 10 ml ethanol) was used as the target. The headspace profile of the ethanolic garlic extract (ethanol only) was compared with the DADS standards in ethanol.

All samples are incubated in the boiling water bath for 5 minutes and the spectra of the headspace of garlic ethanolic extract is shown in Figure 30 (A). In the spectra, all distinct bands, as expected, matched the spectra of headspace of the minced garlic shown in Figure 27 (B) and there are no signature peaks of DAS and DATS observed in the spectra. To be noted, to prevent the interreference, 1% DATS in ethanol (much higher than its inherent concentration in garlic, i.e., 0.08%) in ethanol was also tested in water

bath for 5 min, however, due to its high boiling point of DATS, no signature peaks were observed (data not shown). For the quantification of DADS, its distinct peak at the Raman shift of 1632 cm^{-1} was chosen as the reference band and the intensity was plotted as a function of the concentration of DADS from 1-500 ppm in ethanol to build the calibration curve in Figure 4 (B). A positive correlation was observed between the intensity and the concentration of DADS, however, the trendline seemed to be not linear. According to the literature review, the release of DADS from the food system to the headspace followed a second order saturation decay because its release rate decreased gradually when the headspace is being saturated [154]. This presumably explained why Raman intensity readings were not proportional to the concentration, as the headspace might also be getting saturated by DADS during heating and resulted in a deceleration of releasing. Therefore, a second order prediction model was built in Figure 30 (B) with a goodness of fit of 99.72%. The equation represented the calibration curve was shown below,

$$\text{Raman Intensity} = -0.01 \times \text{concentration}^2 + 11.5 \times \text{concentration} + 86.9$$

In the spectra of the headspace of the garlic extract, the intensity of the peak at 1632 cm^{-2} was measured as 1465. After plotting back to the prediction model, the concentration of DADS in the garlic extract headspace was determined as 135 ppm.

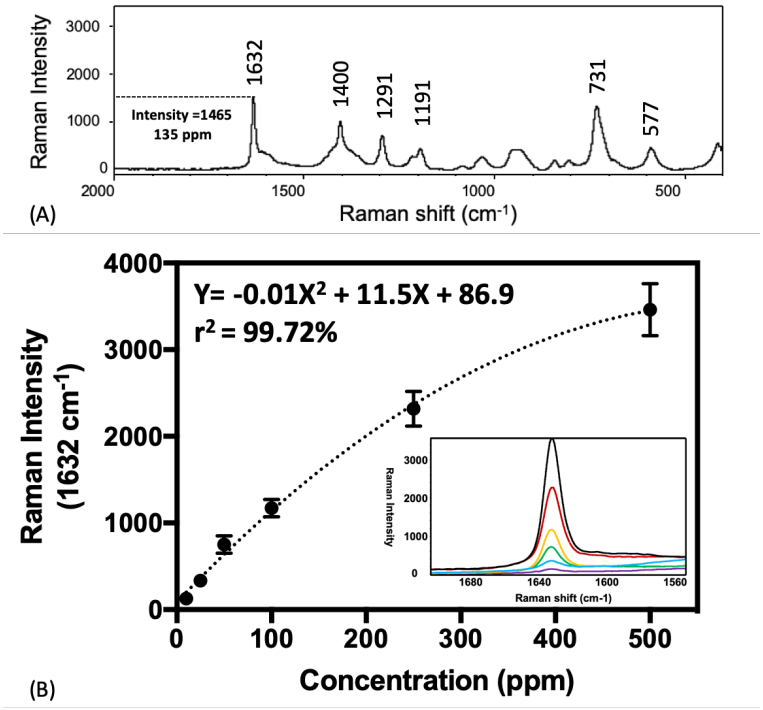

Figure 30 (A) SERS spectra of the headspace of garlic ethanolic extract. (B) Raman intensity at 1632 cm-1 plotted as a function of the DADS concentration. The coefficient of determination and the equation are displayed.

To validate the result obtained from the mirror-in-cap substrate, standard gas chromatography was performed for same samples following a well-established protocol [149]. Figure 31 (A) shows the chromatogram of garlic extract, DADS, and ADS. According to the retention time of DADS (4.85 minutes) and ADS (2.1 minutes), both of them were found to be present in the headspace of the garlic extract, and the DADS is dominating in the chromatogram with a concentration of 112 ppm determined by the calibration curve.

After comparing the results obtained from GC and SERS, it was found that the concentration of DADS obtained from GC method (i.e., 112 ppm) is relatively lower than the SERS (i.e., 135 ppm). In SERS, the peak of 1632 cm^{-1} represents the vibration of the

C=C stretching, which is a functional group not only in the structure of DADS but also in DAS, DATS, and some other garlic constituents. Therefore, the intensity of the 1632 cm^{-1} is considered as the sum of all those compounds, hence, the determined concentration of DADS was slightly higher. However, according to the literature and the GC results, since the DADS is the dominant compound in garlic, the interreference from other compounds can be considered as minimal, and it justified the capability of SERS in the garlic headspace analysis.

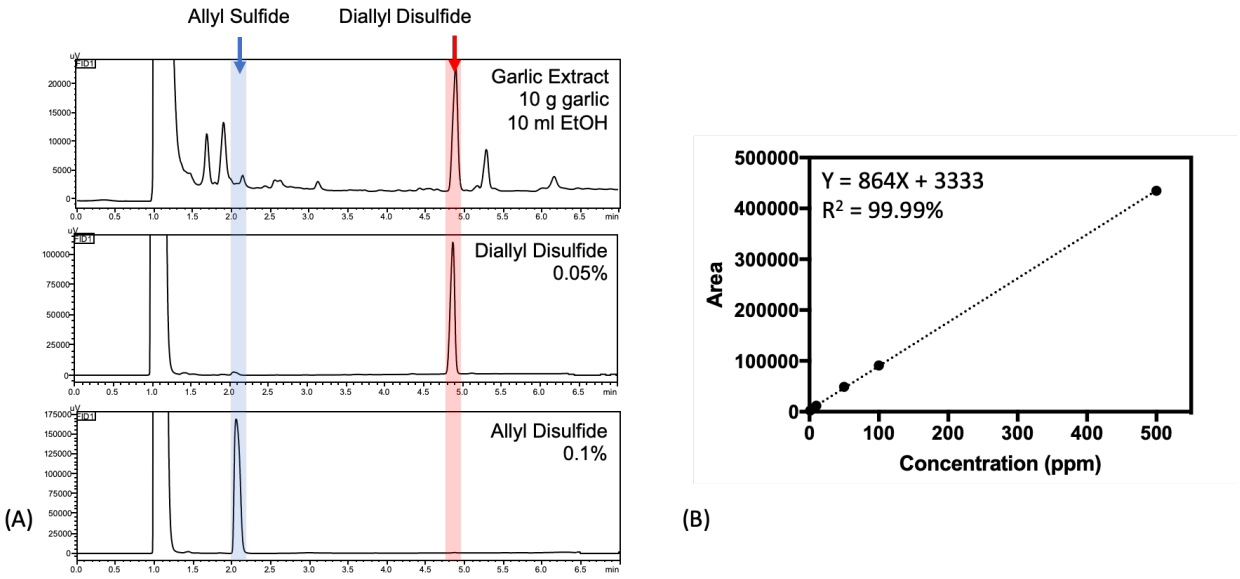

Figure 31 (A) Chromatogram of the garlic extract in ethanol, 0.05% DADS in ethanol, and Allyl Disulfide in ethanol. (B) The calibration curve of the DADS, the area of band plotted as a function of concentration of DADS.

Conclusion

Table 6 Analytical behaviors comparison between GC and SERS

	Gas Chromatography	SERS
Analyzing Time	7 minutes for each sample	**1 minute for each sample**
Sample Pretreatment	Sample might need to be filtered for the protection of columns	**5 min boiling water bath for a batch of samples**
Lowest detectable concentration	**5 ppm**	10 ppm
Coefficient of Determination (r^2)	**99.99%**	99.72%
Determined DADS Concentration in Headspace of Garlic Extract	**112 ppm**	135 ppm

Table 6 showed the analytical behaviors between GC and SERS methods for the characterization of the garlic headspace. Compared to the GC results, the mirror-in-cap SERS method showed a much shorter overall analyzing time and a simpler sample preparation, since GC might require a sample cleaning step to protect the column from cogging which will increase the sample preparation time, but SERS does not require any sample cleaning. Although the SERS method also requires a heating step, since samples can be incubated together in a big batch, the sample preparation time will maintain the same as 5 minutes. However, even though the SERS method is promising in the profiling of DADS in the headspace of garlic, the lowest detectable concentration, the coefficient of determination, and the accuracy still need to be improved. Additionally, many volatile compounds are very unstable which will cause a consistent changing of headspace profile [155]. This is a huge limitation for the current chromatographic headspace detection methods, since samples might take days to be delivered and to be analyzed, when the profile has already changed dramatically, and the target might be lost. On the other hand, the availability of portable Raman device enables the potential on-site measurement of SERS, this technique will have more potentials to be used for the real-time characterization of volatile targets and the monitoring of headspace changing during the manufacture and processing. Future study will focus on the further improvement of the sensitivity and quantitative ability and the extension to study other essential volatile compounds in food products.

7. DEVELOPMENT OF A FACILE ROLLING METHOD TO AMPLIFY THE ANALYTE OF WEAK SERS ACTIVITY IN FOOD

Introduction

Surface enhanced Raman scattering (SERS) combined the nanotechnology and Raman scattering. The SERS techniques have shown great advantages in terms of the sensitivity and speed and has been developed as a rapid analytical tool for various pesticides [40,124,156,157]. However, strong Raman scattering cannot be always obtained, since not all chemical structures are Raman sensitive to produce strong scattering and some molecules do not have strong affinity to the nanoparticles to generate sufficient signal enhancement [7,158].

To date, methods to amplify the weak SERS intensity of interested analytes are based on three mechanisms: (1) generating more hot spots such as the fabrication of ultra-sensitive SERS substrates and inducing aggregation of nanoparticles using ionized agents. However, they suffered from complicated fabrication or uncontrollable aggregation. (2) Enhancing the binding such as using the ligand to improve the affinity of the targeted molecules to nanoparticles, but this will introduce foreign chemicals into the sample and many efforts need to be made to choose the ligand molecule and to optimize the binding enhancement. (3) Increasing the concentration of analytes such as enriching the targets to enhance interaction of the analytes with nanoparticles by using vacuum concentrator, but it is highly dependent on expensive instruments and the final volume of the sample is hard to control [15,159–165]. More importantly, for label-based methods and deliciated substrates, the determination of their amplification performance are mostly

based on the signal enhancement of SERS sensitive probes other than the weak-SERS-signal analytes, which are real concerns in industrial applications [166].

Therefore, in this study, the objective is to develop a simple sample preparation method to enrich the analyte without the use of any instrumentations, and to amplify the weak SERS activities of the target. A organochloride pesticide, chlordane, was chosen as the probe due to its weak affinity to nanoparticles and its Raman inactive inherent chemical structure [160,167].

Materials and Methods

Materials

Chlordane, methanol, and hexane were purchased from Thermo Fisher Scientific in Waltham, MA. Chloroauric acid tetrahydrate (i.e., $HAuCl_4$) and sodium citrate are purchased from Sigma Aldrich in St. Louis, MO. A real livestock oil sample was provided by Diversified laboratories, Chantilly, VA, 20151 and used to challenge the method for real application

Synthesis of gold nanoparticles (AuNPs)

2 ml 1% $HAuCl_4$ was mixed with 200 mL ultrapure water and stirred at 350 rpm under 310 °C. When solution began to boil, 1.4 ml 1% sodium citrate solution was added to the solution. The mixture was kept heating and stirring for another 30 minutes, until the color changed from transparency to black, then to brick red, which indicated the formation of AuNPs. The AuNPs solution was then diluted to 200 ml to reach the final concentration of 0.1 mg/ml. The size of AuNPs was determined as 55 nm using the Malvern Mastersizer.

Sample preparation of chlordane with AuNPs solution using the traditional mixing method

Chlordane was prepared in 50% methanolic solution at the concentration of 0.5 ppm to 10 ppm. 2.5 or 10 μl of chlordane solution was mixed and incubated with 2.5 μl 1 mg/ml AuNPs solution on a parafilm for 30 seconds, then transferred and air dried on a gold covered glass side for the SERS analysis.

Sample preparation of chlordane with AuNPs using the rolling method

Parafilm was washed with 50% methanolic water solution and dried to work as a platform for rolling method. 2.5 μl of chlordane solution was mixed with 2.5 μl 1 mg/ml AuNPs solution on the parafilm and then sucked up and pressed down using a pipette within a pipette tip for 10-20 seconds, until half of the volume of mixture was evaporated (i.e., the final volume of mixture remained at 2.5 μl). Subsequently, another 2.5 μl of chlordane solution was added to the mixture and pipetted until half of the volume was evaporated. Repeat the action for 1-4 times, then the mixture was transferred and dried on a gold covered glass slides for the SERS measurement.

Extract of chlordane form crude oil

Chlordane was initially dissolved into the hexane and added to the crude oil to make the final concentration to 1 ppm. 50 μl methanol was then added to 50 μl oil sample in a microcentrifuge tube and the mixture was vortexed vigorously. The mixture was further centrifuged at 10,000 rpm under refrigerator temperature (i.e. 4 °C). Once the separation of two phases was clearly observed, the methanol phase was transferred out and incubated with AuNPs or rolling method for SERS analysis.

Instrumentation and Data analysis

In this study, the SERS measurements were performed using a Thermo Scientific DXR Raman Spectro-microscope with a 780 nm Laser source under the following conditions: 20× objective, 3.1 μm spot diameter, 5 mW laser power, 2s exposure time and 50 μm slit width for chlordane detection. All Raman spectra were analyzed using Thermo Scientific TQ Analyst 8.0 software. All Raman intensities were averaged from at least ten replicates and standard deviations were recorded. The distinct peak at 552 cm^{-1} was chosen for further characteristic analysis of chlordane. Raman intensity, rolling times, and chlordane concentration were plotted as a surface using the Microsoft Excel. Since chlordane is enriched after the rolling, the overall concentration (i.e., calculated by multiplying the rolling times to the chlordane concentration) was introduced to simplify the correlation. The linear regression analysis was applied to the plot of Raman intensity to the overall concentration and a mathematic model was determined by using the Prism (Graphpad) along with the determination of coefficient (i.e., r^2) and the trendline.

Results and discussion

Evaluation of the amplification capability of the rolling method to enhance chlordane SERS signals

Organochlorine pesticide, chlordane was prepared in a methanolic solution, and then mixed with synthesized AuNPs solution. After the incubation and air-dried on a gold covered glass slide, as shown in Figure 1 (A), chlordane showed its distinct SERS spectra at the 552 cm^{-1}, attributed to the stretching vibration of ν(C-Cl), whereas no obvious SERS peaks were observed at the background spectra of AuNPs [135,168]. However, according to Figure 32 (B), the SERS spectra (i.e., Raman intensity at 552 cm^{-1}) of

chlordane decayed extremely fast with the decrease of concentration of chlordane and became very noisy after the concentration reduced to 2.5 ppm. Once the concentration was below 1 ppm, the signature peak of chlordane can be barely observed. Since the organochlorine pesticides have a weak affinity to nanoparticles, this fast disappearance was presumably caused by weak signal Raman signal enhancement of the vibration stretching of *v*(C-Cl) at low concentrations [164].

Based on the Figure 32, to enhance the interaction between chlordane and AuNPs, sufficiently high concentration of chlordane is required (i.e. 1 ppm). However, according to the EPA report, the required detection limit of chlordane concentration is much lower [169], therefore, an evaporation triggered enriching method to enforce sufficient interactions between analytes and nanoparticles is developed. This approach named as rolling method and the objective of it is to amplify the weak SERS signals of chlordane.

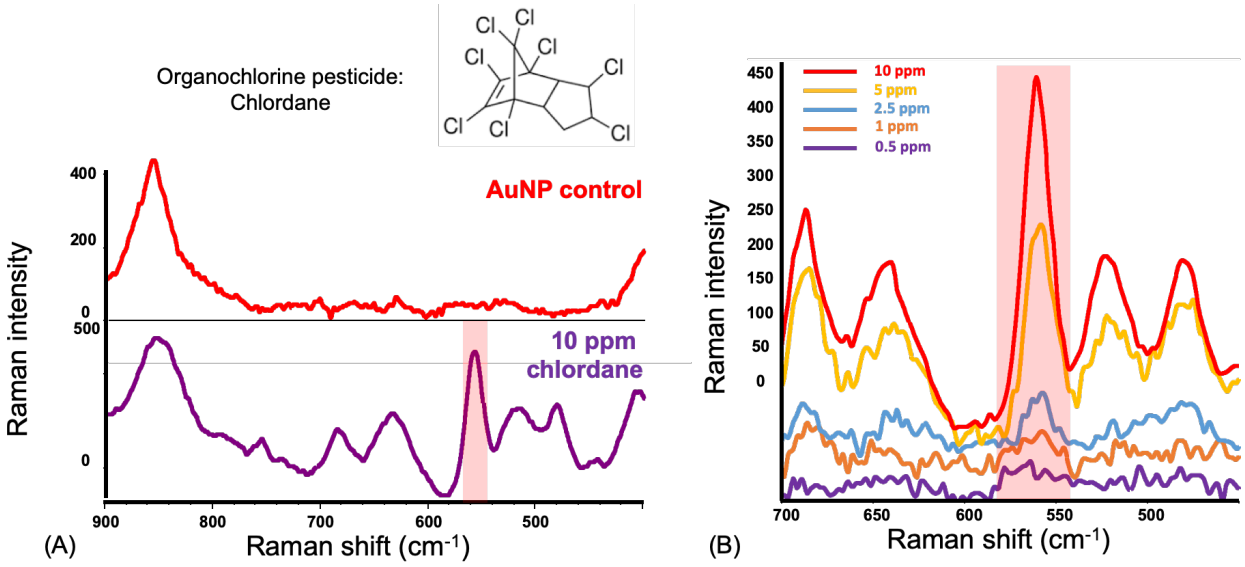

Figure 32 (A) SERS spectra of 10 ppm chlordane and AuNPs. (B) SERS spectra of chlordane at the concentration from 0.5 ppm to 10 ppm.

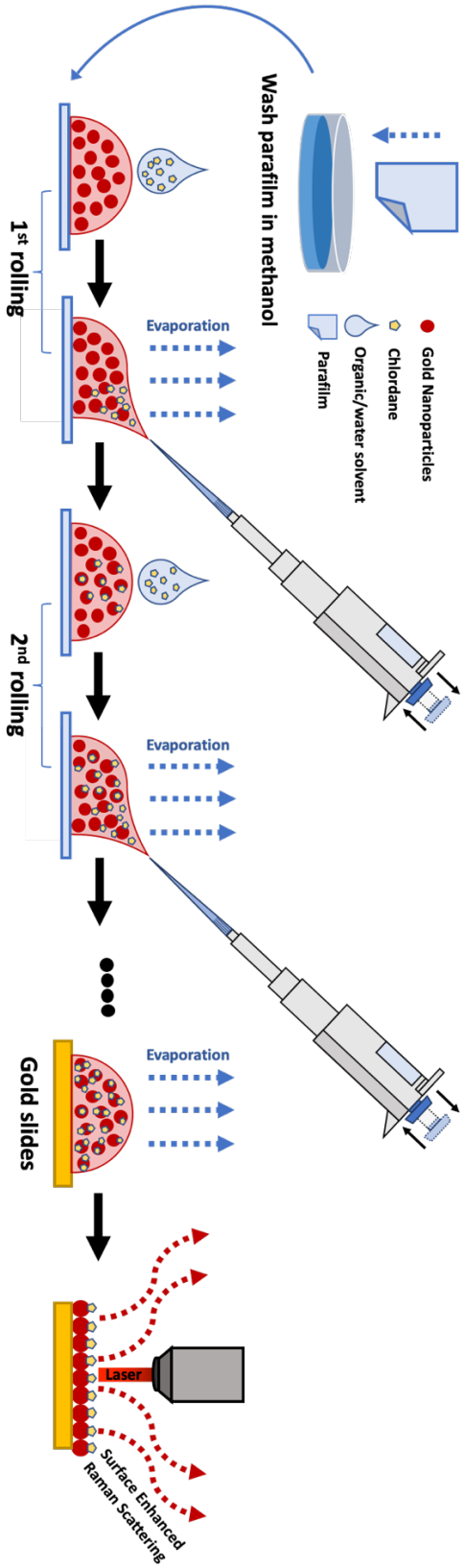

Figure 33 Schematic illustration of the rolling method.

During the solvent evaporation, rolling method is hypothetically to enrich the analyte and to induce the interaction between AuNPs and the chlordane, hence, to amplify the SERS signal. In this study, AuNPs are stabilized by citrate and dispersed in the water solution and then mixed with chlordane in 50% methanolic solution on a parafilm. The parafilm here worked as a hydrophobic platform to prevent the spreading of the sample and to speed up the evaporation. The parafilm was initially washed with methanol to remove the residues that could induce the aggregation of the nanoparticles (to be noted, aggregation of nanoparticles could result in the failure of rolling since aggregated nanoparticles might lose their function to interact with the targets). After washing, a drop of sample (i.e., 2.5 μl chlordane solution) was dripping to a drop of AuNPs dispersion (i.e., 2.5 μl) and the mixture was sucked up and pressed down within a tip using pipetted for 10-20 seconds on the parafilm. Constant pipetting allowed the AuNPs to sufficiently interact with chlordane during the mixing in the pipette tip. At the same time, due to the relatively low sample volume (i.e., 5 μl in total) and the presence of methanol, the mixture was evaporating fast during the pipetting, and the action will stop once the mixture reduced to half of volume (i.e., 2.5 μl). During this process, the solvent volume shrunk half but the concentration of chlordane was doubled compared to the initial sample, and this conclude the process as the first time rolling, as shown in Figure 33. Since the interaction between AuNPs and chlordane was weak, increased concentration of chlordane from one rolling might still not enough to generate a strong SERS signal. Therefore, in the next step, another one drop of sample (i.e., 2.5 μl) was added to the remaining mixture and the pipetting step was repeated. After the mixing, the water and solvents were evaporated to half volume once more, but the total volume still

remained the same level as the finish of the first rolling. However, the concentration of chlordane was further increased, and more analytes were presumably pushed to interact with AuNPs. This repeated action was considered as the second time rolling. The rolling process can be repeated many until the satisfying SERS spectra was observed.

To be noted, the mechanism of rolling method for the enrichment of chlordane is very similar to the vacuum concentrator. However, the rolling method only used the pipette to accelerate the evaporation, and only required smaller volumes of samples. Therefore, this approach offers a more cost effective and faster solution for the concentrating (i.e., 5 μl in total).

With more repeating times of rolling, more chlordane was forced to interact with the AuNPs until hotspots on nanoparticles were saturated. Hypothetically, the SERS intensity of signature peaks of chlordane should also increase along with the increasing times of rolling. Therefore, three concentrations of chlordane in standard solution, 0.5 ppm, 1 ppm, and 2.5 ppm were prepared with one to four rolling times to test the hypothesis.

As shown in Figure 34, with the increase of rolling times, the intensity of chlordane distinct peak at 552 cm^{-1} indeed increased, despite in low or high concentrations, which suggested that rolling method is able to amplify the Raman signals of chlordane, even at low concentration level. In this research, only up to four times of rolling were conducted, but the increasing trend of the Raman signal suggested that this approach could even amplify the signal of analytes to much higher level hypothetically with further rolling, until reach the satisfaction. However, to be noted, too many times of rolling could result in the over aggregation of nanoparticles which could cause the

quenching of Raman signal. Furthermore, sample deposition could be another critical step in the preparation of rolling method. As stated previously, the deposition of sample has to be done one drop by another, not only to achieve an effective evaporation, but also to enhance the weak interactions between the chlordane with AuNPs.

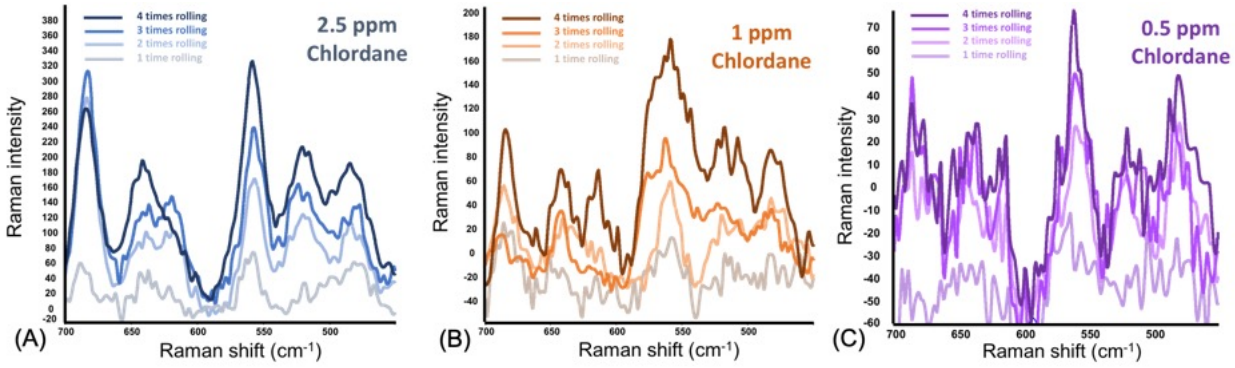

Figure 34 SERS spectra of (A) 2.5 ppm, (B) 1 ppm, (C) 0.5 ppm chlordane with 1-4 times rolling.

The sample went through the rolling method is hypothetically to achieve similar concentration level and SERS signal as a more concentrated sample; for an example, a 1-ppm chlordane sample with four times of rolling presumably owns similar Raman signals with a 4-ppm chlordane sample mixed with AuNPs solution directly.

To test the hypothesis, the performance of the enrichment of the rolling method was compared with the traditional sample preparation method (i.e., the comparation between a sample prepared using rolling method and a sample with higher inherent chlordane concentrations or a sample with higher volume sizes).

As shown in Figure 4, samples were prepared in the following manner, and to simplify the language, they will be named as Method (A): sample with higher inherent chlordane concentration: 2.5 µl concentrated chlordane 50% methanolic solution (i.e., 4 ppm) was mixed with 2.5 µl AuNPs dispersion, Method (B): sample prepared with

rolling method, 2.5 μl 1 ppm chlordane in 50% methanolic solution was prepared with 4 times of rolling with 2.5 μl AuNPs dispersion, and Method (C): sample with larger volume size, three times more volume size of 1 ppm chlordane in 50% methanolic solution (i.e., 10 μl) was mixed with 2.5 μl AuNPs dispersion.

After the Raman measurement, spectra of three samples are shown in Figure 34 (D). Chlordane signature SERS spectra were all observed in three spectra. However, at the distinct area, both Method (A) and Method (B) showed very similar intensity level while significantly lower signals were observed from Method (C). Low Raman intensity from Method (C) is presumably due to the large sample volume size. According to the sample picture in Figure 4 (C), a much larger size "coffee ring" (i.e., Aggregated AuNPs and Chlordane) was formed but sample sizes in Figure 35 (A) and (B) were similar. Therefore, AuNPs were highly diluted with a larger ring size and the interaction between chlordane and AuNPs were also further weakened. This discovery suggested that due to the large volume size and the dilution of AuNPs, Method (C) (i.e., increasing sample volume size) cannot achieve the similar SERS performance as the rolling method.

Compared the Raman intensity of Method (A) and Method (B) at the chlordane distinct area (i.e., 552 cm^{-1}) in Figure 35 (E), no significant differences were observed, which means the intensity of 1 ppm of chlordane with 4 times rolling is equivalent to that of 4 ppm chlordane. According to the previous statement, one time of rolling can double the concentration of chlordane once extra solvents are evaporated and the volume of sample mixture remains the same as that before the rolling. Therefore, with four times of rolling of 1 ppm chlordane sample, the final concentration of the mixture was presumably enriched to 4 ppm, and as shown in Figure 35 (E), the hypothesis was supported.

These results suggested that the rolling method has a very promising enrichment efficiency, and also can amplify the sample signal equivalently.

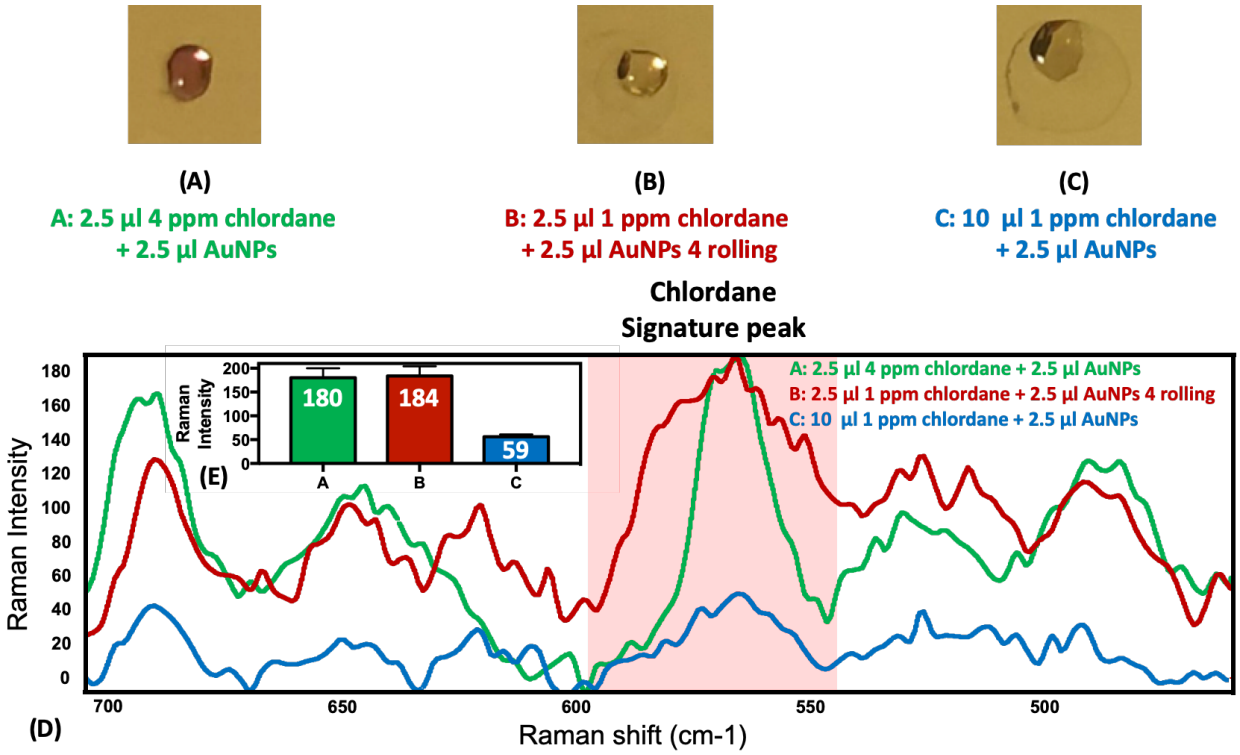

Figure 35 (A)-(C) Different sample preparation of chlordane solution and AuNPs solution, (D) SERS spectra of samples with different preparation, (E) Raman intensity of the distinct peak of chlordane at 552 cm-1 from three sample preparations.

Modeling the correlation between Raman intensity, concentration and rolling times and its application for chlordane detection in oil

In the previous section, all chlordane samples were analyzed with known concentrations, however, in the practical cases, the concentration of chlordane was always unknown and need to be determined. Due to the uncertainty of the chlordane concentration in real samples, it was hard to determine the times of rolling to achieve a satisfied Raman signal. Since Raman signals were amplified with increasing of rolling times and 1 ppm chlordane sample with 4 times of rolling showed an equivalency of the Raman signal with a 4 ppm chlordane sample, a positive correlation could be determined

between Raman intensity and rolling times and the concentration of chlordane in samples. Therefore, to simplify the rolling method, a mathematic model was attempted to build for the deamination of the number of rolling times or the concentration of analytes with an acquired Raman intensity.

With data acquired from different concentrations, rolling times, and Raman intensities in Figure 36, a tridimensional surface map was plotted in Figure 5 (A), where x axis referred to the concentration of chlordane, y axis referred to the number of rolling times, and z axis referred to the Raman intensity. In the surface plot, Raman intensity showed an increasing trend as a function of either the time of rolling or the concentration of chlordane, however, the presence of three variables (i.e., Raman intensity, rolling times, and concentrations) in the model made the correlation hard to be determined, therefore, the plot need to be simplified.

As we know, Raman intensity is positively correlated to the chlordane concentration (in Figure 32 (B)), and Raman intensity of 4 ppm chlordane is equivalent to 1 ppm chlordane with 4 times of rolling (in Figure 35 (E)), therefore, combining sample concentration and the rolling time as one variable (i.e., overall concentration) can presumably simplify the correlation model. In Figure 36 (B), Raman intensities were plotted as a function of the overall concentrations collected from all data points, and a trendline was added with the correlation analysis. The goodness of the fit (i.e., r^2) was determined as 0.8289, and the Raman intensity can be calculated from the following model,

$$\text{Raman Intensity} = 23.96 \times \text{overall concentration} + 33.67$$

where overall concentration can be calculated by,

$$\text{Overall concentration} = \text{Time of rolling} \times \text{sample concentration}$$

Therefore, in the real analysis, with the acquired Raman signal and the number of rolling times, the residual concentration of chlordane in samples can be calculated form the prediction model.

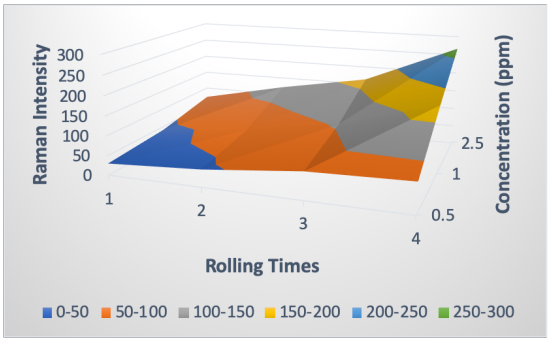

(A)

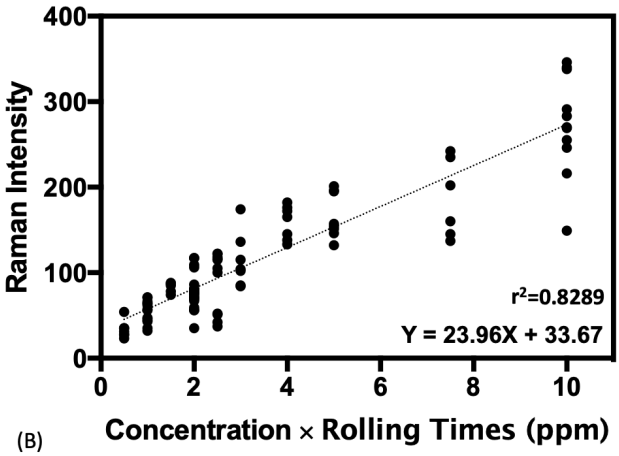

(B)

Figure 36 (A) Actual 3D plot of Raman intensity with concentration of chlordane and rolling times. (B) Predicted mathematic model (Plot of Raman intensity with concentration multiplied by rolling times).

To investigate the reliability of the prediction model, a crude oil sample spiked with 1 ppm chlordane was tested. The spectra of crude oil (control) and 1 ppm chlordane in crude oil with or without rolling were shown in Figure 37. Signature peak of chlordane can be barely observed without rolling in Figure 37 (A) and this could be due to the presence of several interferent peaks from the crude oil in Figure 37 (C). However, the interreference of crude oil did not prevent the detection of distinct peaks of chlordane after 4 times of rolling in Figure 37 (B). The Raman intensity of the signature peak of chlordane at 522 cm^{-1} was measured as 125.2. As shown in Table 7, by plotting the measured Raman signal into the prediction model with 4 times of rolling, the predicted concentration of chlordane was calculated as 0.953 ppm, compared to the actual spiked

chlordane concentration (i.e., 1 ppm), the recovery value of the predicting model reached 95.5% approximately. In another way, by plotting 1 ppm with 4 times of rolling into the prediction model, the predicted Raman intensity was calculated as 129.5, after comparing to the actual Raman intensity reading (i.e., 125.2), the recovery value of the prediction model reached 96.5%. Both prediction models gave fairly satisfactory recovery values, suggesting ed that the rolling method combined with the mathematic model could be used for determining the residual concentration of chlordane, even in complex system with considerable interferences, such as the crude oil. However, as shown in Figure 37, the noise interreference from the matrix could also be accumulated with increasing times of rolling, therefore, a proper extraction step might be needed to provide a cleaner background.

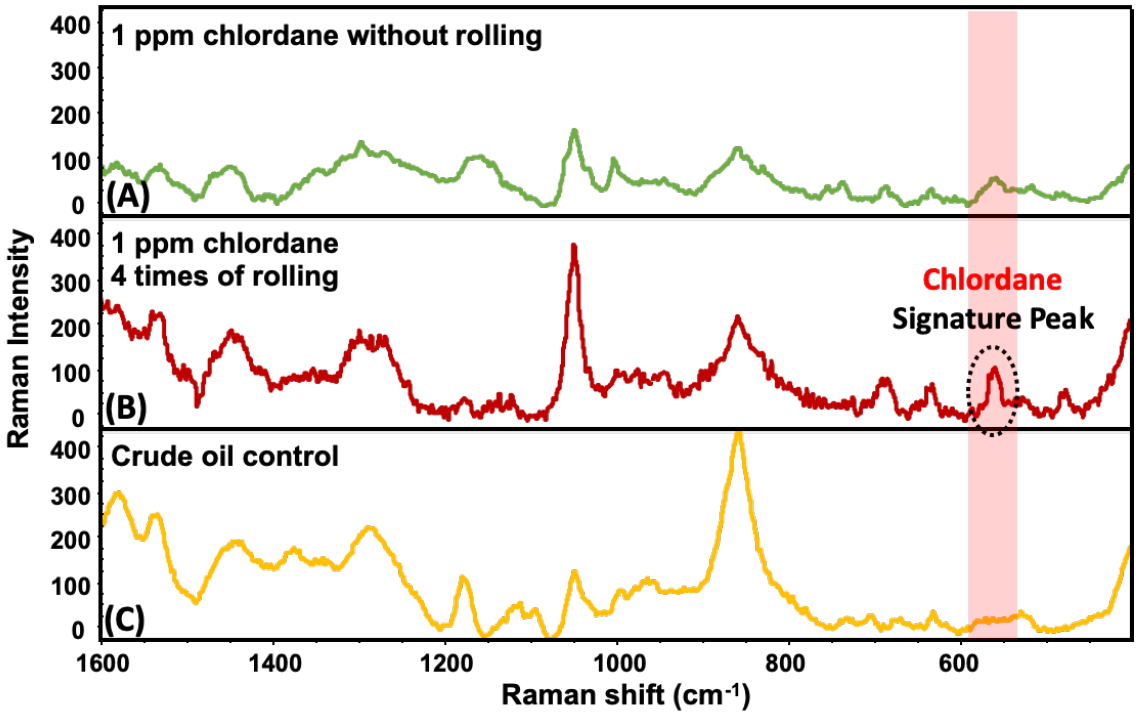

Figure 37 (A) SERS spectra of 1 ppm chlordane in crude oil (B) SERS spectra of 1 ppm chlordane in the crude oil with 4 times of rolling. (C) SERS spectra of the crude oil.

Table 7 Accuracy of the rolling method and mathematic model in the detection of chlordane in crude oil.

	Actual value in crude oil from rolling method	Prediction value from mathematic method	Recovery (%)
Raman Intensity	**125.2**	**129.5**	**96.5**
Concentration	**1.000 ppm**	**0.953 ppm**	**95.5**

Conclusion

As a conclusion, the rolling method provides a very simple sample preparation approach to enrich the analyte in a limited volume of sample, and to amplify the analytes' weak SERS signals. For analytes having weak interactions with nanoparticles, the rolling method can presumably improve the detection to a much better level without using any costly instrumentations such as centrifugal vacuum concentrator or pretreatments such as chemically linking. Combined the rolling method with an established prediction model, concentrations of chlordane in complex samples can be easily determined based on the actual Raman intensity readings and the times of rolling with a promising recovery value. Except for the pesticides tested in this study, the rolling method is expected to be applied in the detection of other analytes showing weak Raman intensities. To be noted, the rolling method is only potentially targeting to amplify the signal of targets with weak affinity to nanoparticles. If the binding of the target is strong to nanoparticles, the rolling step could induce the aggregation and cause the quenching of signals. In the future, the capability of rolling method for other targets and its reliability in other food matrix (such as fruit juices) should be further investigated.

8. SUMMARY

In this dissertation, we demonstrated a facile fabricated self-assembly AgNPs mirror substrate and a simple rolling sample preparation method to improve the sensitivity, selectivity, and quantitative ability of surface-enhanced Raman spectroscopic analysis in food.

Firstly, the successful fabrication of AgNPs mirror substrate using the interface between polar and non-polar solvents provided a very simple approach to manufacture a uniform SERS substrate compared to the currently available reproducible substrates which are suffering from the complicated fabrication.Additionally, the AgNPs mirror showed great reliability in the quantitative analysis of fonofos pesticide in water and commercially available juices and teas. The mirror substrates offered a great control of the arrangement of nanoparticles and solved the reproducibility problem (caused by the randomly aggregation of NPs) that is bothering the SERS to become a reliable quantitative tool in food analysis. The large analytical area of the AgNPs mirror also offered a great compatibility with all kinds of Raman instruments and avoid the dependency of microscope to provide sensitive SERS measurements. The diverse functionality of the mirror substrate in the sample preparation (i.e., in sample immersing, in situ fabrication, sample deposition on the pre-formed mirror) provided more possibilities for SERS to be applied in food analysis.

The red wine chemical profiling using mirror substrate further broaden the analytical application of SERS in complicated food samples. Using the wine extract (in mediating solvent) to form the mirror substrate not only solve the problems of background interference caused by polymerized pigments, but also eliminate the

dominancy of peaks of DNA fractions in the Raman spectra, and generated a comprehensive spectrum (barcode) including tannins, anthocyanins, phenolic acids, and bioactive compounds. Later results found that each red wine has a unique chemical profile, which suggested that SERS bar code can be used for differentiation, authentication, control the and monitor safety and quality of red wines.

The detection of volatile compounds from garlic using the “mirror-in-cap” substrate extended the application of mirror and SERS in the headspace analysis. AgNPs mirror successfully identified the diallyl disulfide as the dominant compound in the garlic headspace and differentiated it from other organosulfur compounds. Compared to the gold standard GC method, AgNPs mirror showed a relatively equivalent analytical performance plus a simpler sample preparation and faster analyzing time and demonstrated a great potential to be a promising electronic nose device

Lastly, the rolling method as a simple sample preparation approach focused on the amplification of weak surface-enhanced Raman scattering of certain targets having a weak interaction with nanoparticles. The rolling method offered a great ability to enrich analytes and enhance signals without complicated pretreatments and instrumentations. Combined with a mathematic model, it even offers a potential to predict the unknown concentration of a target with a certain number of rolling times and the Raman intensity readings.

Future study will focus on the exploration of the analytical performance of the nanoparticle mirror and the rolling method in more challenging food systems including the collection of more chemical profiles of red wines and its combination with data science, expanding the headspace analysis to other aromatic bioactive compounds/plants,

and testing the reliability of rolling method in the detection of other targets with weak SERS activities.

BIBLIOGRAPHY

1. Yang T, Zhang Z, Zhao B, et al. Real-Time and in Situ Monitoring of Pesticide Penetration in Edible Leaves by Surface-Enhanced Raman Scattering Mapping. *Anal Chem*. 2016;88(10):5243-5250. doi:10.1021/acs.analchem.6b00320
2. Tu Q, Hickey ME, Yang T, et al. A simple and rapid method for detecting the pesticide fipronil on egg shells and in liquid eggs by Raman microscopy. *Food Control*. 2018. doi:10.1016/j.foodcont.2018.08.025
3. He L, Liu Y, Lin M, et al. A new approach to measure melamine, cyanuric acid, and melamine cyanurate using surface enhanced Raman spectroscopy coupled with gold nanosubstrates. *Sens Instrum Food Qual Saf*. 2008;2(1):66-71. doi:10.1007/s11694-008-9038-0
4. Gao S, Glasser J, He L. A Filter-based Surface Enhanced Raman Spectroscopic Assay for Rapid Detection of Chemical Contaminants. *J Vis Exp*. 2016;(108):e53791. doi:10.3791/53791
5. Gukowsky JC, Xie T, Gao S, Qu Y, He L. Rapid identification of artificial and natural food colorants with surface enhanced Raman spectroscopy. *Food Control*. 2018;92:267-275. doi:10.1016/j.foodcont.2018.04.058
6. Zhang Z, Guo H, Deng Y, et al. Mapping gold nanoparticles on and in edible leaves in situ using surface enhanced Raman spectroscopy. *RSC Adv*. 2016;6(65):60152-60159. doi:10.1039/C6RA11748A
7. Zheng J, He L. Surface-Enhanced Raman Spectroscopy for the Chemical Analysis of Food. *Compr Rev Food Sci Food Saf*. 2014;13(3):317-328. doi:10.1111/1541-4337.12062
8. Xu ML, Gao Y, Han XX, Zhao B. Detection of Pesticide Residues in Food Using Surface-Enhanced Raman Spectroscopy: A Review. *J Agric Food Chem*. 2017;65(32):6719-6726. doi:10.1021/acs.jafc.7b02504
9. Yaseen T, Pu H, Sun DW. Functionalization techniques for improving SERS substrates and their applications in food safety evaluation: A review of recent research trends. *Trends Food Sci Technol*. 2018;72(October 2017):162-174. doi:10.1016/j.tifs.2017.12.012
10. Fan M, Andrade GFS, Brolo AG. A review on the fabrication of substrates for surface enhanced Raman spectroscopy and their applications in analytical chemistry. *Anal Chim Acta*. 2011;693(1-2):7-25. doi:10.1016/j.aca.2011.03.002
11. Pieczonka NPW, Aroca RF. Inherent complexities of trace detection by surface-enhanced Raman scattering. *ChemPhysChem*. 2005;6(12):2473-2484. doi:10.1002/cphc.200500112
12. Reuhs BL. *Food Analysis*. Vol 184.; 1959. doi:10.1038/1841347a0
13. Pu H, Xiao W, Sun DW. SERS-microfluidic systems: A potential platform for rapid analysis of food contaminants. *Trends Food Sci Technol*. 2017;70(October):114-126. doi:10.1016/j.tifs.2017.10.001
14. Mcgorrin RJ. One Hundred Years of Progress in Food Analysis. *J Agric Food Chem*. 2009;57(18):8076-8088. doi:10.1021/jf900189s
15. Cordella C, Moussa I, Martel AC, Sbirrazzouli N, Lizzani-Cuvelier L. Recent developments in food characterization and adulteration detection: Technique-oriented perspectives. *J Agric Food Chem*. 2002;50(7):1751-1764.

doi:10.1021/jf011096z
16. Ignat T, Lurie S, Nyasordzi J, et al. Forecast of Apple Internal Quality Indices at Harvest and During Storage by VIS-NIR Spectroscopy. *Food Bioprocess Technol*. 2014;7(10):2951-2961. doi:10.1007/s11947-014-1297-7
17. Penner MH. Ultraviolet, Visible, and Fluorescence Spectroscopy. In: *Food Analysis*. Vol 22. ; 2010:389-404. doi:10.1007/978-1-4419-1478-1
18. Y-H. Peggy Hsieh. Immunoassays. In: *Food Analysis*. Vol 17. ; 2010:303-315. doi:10.1007/978-1-4419-1478-1
19. O'sullivan MJ, Bridges JW, Marks V. Enzyme Immunoassay: A Review. *Ann Clin Biochem An Int J Biochem Lab Med*. 1979;16(1-6):221-239. doi:10.1177/000456327901600162
20. Raman C, Krishnan K. A new type of secondary radiation. *Nature*. 1928;121:501.
21. Randall HM. The Infrared Spectrum of SN I. *Phys Rev*. 1931;38.
22. Yang D, Ying Y. Applications of raman spectroscopy in agricultural products and food analysis: A review. *Appl Spectrosc Rev*. 2011;46(7):539-560. doi:10.1080/05704928.2011.593216
23. Craig AP, Franca AS, Irudayaraj J. Surface-Enhanced Raman Spectroscopy Applied to Food Safety. *Annu Rev Food Sci Technol*. 2013;4(1):369-380. doi:10.1146/annurev-food-022811-101227
24. Thygesen LG, Løkke MM, Micklander E, Engelsen SB. Vibrational microspectroscopy of food. Raman vs. FT-IR. *Trends Food Sci Technol*. 2003;14(1-2):50-57. doi:10.1016/S0924-2244(02)00243-1
25. Li YS, Church JS. Raman spectroscopy in the analysis of food and pharmaceutical nanomaterials. *J Food Drug Anal*. 2014;22(1):29-48. doi:10.1016/j.jfda.2014.01.003
26. Gersten J, Nitzan A. Electromagnetic theory of enhanced Raman scattering by molecules adsorbed on rough surfaces. *J Chem Phys*. 1980;73(7):3023-3037. doi:10.1063/1.440560
27. Schatz GC, Van Duyne RP. Electromagnetic Mechanism of Surface-Enhanced Spectroscopy. In: *Surface-Enhanced Raman Scattering Physics and Applications*. Vol 46. ; 2006:19-45. doi:10.1002/0470027320.s0601
28. Anderson DJ, Moskovits M. A SERS-active system based on silver nanoparticles tethered to a deposited silver film. *J Phys Chem B*. 2006;110(28):13722-13727. doi:10.1021/jp055243y
29. Dieringer JA, McFarland AD, Shah NC, et al. Surface enhanced Raman spectroscopy: New materials, concepts, characterization tools, and applications. *Faraday Discuss*. 2006;132:9-26. doi:10.1039/b513431p
30. Lombardi JR, Birke RL, Lu T, Xu J. Charge-transfer theory of surface enhanced Raman spectroscopy: Herzberg-Teller contributions. *J Chem Phys*. 1986;84(8):4174-4180. doi:10.1063/1.450037
31. McNay G, Eustace D, Smith WE, Faulds K, Graham D. Surface-enhanced Raman scattering (SERS) and surface-enhanced resonance raman scattering (SERRS): A review of applications. *Appl Spectrosc*. 2011;65(8):825-837. doi:10.1002/jca.21312
32. Yang T, Wang P, Guo H, He L. Surface-Enhanced Raman Spectroscopy: A Tool for All Classes of Food Contaminants. *Ref Modul Food Sci*. 2017;(January 2019).

doi:10.1016/B978-0-08-100596-5.21090-1
33. Li L, Hutter T, Steiner U, Mahajan S. Single molecule SERS and detection of biomolecules with a single gold nanoparticle on a mirror junction. *Analyst*. 2013;138:4574-4578. doi:10.1039/c3an00447c
34. Si M, Li L, Chuanyun Z. Identification and Characterization of Volatile Organic Compounds of Fresh Plant Using Headspace Combined with Surface-Enhanced Raman Scattering. *J Food Process Technol*. 2016;6(12). doi:10.4172/2157-7110.1000520
35. Chen H, Wang C, Zhang Z, He L. Combining Headspace Solid-Phase Microextraction and Surface-Enhanced Raman Spectroscopy To Detect the Pesticide Fonofos in Apple Juice. *J Food Prot*. 2018;81(7):1087-1092. doi:10.4315/0362-028X.JFP-17-505
36. He L, Haynes CL, Diez-Gonzalez F, Labuza TP. Rapid detection of a foreign protein in milk using IMS-SERS. *J Raman Spectrosc*. 2011;42(6):1428-1434. doi:10.1002/jrs.2880
37. Chen M, Yang H, Rong L, Chen X. A gas-diffusion microfluidic paper-based analytical device (μPAD) coupled with portable surface-enhanced Raman scattering (SERS): facile determination of sulphite in wines. *Analyst*. 2016;141(19):5511-5519. doi:10.1039/C6AN00788K
38. Martin C, Bruneel JL, Castet F, et al. Spectroscopic and theoretical investigations of phenolic acids in white wines. *Food Chem*. 2017;221:568-575. doi:10.1016/j.foodchem.2016.11.137
39. Jung J, Chen L, Lee S, et al. Fast and sensitive DNA analysis using changes in the FRET signals of molecular beacons in a PDMS microfluidic channel. *Anal Bioanal Chem*. 2007;387(8):2609-2615. doi:10.1007/s00216-007-1158-6
40. Pang S, Yang T, He L. Review of surface enhanced Raman spectroscopic (SERS) detection of synthetic chemical pesticides. *TrAC - Trends Anal Chem*. 2016;85:73-82. doi:10.1016/j.trac.2016.06.017
41. Kneipp K. *Surface-Enhanced Raman Scattering*. Vol 60.; 2007. doi:10.1063/1.2812122
42. Tan C, Zhang Z, Qu Y, He L. Ag2O/TiO2 Nanocomposite Heterostructure as a Dual Functional Semiconducting Substrate for SERS/SEIRAS Application. *Langmuir*. 2017;33(22):5345-5352. doi:10.1021/acs.langmuir.7b00229
43. Panacek A, Libor Kvıtek,† Robert Prucek MK, Vecˇerˇova´ ‡ Renata, et al. Silver colloid nanoparticles: Synthesis, characterization, and their antibacterial activity. *J Optoelectron Adv Mater*. 2014;16(1-2):182-187. doi:10.1021/jp063826h
44. Moulton MC, Braydich-Stolle LK, Nadagouda MN, Kunzelman S, Hussain SM, Varma RS. Synthesis, characterization and biocompatibility of "green" synthesized silver nanoparticles using tea polyphenols. *Nanoscale*. 2010;2(5):763-770. doi:10.1039/c0nr00046a
45. Ratna T, Brown RJC, Martin MJT. Strategy to improve the reproducibility of colloidal SERS. *J Raman Spectrosc*. 2007;38(April):1538-1553. doi:10.1002/jrs
46. El-Aal MA, Seto T, Kumita M, Abdelaziz AA, Otani Y. Synthesis of silver nanoparticles film by spark discharge deposition for surface-enhanced Raman scattering. *Opt Mater (Amst)*. 2018;83(June):263-271. doi:10.1016/j.optmat.2018.06.029

47. Aroca RF, Alvarez-Puebla RA, Pieczonka N, Sanchez-Cortez S, Garcia-Ramos J V. Surface-enhanced Raman scattering on colloidal nanostructures. *Adv Colloid Interface Sci*. 2005;116(1-3):45-61. doi:10.1016/j.cis.2005.04.007
48. Aroca RF, Ross DJ. Surface-Enhanced Infrared Spectroscopy. *Appl Spectrosc*. 2004;58(11):324A-338A(15). doi:http://dx.doi.org/10.1366/0003702042475420
49. Zhao Y, Luo W, Kanda P, et al. Silver deposited polystyrene (PS) microspheres for surface-enhanced Raman spectroscopic-encoding and rapid label-free detection of melamine in milk powder. *Talanta*. 2013;113:7-13. doi:10.1016/j.talanta.2013.03.075
50. Liu X, Zong C, Ai K, He W, Lu L. Engineering natural materials as surface-enhanced Raman spectroscopy substrates for in situ molecular sensing. *ACS Appl Mater Interfaces*. 2012;4(12):6599-6608. doi:10.1021/am302376q
51. Chen LM, Liu YN. Surface-enhanced Raman detection of melamine on silver-nanoparticle- decorated silver/carbon nanospheres: Effect of metal ions. *ACS Appl Mater Interfaces*. 2011;3(8):3091-3096. doi:10.1021/am200603y
52. Hu H, Wang Z, Pan L, Zhao S, Zhu S. Ag-Coated Fe3O4@SiO2three-ply composite microspheres: Synthesis, characterization, and application in detecting melamine with their surface-enhanced Raman scattering. *J Phys Chem C*. 2010;114(17):7738-7742. doi:10.1021/jp100141c
53. Moskovits M. Surface-Enhanced Raman Spectroscopy: a Brief Perspective. In: *Surface-Enhanced Raman Scattering Physics and Applications*. Vol 18. ; 2006:1-17. http://www1.folha.uol.com.br/mercado/2015/11/1702797-crise-nao-freia-avanco-de-grandes-varejistas.shtml.
54. Freeman RG, Grabar KC, Allison KJ, et al. Self-Assembled Metal Colloid Monolayers: An Approach to SERS Substrates. *Science (80-)*. 1995;267(March):1629-1632.
55. Zhai J, Wang Y, Zhai Y, Dong S. Rapid fabrication of Au nanoparticle films with the aid of centrifugal force. *Nanotechnology*. 2009;20(5). doi:10.1088/0957-4484/20/5/055609
56. Makiabadi T, Bouvrée A, Le Nader V, Terrisse H, Louarn G. Preparation, optimization, and characterization of SERS sensor substrates based on two-dimensional structures of gold colloid. *Plasmonics*. 2010;5(1):21-29. doi:10.1007/s11468-009-9110-6
57. Toderas F, Baia M, Baia L, Astilean S. Controlling gold nanoparticle assemblies for efficient surface-enhanced Raman scattering and localized surface plasmon resonance sensors. *Nanotechnology*. 2007;18(25). doi:10.1088/0957-4484/18/25/255702
58. Muniz-Miranda M, Pergolese B, Bigotto A, Giusti A. Stable and efficient silver substrates for SERS spectroscopy. *J Colloid Interface Sci*. 2007;314(2):540-544. doi:10.1016/j.jcis.2007.05.089
59. Crespo-Biel O, Ravoo BJ, Reinhoudt DN, Huskens J. Noncovalent nanoarchitectures on surfaces: From 2D to 3D nanostructures. *J Mater Chem*. 2006;16(41):3997-4021. doi:10.1039/b608858a
60. Ko H, Singamaneni S, Tsukruk V V. Nanostructured surfaces and assemblies as SERS media. *Small*. 2008;4(10):1576-1599. doi:10.1002/smll.200800337
61. Cottart CH, Nivet-Antoine V, Laguillier-Morizot C, Beaudeux JL. Resveratrol

bioavailability and toxicity in humans. *Mol Nutr Food Res*. 2010;54(1):7-16. doi:10.1002/mnfr.200900437
62. Kaminska A, Inya-Agha O, Forster RJ, Keyes TE. Chemically bound gold nanoparticle arrays on silicon: Assembly, properties and SERS study of protein interactions. *Phys Chem Chem Phys*. 2008;10(28):4172-4180. doi:10.1039/b803007c
63. Daniels JK, Chumanov G. Nanoparticle - Mirror sandwich substrates for surface-enhanced Raman scattering. *J Phys Chem B*. 2005;109(38):17936-17942. doi:10.1021/jp053432a
64. Wang H, Kundu J, Halas NJ. Plasmonic nanoshell arrays combine surface-enhanced vibrational spectroscopies on a single substrate. *Angew Chemie - Int Ed*. 2007;46(47):9040-9044. doi:10.1002/anie.200702072
65. Yun S, Park YK, Seong KK, Park S. Linker-molecule-free gold nanorod layer-by-layer films for surface-enhanced Raman scattering. *Anal Chem*. 2007;79(22):8584-8589. doi:10.1021/ac071440c
66. Wang Y, Chen H, Wang E. Facile fabrication of gold nanoparticle arrays for efficient surface-enhanced Raman scattering. *Nanotechnology*. 2008;19(10). doi:10.1088/0957-4484/19/10/105604
67. Oh MK, Yun S, Kim SK, Park S. Effect of layer structures of gold nanoparticle films on surface enhanced Raman scattering. *Anal Chim Acta*. 2009;649(1):111-116. doi:10.1016/j.aca.2009.07.025
68. Tao AR, Kim F, Hess C, et al. Langmuir−Blodgett Silver Nanowire Monolayers for Molecular Sensing Using Surface-Enhanced Raman Spectroscopy. *Nano Lett*. 2003;3(9):1229-1233. doi:10.1021/nl0344209
69. Orendorff CJ, Gole A, Sau TK, Murphy CJ. Surface-enhanced Raman spectroscopy of self-assembled monolayers: Sandwich architecture and nanoparticle shape dependence. *Anal Chem*. 2005;77(10):3261-3266. doi:10.1021/ac048176x
70. Dos Santos DS, Goulet PJG, Pieczonka NPW, Oliveira ON, Aroca RF. Gold nanoparticle embedded, self-sustained chitosan films as substrates for surface-enhanced Raman scattering. *Langmuir*. 2004;20(23):10273-10277. doi:10.1021/la048328j
71. M.Kahla, E.Voges, S.Kostrewa, C.Viets, W.Hill. Periodically structured metallic substrates for SERS. *J Inst Electr Eng Japan*. 2012;132(8):554-557. doi:10.1016/S0925-4005(98)00219-6
72. Hidi IJ, Jahn M, Weber K, et al. Lab-on-a-Chip-Surface Enhanced Raman Scattering Combined with the Standard Addition Method: Toward the Quantification of Nitroxoline in Spiked Human Urine Samples. *Anal Chem*. 2016;88(18):9173-9180. doi:10.1021/acs.analchem.6b02316
73. Zhou Q, Kim T. Review of microfluidic approaches for surface-enhanced Raman scattering. *Sensors Actuators, B Chem*. 2016;227:504-514. doi:10.1016/j.snb.2015.12.069
74. Galarreta BC, Tabatabaei M, Guieu V, Peyrin E, Lagugné-Labarthet F. Microfluidic channel with embedded SERS 2D platform for the aptamer detection of ochratoxin A. *Anal Bioanal Chem*. 2013;405(5):1613-1621. doi:10.1007/s00216-012-6557-7

75. Parisi J, Su L, Lei Y. In situ synthesis of silver nanoparticle decorated vertical nanowalls in a microfluidic device for ultrasensitive in-channel SERS sensing. *Lab Chip*. 2013;13(8):1501-1508. doi:10.1039/c3lc41249k
76. Parisi J, Dong Q, Lei Y. In situ microfluidic fabrication of SERS nanostructures for highly sensitive fingerprint microfluidic-SERS sensing. *RSC Adv*. 2015;5(19):14081-14089. doi:10.1039/c4ra15174g
77. Xu B Bin, Ma ZC, Wang L, et al. Localized flexible integration of high-efficiency surface enhanced Raman scattering (SERS) monitors into microfluidic channels. *Lab Chip*. 2011;11(19):3347-3351. doi:10.1039/c1lc20397e
78. Peksa V, Jahn M, Štolcová L, et al. Quantitative SERS analysis of azorubine (E 122) in sweet drinks. *Anal Chem*. 2015;87(5):2840-2844. doi:10.1021/ac504254k
79. Chen J, Li Y, Huang K, et al. Nanoimprinted Patterned Pillar Substrates for Surface-Enhanced Raman Scattering Applications. *ACS Appl Mater Interfaces*. 2015;7(39):22106-22113. doi:10.1021/acsami.5b07879
80. Shanmukh S, Jones L, Driskell J, Zhao Y, Dluhy R, Tripp RA. Rapid and sensitive detection of respiratory virus molecular signatures using a silver nanorod array SERS substrate. *Nano Lett*. 2006;6(11):2630-2636. doi:10.1021/nl061666f
81. Shen W, Lin X, Jiang C, et al. Reliable quantitative SERS analysis facilitated by core-shell nanoparticles with embedded internal standards. *Angew Chemie - Int Ed*. 2015;54(25):7308-7312. doi:10.1002/anie.201502171
82. Li JF, Huang YF, Ding Y, et al. LETTERS Shell-isolated nanoparticle-enhanced Raman spectroscopy. *Nature*. 2010;464(7287):392-395. doi:10.1038/nature08907
83. Park YK, Yoo SH, Park S. Assembly of highly ordered nanoparticle monolayers at a water/ hexane interface. *Langmuir*. 2007;23(21):10505-10510. doi:10.1021/la701445a
84. Duan H, Wang D, Kurth DG, Möhwald H. Directing self-assembly of nanoparticles at water/oil interfaces. *Angew Chemie - Int Ed*. 2004;43(42):5639-5642. doi:10.1002/anie.200460920
85. Reincke F, Hickey SG, Kegel WK, Vanmaekelbergh D. Spontaneous Assembly of a Monolayer of Charged Gold Nanocrystals at the Water/Oil Interface. *Angew Chemie - Int Ed*. 2004;43(4):458-462. doi:10.1002/anie.200352339
86. Li YJ, Huang WJ, Sun SG. A universal approach for the self-assembly of hydrophilic nanoparticles into ordered monolayer films at a toluene/water interface. *Angew Chemie - Int Ed*. 2006;45(16):2537-2539. doi:10.1002/anie.200504595
87. Liao W, Lu X. Determination of chemical hazards in foods using surface-enhanced Raman spectroscopy coupled with advanced separation techniques. *Trends Food Sci Technol*. 2016;54:103-113. doi:10.1016/j.tifs.2016.05.020
88. Zhang X, Chu Y, Yang H, et al. Ultrasensitive and Specific Detection of Salbutamol in Swine Feed, Meat, and Urine Samples by a Competitive Immunochromatographic Test Integrated with Surface-Enhanced Raman Scattering. *Food Anal Methods*. 2016;9(12):3396-3406. doi:10.1007/s12161-016-0533-3
89. Schmit VL, Martoglio R, Carron KT. Lab-on-a-bubble surface enhanced raman indirect immunoassay for cholera. *Anal Chem*. 2012;84(9):4233-4236. doi:10.1021/ac300242k

90. Pang S, Labuza TP, He L. Development of a single aptamer-based surface enhanced Raman scattering method for rapid detection of multiple pesticides. *Analyst*. 2014;139(8):1895-1901. doi:10.1039/c3an02263c
91. Farka Z, Juřík T, Kovář D, Trnková L, Skládal P. Nanoparticle-Based Immunochemical Biosensors and Assays: Recent Advances and Challenges. *Chem Rev*. 2017;117(15):9973-10042. doi:10.1021/acs.chemrev.7b00037
92. Negri P, Kage A, Nitsche A, Naumann D, Dluhy RA. Detection of viral nucleoprotein binding to anti-influenza aptamers via SERS. *Chem Commun*. 2011;47(30):8635-8637. doi:10.1039/c0cc05433j
93. He L, Lamont E, Veeregowda B, et al. Aptamer-based surface-enhanced Raman scattering detection of ricin in liquid foods. *Chem Sci*. 2011;2(8):1579-1582. doi:10.1039/c1sc00201e
94. He L, Deen BD, Pagel AH, Diez-Gonzalez F, Labuza TP. Concentration, detection and discrimination of Bacillus anthracis spores in orange juice using aptamer based surface enhanced Raman spectroscopy. *Analyst*. 2013;138(6):1657-1659. doi:10.1039/c3an36561a
95. Kamra T, Chaudhary S, Xu C, Montelius L, Schnadt J, Ye L. Covalent immobilization of molecularly imprinted polymer nanoparticles on a gold surface using carbodiimide coupling for chemical sensing. *J Colloid Interface Sci*. 2016;461:1-8. doi:10.1016/j.jcis.2015.09.009
96. Gao F, Grant E, Lu X. Determination of histamine in canned tuna by molecularly imprinted polymers-surface enhanced Raman spectroscopy. *Anal Chim Acta*. 2015;901:68-75. doi:10.1016/j.aca.2015.10.025
97. Gao F, Hu Y, Chen D, Li-Chan ECY, Grant E, Lu X. Determination of Sudan I in paprika powder by molecularly imprinted polymers-thin layer chromatography-surface enhanced Raman spectroscopic biosensor. *Talanta*. 2015;143:344-352. doi:10.1016/j.talanta.2015.05.003
98. Gao J, Hu Y, Li S, Zhang Y, Chen X. Adsorption of benzoic acid, phthalic acid on gold substrates studied by surface-enhanced Raman scattering spectroscopy and density functional theory calculations. *Spectrochim Acta - Part A Mol Biomol Spectrosc*. 2013;104:41-47. doi:10.1016/j.saa.2012.11.103
99. Peica N, Lehene C, Leopold N, Cozar O, Kiefer W. Raman and surface-enhanced Raman studies of the food additive sodium benzoate. *J Optoelectron Adv Mater*. 2007;9(9):2943-2948.
100. Yao W, Sun Y, Xie Y, et al. Development and evaluation of a surface-enhanced Raman scattering (SERS) method for the detection of the antioxidant butylated hydroxyanisole. *Eur Food Res Technol*. 2011;233(5):835-840. doi:10.1007/s00217-011-1576-8
101. Peica N, Lehene C, Leopold N, Schlücker S, Kiefer W. Monosodium glutamate in its anhydrous and monohydrate form: Differentiation by Raman spectroscopies and density functional calculations. *Spectrochim Acta - Part A Mol Biomol Spectrosc*. 2007;66(3):604-615. doi:10.1016/j.saa.2006.03.037
102. Dasary SSR, Ray PC, Singh AK, Arbneshi T, Yu H, Senapati D. A surface enhanced Raman scattering probe for highly selective and ultra sensitive detection of iodide in water and salt samples. *Analyst*. 2013;138(4):1195-1203. doi:10.1039/c2an36293g

103. Olavarría-Fullerton J, Wells S, Ortiz-Rivera W, Sepaniak MJ, De Jesú MA. Surface-enhanced Raman scattering (SERS) characterization of trace organoarsenic antimicrobials using silver/polydimethylsiloxane nanocomposites. *Appl Spectrosc*. 2011;65(4):423-428. doi:10.1366/10-06116
104. Podstawka E, Światłowska M, Borowiec E, Proniewicz LM. Food additives characterization by infrared, Raman, and surface-enhanced Raman spectroscopies. *J Raman Spectrosc*. 2007;38:357-364. doi:10.1002/jrs
105. Cheung W, Shadi IT, Xu Y, Goodacre R. Quantitative analysis of the banned food dye sudan-1 using surface enhanced raman scattering with multivariate chemometrics. *J Phys Chem C*. 2010;114(16):7285-7290. doi:10.1021/jp908892n
106. Feng S, Gao F, Chen Z, et al. Determination of α-tocopherol in vegetable oils using a molecularly imprinted polymers-surface-enhanced Raman spectroscopic biosensor. *J Agric Food Chem*. 2013;61(44):10467-10475. doi:10.1021/jf4038858
107. Yang T, Zhao B, Kinchla AJ, Clark JM, He L. Investigation of Pesticide Penetration and Persistence on Harvested and Live Basil Leaves Using Surface-Enhanced Raman Scattering Mapping. *J Agric Food Chem*. 2017;65(17):3541-3550. doi:10.1021/acs.jafc.7b00548
108. Wang P, Pang S, Chen J, et al. Label-free mapping of single bacterial cells using surface-enhanced Raman spectroscopy. *Analyst*. 2016;141(4):1356-1362. doi:10.1039/C5AN02175H
109. Serrano-Montes AB, De Aberasturi DJ, Langer J, et al. A General Method for Solvent Exchange of Plasmonic Nanoparticles and Self-Assembly into SERS-Active Monolayers. *Langmuir*. 2015;31(33):9205-9213. doi:10.1021/acs.langmuir.5b01838
110. Alessi P, Fermeglia M, Kikic I. Liquid-Liquid Equilibrium of Cyclohexane-n-Hexane-Methanol Mixtures: Effect of Water Content. *J Chem Eng*. 1989;34:236-240. doi:10.1021/je00056a026
111. Guo H, Zhang Z, Xing B, et al. Analysis of Silver Nanoparticles in Antimicrobial Products Using Surface-Enhanced Raman Spectroscopy (SERS). *Environ Sci Technol*. 2015;49(7):4317-4324. doi:10.1021/acs.est.5b00370
112. Shrivastava A, Gupta V. Methods for the determination of limit of detection and limit of quantitation of the analytical methods. *Chronicles Young Sci*. 2011;2(1):21-25. doi:10.4103/2229-5186.79345
113. Vongsvivut J, Robertson EG, McNaughton D. Surface-enhanced Raman spectroscopic analysis of fonofos pesticide adsorbed on silver and gold nanoparticles. *J Raman Spectrosc*. 2010;41(10):1137-1148. doi:10.1002/jrs.2579
114. Waterhouse, A. L., Sacks, G. L. and Jeffery DW. *Anthocyanins*.; 2016. doi:doi:10.1002/9781118730720.ch16
115. Waterhouse AL. Wine Phenolics. *Ann N Y Acad Sci*. 2002;957(1):21-36. doi:10.1111/j.1749-6632.2002.tb02903.x
116. Kelebek H, Selli S, Canbas A, Cabaroglu T. HPLC determination of organic acids, sugars, phenolic compositions and antioxidant capacity of orange juice and orange wine made from a Turkish cv. Kozan. *Microchem J*. 2009;91(2):187-192. doi:10.1016/j.microc.2008.10.008
117. Martin JS, Martin MM. Tannin Assays in Ecological Studies : Lack of Correlation between Phenolics , Proanthocyanidins and Protein-Precipitating. *Oecologia*.

1982;54(2):205-211.
118. Teixeira dos Santos CA, Páscoa RNMJ, Lopes JA. A review on the application of vibrational spectroscopy in the wine industry: From soil to bottle. *TrAC - Trends Anal Chem*. 2017;88:100-118. doi:10.1016/j.trac.2016.12.012
119. Veale R, Quester P. Consumer Sensory Evaluations of Wine Quality: The Respective Influence of Price and Country of Origin. *J Wine Econ*. 2008;3(01):10-29. doi:10.1017/S1931436100000535
120. Wine Enthusiast Magazine. Gallo Family Vineyards NV Hearty Burgundy Red (California) Rating and Review | Wine Enthusiast Magazine. Wine Enthusiast Magazine. https://www.winemag.com/buying-guide/gallo-family-vineyards-nv-hearty-burgundy-red-california-190292. Published 2014. Accessed April 11, 2018.
121. Wang Q, Li Z, Ma Z, Liang L. Real time monitoring of multiple components in wine fermentation using an on-line auto-calibration Raman spectroscopy. *Sensors Actuators, B Chem*. 2014;202:426-432. doi:10.1016/j.snb.2014.05.109
122. Pinzaru SC, Magdas DA. Ag nanoparticles meet wines: SERS for wine analysis. *Food Anal Methods*. 2018;11(3):892-900. doi:10.1007/s12161-017-1056-2
123. Martin C, Bruneel JL, Guyon F, et al. Raman spectroscopy of white wines. *Food Chem*. 2015;181:235-240. doi:10.1016/j.foodchem.2015.02.076
124. Qu Y, Tan C, Zhang Z, He L. A facile solvent mediated self-assembly silver nanoparticle mirror substrate for quantitatively improved surface enhanced Raman scattering. *Analyst*. 2017;142(21):4075-4082. doi:10.1039/C7AN00784A
125. Wine Enthusiast Magazine. Château de Chantegrive 2012 Graves Rating and Review. Wine Enthusiast Magazine. https://www.winemag.com/buying-guide/chateau-de-chantegrive-2012-graves/. Published 2016. Accessed April 11, 2018.
126. Wine Enthusiast Magazine. Corley 2011 State Lane Vineyard Cabernet Sauvignon (Yountville) Rating and Review. Wine Enthusiast Magazine. https://www.winemag.com/buying-guide/corley-2011-state-lane-vineyard-cabernet-sauvignon-napa-yountville. Published 2015. Accessed April 11, 2018.
127. Jolliffe I. Principal Component Analysis BT - International Encyclopedia of Statistical Science. In: Lovric M, ed. Berlin, Heidelberg: Springer Berlin Heidelberg; 2011:1094-1096. doi:10.1007/978-3-642-04898-2_455
128. Kneipp K, Kneipp H, Kartha V, et al. Detection and identification of a single DNA base molecule using surface-enhanced Raman scattering (SERS). *Phys Rev E*. 1998;57(6):6281-6284. doi:10.1103/PhysRevE.57.R6281
129. Siret R, Boursiquot JM, Merle MH, Cabanis JC, This P. Toward the authentication of varietal wines by the analysis of grape (Vitis vinifera L.) Residual DNA in must and wine using microsatellite markers. *J Agric Food Chem*. 2000;48(10):5035-5040. doi:10.1021/jf991168a
130. Scruggs RL, Achter EK. The Thermodynamic Effects of Exposing Nucleic Acid Bases to Water : Solubility Measurements in Water and Organic Solvents. *Biopolymers*. 1972;11:1961-1972.
131. Zaffino C, Russo B, Bruni S. Surface-enhanced Raman scattering (SERS) study of anthocyanidins. *Spectrochim Acta - Part A Mol Biomol Spectrosc*. 2015;149:41-47. doi:10.1016/j.saa.2015.04.039
132. Waterhouse, A. L., Sacks, G. L. and Jeffery DW. *New Approaches to Tannin*

Characterization.; 2016. doi:doi:10.1002/9781118730720.ch33
133. Burns J, Gardner PT, O'Neil J, et al. Relationship among antioxidant activity, vasodilation capacity, and phenolic content of red wines. *J Agric Food Chem*. 2000;48(2):220-230. doi:10.1021/jf9909757
134. Deng Z, Chen X, Wang Y, Fang E, Zhang Z, Chen X. Headspace Thin-Film Microextraction Coupled with Surface- Enhanced Raman Scattering as a Facile Method for Reproducible and Speci fi c Detection of Sulfur Dioxide in Wine. *Anal Chem*. 2015;87:633-640.
135. Socrates G. *Infrared and Raman Characteristic Group Frequencies: Tables and Charts*.; 2004.
136. Aking W. Sulfur Dioxide : Science behind this anti-microbial , anti-oxidant , wine additive. *Pract Winer Vineyard J*. 2014;January/Fa:1-7.
137. Bartowsky EJ, Henschke PA. Acetic acid bacteria spoilage of bottled red wine-A review. *Int J Food Microbiol*. 2008;125(1):60-70. doi:10.1016/j.ijfoodmicro.2007.10.016
138. Bartowsky EJ. Bacterial spoilage of wine and approaches to minimize it. *Lett Appl Microbiol*. 2009;48:149-156. doi:10.1111/j.1472-765X.2008.02505.x
139. Kim SM, Wu CM, Kobayashi A, Kubota K, Okumura J. Volatile Compounds in Stir-Fried Garlic. *J Agric Food Chem*. 1995;43(11):2951-2955. doi:10.1021/jf00059a033
140. Lanzotti V. The analysis of onion and garlic. *J Chromatogr A*. 2006;1112(1-2):3-22. doi:10.1016/j.chroma.2005.12.016
141. Amagase H, Petesch BL, Matsuura H, Kasuga S, Itakura* Y. Intake of Garlic and Its Bioactive Components. *J Nutr*. 2001;131(3s):951s-1123s.
142. Calvo-Gómez O, Morales-López J, López MG. Solid-phase microextraction-gas chromatographic-mass spectrometric analysis of garlic oil obtained by hydrodistillation. *J Chromatogr A*. 2004;1036(1):91-93. doi:10.1016/j.chroma.2004.02.072
143. Avato P, Tursi F, Vitali C, Miccolis V, Candido V. Allylsulfide constituents of garlic volatile oil as antimicrobial agents. *Phytomedicine*. 2000;7(3):239-243. doi:10.1016/S0944-7113(00)80010-0
144. Nakagawa H. Growth inhibitory effects of diallyl disulfide on human breast cancer cell lines. *Carcinogenesis*. 2001;22(6):891-897. doi:10.1093/carcin/22.6.891
145. Yi L, Su Q. Molecular mechanisms for the anti-cancer effects of diallyl disulfide. *Food Chem Toxicol*. 2013;57:362-370. doi:10.1016/j.fct.2013.04.001
146. Deng Z, Chen X, Wang Y, Fang E, Zhang Z, Chen X. Headspace thin-film microextraction coupled with surface-enhanced raman scattering as a facile method for reproducible and specific detection of sulfur dioxide in wine. *Anal Chem*. 2015;87(1):633-640. doi:10.1021/ac503341g
147. Li D, Duan H, Ma Y, Deng W. Headspace-Sampling Paper-Based Analytical Device for Colorimetric/Surface-Enhanced Raman Scattering Dual Sensing of Sulfur Dioxide in Wine. *Anal Chem*. 2018;90(9):5719-5727. doi:10.1021/acs.analchem.8b00016
148. Schulz H, Baranska M, Belz HH, Rösch P, Strehle MA, Popp J ürgen. Chemotaxonomic characterisation of essential oil plants by vibrational spectroscopy measurements. *Vib Spectrosc*. 2004;35(1-2):81-86.

doi:10.1016/j.vibspec.2003.12.014
149. Doi T, Wang M, McClements DJ. Emulsion-based control of flavor release profiles: Impact of oil droplet characteristics on garlic aroma release during simulated cooking. *Food Res Int*. 2019;116(October 2018):1-11. doi:10.1016/j.foodres.2018.12.056
150. Martins N, Petropoulos S, Ferreira ICFR. Chemical composition and bioactive compounds of garlic (Allium sativum L.) as affected by pre- and post-harvest conditions: A review. *Food Chem*. 2016;211:41-50. doi:10.1016/j.foodchem.2016.05.029
151. Wang HC, Pao J, Lin SY, Sheen LY. Molecular mechanisms of garlic-derived allyl sulfides in the inhibition of skin cancer progression. *Ann N Y Acad Sci*. 2012;1271(1):44-52. doi:10.1111/j.1749-6632.2012.06743.x
152. Lee S-N, Kim N-S, Lee D-S. Comparative study of extraction techniques for determination of garlic flavor components by gas chromatography?mass spectrometry. *Anal Bioanal Chem*. 2003;377(4):749-756. doi:10.1007/s00216-003-2163-z
153. Brodnitz MH, Pascale J V., Van Derslice L. Flavor Components of Garlic Extract. *J Agric Food Chem*. 1971;19(2):273-275. doi:10.1021/jf60174a007
154. Springett MB, Rozier V, Bakker J. Use of fiber interface direct mass spectrometry for the determination of volatile flavor release from model food systems. *J Agric Food Chem*. 1999;47(3):1125-1131. doi:10.1021/jf980199n
155. Voice TC, Kolb B. Static and Dynamic Headspace Analysis of Volatile Organic Compounds in Soils. *Environ Sci Technol*. 1993;27(4):709-713. doi:10.1021/es00041a014
156. He L, Chen T, Labuza TP. Recovery and quantitative detection of thiabendazole on apples using a surface swab capture method followed by surface-enhanced Raman spectroscopy. *Food Chem*. 2014;148:42-46. doi:10.1016/j.foodchem.2013.10.023
157. Yang T, Doherty J, Zhao B, Kinchla AJ, Clark JM, He L. Effectiveness of Commercial and Homemade Washing Agents in Removing Pesticide Residues on and in Apples. *J Agric Food Chem*. 2017;65(44):9744-9752. doi:10.1021/acs.jafc.7b03118
158. Stiles PL, Dieringer JA, Shah NC, Duyne RP Van. Surface-Enhanced Raman Spectroscopy. *Annu Rev ofAnalytical Chem*. 2008;1:601-626. doi:10.1146/annurev.anchem.1.031207.112814
159. Chen Q, Yang M, Yang X, Li H, Guo Z, Rahma MH. A large Raman scattering cross-section molecular embedded SERS aptasensor for ultrasensitive Aflatoxin B1 detection using CS-Fe3O4 for signal enrichment. *Spectrochim Acta - Part A Mol Biomol Spectrosc*. 2018;189:147-153. doi:10.1016/j.saa.2017.08.029
160. Kubackova J, Fabriciova G, Miskovsky P, Jancura D, Sanchez-Cortes S. Sensitive surface-enhanced Raman spectroscopy (SERS) detection of organochlorine pesticides by alkyl dithiol-functionalized metal nanoparticles-induced plasmonic hot spots. *Anal Chem*. 2015;87(1):663-669. doi:10.1021/ac503672f
161. Gao S, Pearson B, He L. Mapping bacteria on filter membranes, an innovative SERS approach. *J Microbiol Methods*. 2018;147(December 2017):69-75. doi:10.1016/j.mimet.2018.03.005

162. Zhang Z, Guo H, Carlisle T, et al. Evaluation of Postharvest Washing on Removal of Silver Nanoparticles (AgNPs) from Spinach Leaves. *J Agric Food Chem*. 2016;64(37):6916-6922. doi:10.1021/acs.jafc.6b02705
163. Wang X, Du Y, Zhang H, et al. Fast enrichment and ultrasensitive in-situ detection of pesticide residues on oranges with surface-enhanced Raman spectroscopy based on Au nanoparticles decorated glycidyl methacrylate-ethylene dimethacrylate material. *Food Control*. 2014;46:108-114. doi:10.1016/j.foodcont.2014.04.035
164. Guerrini L, Aliaga AE, Cárcamo J, et al. Functionalization of Ag nanoparticles with the bis-acridinium lucigenin as a chemical assembler in the detection of persistent organic pollutants by surface-enhanced Raman scattering. *Anal Chim Acta*. 2008;624(2):286-293. doi:10.1016/j.aca.2008.06.038
165. Saito Y, Wang JJ, Smith DA, Batchelder DN. A Simple Chemical Method for the Preparation of Silver Surfaces for Efficient SERS. *Langmuir*. 2002;18(8):2959-2961. doi:10.1021/la011554y
166. Alvarez-Puebla RA, Liz-Marzán LM. Traps and cages for universal SERS detection. *Chem Soc Rev*. 2012;41(1):43-51. doi:10.1039/c1cs15155j
167. Yang C, Chen S. Two organochlorine pesticides, toxaphene and chlordane, are antagonists for estrogen-related receptor alpha-1 orphan receptor. *Cancer Res*. 1999;59(18):4519-4524. http://www.ncbi.nlm.nih.gov/pubmed/10493499.
168. Horiba. *Raman Bands*.; 2016.
169. EPA. *Chlordane*.; 2016.